

ไมโครอิเล็กทรอนิกส์ สำหรับไบโอเซนเซอร์ที่ใช้ฮอสเตรดสเปร์ออกซิเดส



นางสาวเลิศลักษณ์ แก้ววิมล

ศูนย์วิทยทรัพยากร
วิทยานิพนธ์นี้เป็นส่วนหนึ่งของการศึกษาตามหลักสูตรปริญญา ดุษฎีบัณฑิต

สาขาวิชาวิศวกรรมเคมี ภาควิชาวิศวกรรมเคมี
คณะวิศวกรรมศาสตร์ จุฬาลงกรณ์มหาวิทยาลัย

ปีการศึกษา 2552

ลิขสิทธิ์ของจุฬาลงกรณ์มหาวิทยาลัย

MICROELECTRODE ARRAYS FOR HORSERADISH PEROXIDASE BASED
BIOSENSOR



Miss Lerdluck Kaewvimol

A Dissertation Submitted in Partial Fulfillment of the Requirements
for the Degree of Doctor of Engineering Program in Chemical Engineering

Department of Chemical Engineering

Faculty of Engineering


Chulalongkorn University

Academic year 2009

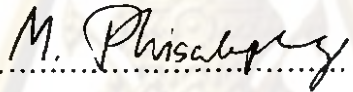
Copyright of Chulalongkorn University

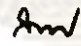
Thesis Title MICROELECTRODE ARRAYS FOR HORSE RADISH
PEROXIDASE BASED BIOSENSOR
By Miss Lerdluck Kaewvimol
Field of Study Chemical Engineering
Advisor Associate Professor Seeroong Prichanont, Ph.D.
Co-Advisor Professor Seamus P. J. Higson, Ph.D.

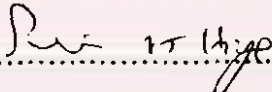
Accepted by the Faculty of Engineering, Chulalongkorn University in Partial
Fulfillment of the Requirements for the Doctoral Degree

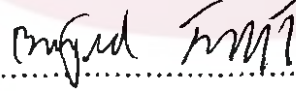
.....  Dean of the Faculty of Engineering
(Associate Professor Boonsom Lerdhirunwong, Dr. Ing)


THESIS COMMITTEE

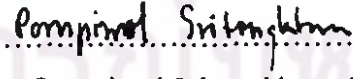
.....  Chairman
(Associate Professor Muenduen Phisalaphong, Ph.D.)

.....  Advisor
(Associate Professor Seeroong Prichanont, Ph.D.)

.....  Co-Advisor
(Professor Seamus P. J. Higson, Ph.D.)

.....  Examiner
(Associate Professor Bunjerd Jongsomjit, Ph.D.)

.....  Examiner
(Dr. Chanchana Thanachayanont, Ph.D.)

.....  External Examiner
(Dr Pornpimol Sritongkham, Ph.D.)

เลิศลักษณ์ แก้ววิมล : ไมโครอิเล็กโทรดอาร์เรย์ สำหรับไปโอเซนเซอร์ที่ใช้ฮอสเรดิสเปอร์ออกซิเดส. (MICROELECTRODE ARRAYS FOR HORSE RADISH PEROXIDASE BASED BIOSENSOR) อ.ที่ปรึกษาวิทยานิพนธ์หลัก : รองศาสตราจารย์ ดร. สิริรุ่งปรีชา นนท์, อ.ที่ปรึกษาวิทยานิพนธ์ร่วม: ศาสตราจารย์ ดร.เชมัส พี เจ อิกสัน, 150 หน้า.

วัตถุประสงค์ของงานวิจัยนี้คือการผลิต พอลิโอฟีนิลินไดเอมีนไดไฮโดรคลอไรด์/ฮอสเรดิสเปอร์ออกซิเดส/พอลิอะนิลีน และพอลิโอฟีนิลินไดเอมีนไดไฮโดรคลอไรด์/ฮอสเรดิสเปอร์ออกซิเดส/อนุภาคทอง/พอลิอะนิลีน ไมโครอิเล็กโทรดอาร์เรย์ ซึ่งงานวิจัยฉบับนี้แบ่งเป็นสามส่วน คือ การสร้างไมโครอิเล็กโทรดอาร์เรย์ ฮอสเรดิสเปอร์ออกซิเดส/พอลิอะนิลีน ไมโครอิเล็กโทรดอาร์เรย์ และ ฮอสเรดิสเปอร์ออกซิเดส/อนุภาคทอง/พอลิอะนิลีน ไมโครอิเล็กโทรดอาร์เรย์ ในส่วนแรก พิล์มที่เป็นขบวนการของพอลิโอฟีนิลินไดเอมีนไดไฮโดรคลอไรด์ ถูกตรึงลงบนกลาสคาร์บอนด้วยวิธีการทางไฟฟ้าเป็นจำนวน 50 รอบ พิล์มจนวน ถูกโชนิกที่เวลา 17.30 นาที เพื่อสร้างไมโครอิเล็กโทรด ด้วยค่าความเบี่ยงเบนมาตรฐานสัมพัทธ์ ของความสามารถในการผลิตซ้ำ 3.15 เปอร์เซ็นต์ โดยพบรูสองขนาด คือ ขนาดไมครอน และสับไมครอน ที่มีความหนาแน่น ประมาณ 7×10^4 และ 17×10^4 รูต่อตารางเซนติเมตร ตามลำดับ ในส่วนที่สอง เอนไซม์และอะนิลีนถูกตรึงลงบนรูไมโครอิเล็กโทรด เป็นจำนวน 20 รอบ เพื่อสร้างเป็น ฮอสเรดิสเปอร์ ออกซิเดส/อนิลีน ที่ยื่นออกมา พบการตอบสนองเชิงเส้น ในช่วงความเข้มข้นของฟีนอล 1×10^{-5} ถึง 1×10^{-6} ในส่วนที่สาม อนุภาคทองถูกตรึงลงบนรูของไมโครอิเล็กโทรด ค่าความต่างศักย์คงที่ ที่ -200 มิลลิโวลต์ เป็นเวลา 30 วินาที อนุภาคทรงกลมของทอง เกิดขึ้นในรูของไมโครอิเล็กโทรด และ ให้ผลเป็นลักษณะซิกมอยดอลของกราฟ ไชคลิกโวลต์แอมเพทรี ซึ่งแสดงถึงลักษณะของไมโครอิเล็กโทรด มีความสามารถในการผลิตซ้ำที่ 8.17 เปอร์เซ็นต์ ค่าความเบี่ยงเบนมาตรฐานสัมพัทธ์ เอนไซม์และอะนิลีนถูกตรึงด้วยวิธีการทางไฟฟ้าเป็นลำดับต่อไป พิล์มบางของเอนไซม์/พอลิอะนิลีน ถูกพบว่าเคลือบอยู่บนผิวของอนุภาคทอง ช่วงของการวัดฟีนอลพบว่าอยู่ในระดับและ 1×10^{-5} ถึง 1×10^{-3} โมลาร์ การมีอนุภาคทองรวมอยู่ด้วยส่งผลให้ ศักยภาพการวัดกระแสไฟฟ้าเพิ่มขึ้น 74.30 เปอร์เซ็นต์ เมื่อเปรียบเทียบกับกรณีไม่มีอนุภาคทอง นอกจากนี้ ค่าการตอบสนองทางไฟฟ้าหลังจากใช้ซ้ำ 10 ครั้ง เหลือประมาณ 43.92 และ 58.94 เปอร์เซ็นต์ สำหรับไมโครอิเล็กโทรดอาร์เรย์ที่มีอนุภาคทองและ ไม่มีอนุภาคทอง ของค่ากระแสเริ่มต้น

ศูนย์วิทยทรัพยากร

จุฬาลงกรณ์มหาวิทยาลัย

ภาควิชา วิศวกรรมเคมี

ลายมือชื่อผู้นิสิตเลิศลักษณ์ แก้ววิมล

สาขาวิชา วิศวกรรมเคมี

ลายมือชื่ออ.ที่ปรึกษาวิทยานิพนธ์หลัก สิริรุ่งปรีชา นนท์

ปีการศึกษา 2552

ลายมือชื่ออ.ที่ปรึกษาวิทยานิพนธ์ร่วม สิริรุ่งปรีชา นนท์

4971826721 : MAJOR CHEMICAL ENGINEERING

KEYWORDS : SONOCHEMICAL FABRICATION / MICROELECTRODE ARRAYS / ENZYME BIOSENSOR / HORSERADISH PEROXIDASE / GOLD PARTICLES

LERDLUCK KAEWVIMOL : MICROELECTRODE ARRAYS FOR HORSERADISH PEROXIDASE BASED BIOSENSOR. ADVISOR : ASSOCIATE PROFESSOR SEEROONG PRICHANONT, Ph.D, CO-ADVISOR: PROFESSOR SEAMUS P.J. HIGSON, Ph.D, 150 pp.

The overall aims of this research were to fabricate the poly(*o*-phenylenediamine dihydrochloride/ horseradish peroxidase/polyaniline and poly(*o*-phenylenediamine dihydrochloride/ horseradish peroxidase/ gold particles/ polyaniline microelectrode arrays. The thesis, therefore, was divided into three different sections namely; microelectrode arrays fabrication, horseradish peroxidase/poly aniline microelectrode arrays, and horseradish peroxidase/gold particles/polyaniline microelectrode arrays. In first part, an insulating film poly(*o*-phenylenediamine dihydrochloride) was firstly electrodeposited on glassy carbon electrode for 50 cycles. An insulating film was achieved and was then sonicated for 17.30 min for microelectrode formation with 3.15% RSD reproducibility. The two cavity sizes were found, microns and submicrons of microelectrode cavity population were approximately at 7×10^4 and 17×10^4 pores cm^{-2} , respectively. In the second part, the enzyme and aniline were electrodeposited on microelectrode cavities for 20 cycles to form the horseradish peroxidase/polyaniline protrusions. The 1×10^{-15} to 1×10^{-6} M range of phenol detection was achieved. In the final part, gold particles were electrodeposited on the microelectrode cavities by applying a fixed potential of -200 mV for 30 sec. The spherical gold particles were formed in microelectrode cavities and the resulting CV of sigmoidal shape was obtained indicating microelectrode characteristics. The reproducibility of these gold incorporated microelectrodes was determined at 8.17 % RSD. An enzyme and aniline were then electrodeposited, the enzyme/polyaniline thin film was found to cover the gold particle surfaces. The phenol detection range was determined from 1×10^{-15} - 1×10^{-3} M. The incorporation of gold particles resulted in current enhancement of 74.30 % compared with those of without. Moreover, the current responses after ten repeated uses were approximately 43.92% and 58.94% for with and without gold particles microelectrode arrays of the initial responses.

Department : Chemical Engineering Student's Signature L. Kaewvimol
 Field of Study : Chemical Engineering Advisor's Signature And
 Academic Year : 2009 Co-Advisor's Signature Seamus P.J. Higson

ACKNOWLEDGEMENTS

In the preparation of this thesis, the author would firstly like to express her sincere gratitude and appreciation to her supervisor, Associate Professor Seeroong Prichanont for her supervision, encouraging guidance, advice, discussion and helpful suggestions throughout the course of this research. Also, she would like to give the very grateful to her co-supervisor, Professor Seamus P.J. Higson, who gave her very kind and advice during she was staying at Cranfield University, UK, for her research.

The author would like to thank The Office of the Higher Education Commission, Thailand for the funding under the program Strategic Scholarships for Frontier Research Network for the Join Ph.D. Program Thai Doctoral degree.

In addition, the author would also be grateful to Associate Professor Muenduen Phisalaphong, as the chairman, Associate Professor Bunjerd Jongsomjit, Dr. Chanchana Thanachayanont, and Dr Pornpimol Sritongkham as the members of the thesis committee.

She would also like to thank her colleagues both from Chulalongkorn University namely, Panjai Rujisomnapa, Yusran Da-oa and from Cranfield University namely, Sarah Caygill, Matthew Partridge, Phillip Derbyshire, Jo Holmes, Dr Frank Davis, and Timothy Holford for their kind and friendship.

Special thanks to Dr Stuart Collyer from Cranfield University for many helpful suggestions and advice, without him this research would never been possible.

Most of all, the author would like to express her highest gratitude to her family, her parents and her sisters who always pay attention all the times for suggestions and advice. The most success of graduation is devoted to my family.

ศูนย์วิทยทรัพยากร

จุฬาลงกรณ์มหาวิทยาลัย

CONTENT

	Page
ABSTRACT (THAI).....	iv
ABSTRACT (ENGLISH).....	v
ACKNOWLEDGEMENTS.....	vi
CONTENTS.....	vii
LIST OF TABLES.....	x
LIST OF FIGURES.....	xi
CHAPTER I INTRODUCTION	
1.1 Motivation.....	17
1.2 Objective.....	19
1.3 Research scope.....	19
CHAPTER II THEORETICAL BACKGROUND	
2.1 Biosensor.....	21
2.2 Electrochemical method.....	22
2.2.1 Potentiometry detection method.....	22
2.2.2 Voltammetry detection method.....	23
2.2.3 Coulometry detection method.....	25
2.2.4 Conductimetry detection method.....	25
2.2.5 Mass transport.....	25
2.3 Horseradish peroxidase for phenol detection.....	27
2.4 Enzyme immobilization.....	27
2.4.1 Physical Adsorption.....	28
2.4.2 Covalent bonding.....	29
2.4.3 Affinity immobilization.....	29
2.4.4 Entrapment.....	30

	Page
2.5 Microelectrode arrays.....	30
2.5.1 Diffusion at microelectrode.....	31
2.5.2 Fabrication of microelectrode arrays	35
2.5.3 Sonochemistry.....	38
 CHAPTER III LITERATURE REVIEW	
3.1 Horseradish peroxidase (HRP) enzyme biosensor.....	42
3.1.1 HRP immobilization method for biosensor application.....	44
3.1.2 Polymer for HRP biosensor.....	47
3.1.3 Nanoparticles for HRP biosensor.....	51
3.2 Microelectrode arrays.....	54
3.2.1 Classification of microelectrode arrays.....	54
3.2.2 Nanoparticles in microelectrode arrays.....	57
3.2.3 Electrodeposition in microelectrode arrays.....	58
3.2.4 Application of microelectrode arrays.....	62
 CHAPTER IV MATERIAL AND METHOD	
4.1 Reagents.....	65
4.2 Equipments.....	65
4.3 Buffer and solution.....	67
4.4 Experimental procedure.....	67
4.4.1 The electrode pretreatment.....	67
4.4.2 The thin poly-phenylenediamine film polymerization.....	67
4.4.3 Sonochemical ablation for polymer thin film.....	68
4.4.4 The Electropolymerisation of PPD/HRP/PANI and.....	68
PPD/Au/HRP/PANI microelectrode arrays	
4.4.5 The microelectrode arrays for phenol detection.....	69
4.4.6 The microelectrode surface characterisation.....	69

	Page
CHAPTER V RESULT AND DISCUSSION	
5.1 Microelectrode arrays fabrication.....	70
5.1.1 Electropolymerisation of <i>o</i> -phenylenediamine dihydrochloride (<i>o</i> PD)	70
5.1.2 Sonochemically for microelectrode arrays fabrication and Characterisation	81
5.2 HRP/PANI microelectrode arrays.....	101
5.2.1 Planar electrode.....	101
5.2.2 Microelectrode arrays	107
5.3 The PPD/Au/HRP/PANI microelectrode arrays	112
5.3.1 Gold particles electrodeposition.....	114
5.3.2 The PPD/Au/HRP/PANI microelectrode array for phenol detection	118
5.3.3 Microscopic characterisation of PPD/Au/HRP/PANI microelectrode arrays	120
5.4 The comparison between PPD/HRP/PANI and PPD/Au/HRP/PANI microelectrode array	122
5.4.1 An electrochemical analysis.....	122
5.4.2 Microelectrode arrays reusability.....	125
5.5 Conclusion.....	127
5.6 Suggestion for future work.....	128
REFERENCES.....	129
APPENDICES	
APPENDIX A.....	141
VITA.....	150

LIST OF TABLES

	Page	
Table 3.1	Examples of polymer for HRP immobilization biosensor	48
Table 5.1	Summary of the effect of sonication time	97



ศูนย์วิทยทรัพยากร
จุฬาลงกรณ์มหาวิทยาลัย

LIST OF FIGURES

	Page
Figure 2.1	Schematic layout of a biosensor 22
Figure 2.2	Current-potential plot for cyclic voltammetry 24
Figure 2.3	Potential-time plot for cyclic voltammetry 24
Figure 2.4	Schematic representations of various enzyme (E) immobilization strategies 28
Figure 2.5	Diffusion profile to a macroelectrode and a hemispherical microelectrode 32
Figure 2.6	Characteristic sigmoidal shaped cyclic voltammogram for a reversible electron transfer reaction at a microelectrode. 33
Figure 2.7	Schematic representation of diffusion at a microelectrode array 34
Figure 2.8	The 3D AFM micrograph of anodic aluminum oxide (AAO) membrane and Zn–Ni alloy nanorods obtained from aqueous bath 35
Figure 2.9	Fabrication of microelectrode array tips using meniscus etching. 36
Figure 2.10	The SEM analysis of the array film of conductive polymer, poly(pyrrole-benzophenone), on indium tin oxide ITO 37
Figure 2.11	The development and collapse of cavitation bubbles 40
Figure 2.12	Cavitation bubble collapse near a solid surface 41
Figure 3.1	Mechanism of mediated electron transfer at HRP modified carbon paste electrode. M_{ox} and M_{red} are the oxidised and reduced forms of the mediator, respectively 43
Figure 3.2	Mechanism of the direct electron transfer between HRP and base electrode 44
Figure 3.3	The chitosan film cross-linked with glyoxal diagram 47
Figure 3.4	The chemical structure of aniline 50
Figure 3.5	AFM images showing the 2D (left) and 3D (right) surfaces of the bare BDD electrode; the MoO_2 nanoparticle modified electrode; the polymer film covered electrode the RAN BDD electrode 56

	Page
Figure 3.6	Cyclic voltammetry experiments show the performances of three working electrodes. 57
Figure 3.7	The chemical structure of <i>o</i> -phenylenediamine 59
Figure 3.8	Initial oxidation of the <i>o</i> PD monomer to form a radical monocation , the dimerization following the oxidation od <i>o</i> PD, and the chain propagation . 60
Figure 3.9	Proposed structure of poly(<i>o</i> -phenylenediamine) 61
Figure 3.10	The structure of aniline , and polyaniline 62
Figure 4.1	Sycopel AEW2 potentiostat 65
Figure 4.2	GC electrode (a), Pt electrode (b), and Ag/AgCl electrode were used as working, counter and reference electrode, respectively in this research 66
Figure 5.1	The schematic of polymer (PPD) to form an insulating film on GC electrode 73
Figure 5.2	Cyclic voltammogram for electropolymerization of 5 mM <i>o</i> PD at apotential scan rate 20 mVs ⁻¹ vs Ag/AgCl 73
Figure 5.3	Schematic representation of the <i>o</i> PD polymerisation mechanism proposed by Losito et al. (2003). 74
Figure 5.4	Cyclic voltammetry of 5 mM Ferri/Ferro cyanide at (a) a bare GC electrode and (b) a similar electrode coated by an electrodeposited film of PPD or poly(<i>o</i> -phenylenediamine) at scan rate 20 mVs ⁻¹ . 76
Figure 5.5	Cyclic voltammetry of 5 mM Hexaamineruthenium(III) chloride at (a) a bare GC electrode and (b) a similar electrode coated by an electrodeposited film of PPD or poly(<i>o</i> -phenylenediamine) at scan rate 20 mVs ⁻¹ . 77
Figure 5.6	Cyclic voltammetry of 5 mM Ferrocenecarboxlic acid at (a) a bare GC electrode and (b) a similar electrode coated by an electrodeposited film of PPD or poly(<i>o</i> -phenylenediamine) at scan rate 20 mVs ⁻¹ . 77

Figure 5.7	Electron micrograph of PPD insulated (a), bare GC electrode (b) and AFM image for PPD insulated on GC electrode (c), the 5 mM oPD oPD electropolymerization for 50 cycles at scan rate 20 mVs ⁻¹ and between 0 to 1000 mV.	80
Figure 5.8	The schematic of sonochemical ablation formation of microelectrode arrays	82
Figure 5.9	Laboratory-scale microelectrode arrays fabrication via ultrasonic ablation	83
Figure 5.10	Positioning of electrode during ultrasonication	83
Figure 5.11	Schematic representation of ultrasonic wave propagation and acoustic cavitation	85
Figure 5.12	The current response at 0 mV from cyclic voltammogram in 5 mM Ferri/Ferro cyanide scan rate 20 mVs ⁻¹ of the sonochemically ablation of electrodeposited film of PPD or poly(o-phenylenediamine) at different position.	87
Figure 5.13	Cyclic voltammetry of 5 mM Hexaamineruthenium(III)chloride of the sonochemically ablation PPD coated GC electrode at various sonication time at scan rate 20 mVs ⁻¹	90
Figure 5.14	Cyclic voltammetry of 5 mM Ferrocenecarboxylic acid of the sonochemically ablation PPD coated GC electrode at various sonication time at scan rate 20 mVs ⁻¹ .	90
Figure 5.15	Cyclic voltammetry of 5 mM Hexaamineruthenium (III) chloride at (a) a bare GC electrode (b) a PPD coated GC electrode and (c) a PPD coated electrode subsequently sonicated for 17.30 min at scan rate 20 mVs ⁻¹ .	92
Figure 5.16	Cyclic voltammetry of 5 mM Ferrocenecarboxylic acid at (a) a bare GC electrode (b) a PPD coated GC electrode and (c) a PPD coated electrode subsequently sonicated for 17.30 min at scan rate 20mVs ⁻¹ .	92

Figure 5.17	Scanning electron micrographs of GC electrode coated with PPD at 16 min, 17.30 min, 18 min, and 19 min of sonication in water at 35 kHz.	96
Figure 5.18	Calibration curves of current resulting from the amperometric reduction of hexaamineruthenium (III) chloride at sonochemically fabricated microelectrode arrays 17.30 min at the potential -40 mV	99
Figure 5.19	Calibration curves of current resulting from the amperometric reduction of hexaamineruthenium (III) chloride at sonochemically fabricated microelectrode arrays 17.30 min at the potential -40 mV	99
Figure 5.20	Comparison of the negative current in 5 mM Hexaamineruthenium (III) chloride for different 17.30 min of sonochemically ablation on PPD modified electrode at -40 mV	100
Figure 5.21	Comparison of the negative current in 5 mM Ferrocenecarboxylic acid for different 17.30 min of sonochemically ablation on PPD modified electrode at 50 mV	100
Figure 5.22	The schematic of sonochemical ablation formation of microelectrode arrays	102
Figure 5.23	Schematic representation of the aniline polymerisation mechanism proposed by Deng and Berkel (1999)	103
Figure 5.24	Linear sweep of HRP/PANI coated GC electrode (a) and 50 mV peak current at various aniline concentration at 500 μM HRP in Hydrogen peroxide: Phenol concentration ration (H:P) 0.35 (Rosatto et al., 1999) at scan rate 20 mVs^{-1}	105
Figure 5.25	Linear sweep of HRP/PANI coated GC electrode (a) and 50 mV peak current at various HRP concentration at 0.3 mM aniline concentration in Hydrogen peroxide: Phenol concentration ration (H:P) 0.35 (Rosatto et al., 1999) at scan rate 20 mVs^{-1}	106

	Page
Figure 5.26 Electrochemical deposition (-0.2 V to 0.8 V) of 0.3 mM aniline/ 300 Uml ⁻¹ HRP electrodeposition on a PPD modified GC electrode in acetate buffer pH 5.5 at scan rate 20 mVs ⁻¹	108
Figure 5.27 Scanning electron micrographs of PPD/HRP/PANI microelectrode arrays.	109
Figure 5.28 Current response at 50 mV of PPD/HRP/PANI microelectrode arrays for various Hydrogen peroxide concentration at 1 μM Phenol concentration ration scan rate 20 mVs ⁻¹	111
Figure 5.29 Linear sweep of PPD/HRP/PANI microelectrode arrays and 50 mV peak current for various phenol concentration at 0.7 H:P ratio, scan rate 20 mVs ⁻¹ .	113
Figure 5.30 The schematic of sonochemical ablation formation of PPD/Au/HRP/PANI microelectrode arrays	114
Figure 5.31 Cyclic voltammety of 5 mM Ferri/Ferro cyanide of Au nanoparticle microelectrode arrays at the electrodeposition time 30 sec, -20 mV.	116
Figure 5.33 Scanning electron micrographs of Au particles on micro arrays cavities	117
Figure 5.34 Linear sweep of PPD/Au/HRP/PANI microelectrode arrays (a) and 50 mV peak current for various phenol concentration at 0.7 H:P ratio, scan rate 20 mVs ⁻¹ .	119
Figure 5.35 Scanning electron micrographs of and PPD/HRP/PANI microelectrode arrays.	121
Figure 5.36 The comparison between PPD/HRP/PANI and PPD/Au/HRP/PANI microelectrode arrays peak current at applied voltage 50 mV	124
Figure 5.37 Reusability of PPD/HRP/PANI microelectrode arrays(b),the phenol samples (1x10 ⁻⁶ M) were analyzed repeatedly using single electrode.	

Figure 5.38 Reusability of PPD/Au/HRP/PANI microelectrode arrays(b),the phenol samples (1×10^{-6} M) were analyzed repeatedly using single electrode.

123



ศูนย์วิทยทรัพยากร
จุฬาลงกรณ์มหาวิทยาลัย

CHAPTER I INTRODUCTION

1.1 Motivation

Microelectrode arrays (MEAs) have been used for the last three decades in the field of cellular biology as tools for probing electrophysiological activity either *in vitro* or *in vivo*. The preparation procedures of microelectrode arrays are not complicated but require very careful work and experiences. There are several basic approaches, such as dispersing sufficiently small particles of a conductive material in an insulator. These arrays are poorly defined electrochemically. Another approach involves coverage of the conductive electrode surface with a monomolecular, nonconductive Langmuir–Blodgett film and formation of conductive channels in the film by uniformly dispersing in it molecules of a suitable substance. Single-molecule electron and ion gate sites are thus obtained forming a random array. Barton, et al. (2004) applied this approach to fabricate microelectrode arrays assisted by ultrasonication and entrapped glucose oxidase for the detection of glucose. Other published works also followed this technique to fabricate microelectrode arrays as biosensors for various substances. For example, Myler, et al. (2005) used alcohol oxidase to detect aqueous ethanol concentration; Law et al., (2005) as well as Pritchard et al., (2004) used acetylcholinesterase for determination of pesticides. Microelectrode arrays of this type were found to be able to determine substances at very low concentrations, for example, respectively down to 1×10^{-17} M, 1×10^{-16} M, and 1×10^{-16} M, for dichlorvos, Parathion, and Azinphos (Law et al., 2005). Moreover, these microelectrodes endured unique hemispherical diffusional profiles, and could impart stir-independence to sensor responses.

Meanwhile, the emergence of nanoparticles is opening new horizons for highly sensitive electrochemical assays. By incorporation with nanoparticles (NPs), electrochemical sensors have shown great promises for the diagnosis of trace molecules because the nanoparticle-based amplification platforms and amplification processes have been reported to dramatically enhance the intensity of the electrochemical signal and lead to ultrasensitive assays (Du, et al., 2008). Gold, silver,

and other noble metal nanoparticles have been intensively studied for the past few decades due to their unusual optical, electronic and catalytic properties. Gold nanoparticles were immobilized to provide a suitable microenvironment for biomolecules to retain their biological activity, and to facilitate electron transfer between the immobilized proteins and electrode surfaces (Lei, et al., 2003; Luo, et al., 2005; Pingarron, et al., 2008). Furthermore, carbon nanotube (Korkut, et al., 2008; Zhu, et al., 2007) and silver nanoparticles (Du, et al., 2008; Xu, et al., 2004) were immobilized together with horseradish peroxidase (HRP) for a modified electrode.

Gold nanoparticles (Au) have been extensively applied for construction of biosensing devices due to their extraordinary properties which allow the success of enhanced biosensor performances (Orozco et al., 2009, Pingarrón et al., 2008, Njagi et al., 2007, Yin et al., 2009). The propitious properties of Au-NPs include the provision of favourable surfaces for stable enzyme immobilization, allowance of direct electron transfer between redox enzyme and electrode surface without the needs of electron mediators, provision of high surface-to-volume ratio for enzyme immobilization, and lessening enzyme-nanoparticles distance (Pingarrón et al., 2008). Thus, biosensors incorporated with Au-NPs have generally proved to be increased in their sensitivity, stability, and selectivity (Yin et al., 2009, Abdullin et al., 2009).

Microelectrode arrays have been used in various type of enzyme such as glucose oxidase (Barton, et al. 2004), alcohol oxidase (Myler, et al. 2005), and acetylcholine esterase (Law et al., 2005 and Pritchard et al., 2004). Nevertheless, no publish reported horseradish peroxidase (HRP) immobilization in microelectrode arrays. Horseradish peroxidase (HRP) have been vastly used for phenolic compound due to their advantages such as good selectivity in the presence of phenol oxidases, relatively low cost of realization and storage, and the potential for miniaturization and automation (Korkut, et al., 2008). Horseradish peroxidase (HRP) based biosensors are most sensitive for a great number of phenolic compounds since phenols can act as electron donors for peroxidase (Yang, et al., 2006).

In comparison with macroelectrode, microelectrode displayed lower current limit. Furthermore, microelectrode can work with small material concentrations (Zoski, G., 2007). For this project, the sonochemically fabricated microelectrode arrays with immobilized HRP based biosensors are proposed. Then the modified

microelectrode arrays by electrodepositing gold nanoparticle on electrode is compared in wish of more improving the current limitation.

1.2 Objective

- 1.2.1 To study the poly-phenylenediamine/ polyaniline/ HRP based microelectrode arrays biosensors.
- 1.2.2 To study the Au nanoparticles/ poly-phenylenediamine / polyaniline/ HRP based microelectrode arrays biosensors.

1.3 Research scopes

Glassy carbon, Ag/AgCl₂, and platinum are used as working, reference, and counter electrodes, respectively.

- 1.3.1 The poly-phenylenediamine / PANI / HRP microelectrode arrays for phenol biosensor.
 - 1.3.1.1 Investigation of suitable fabricating conditions:
 - 1.3.1.1.1 Suitable of aniline concentration.
 - 1.3.1.1.2 Optimum of sonication time for pore formation.
 - 1.3.1.2 Physical characterization of microelectrode arrays
 - 1.3.1.2.1 Scanning electron microscopy (SEM) for surface characteristic.
 - 1.3.1.2.2 *Atomic force microscope* (AFM) for determine surface roughness
 - 1.3.1.3 Electrochemical analysis of microelectrode arrays
 - 1.3.1.3.1 Cyclic voltamogram is recorded
 - 1.3.1.3.2 Linear sweep voltammogram is determined
- 1.3.2 The Au/ poly-phenylenediamine / PANI / HRP based microelectrode arrays biosensor.

1.3.2.1 Physical characterization of gold nanoparticle coated on poly-phenylenediamine film.

1.3.2.1.1 Scanning electron microscopy (SEM) for surface characteristic.

1.3.2.2 Physical characterization of microelectrode arrays

1.3.2.2.1 Scanning electron microscopy (SEM) for surface characteristic.

1.3.2.3 Electrochemical analysis

1.3.2.3.1 Cyclic voltamogram is recorded

1.3.2.3.2 Linear sweep voltammogram is determined

1.3.3 Comparative study of the poly-phenylenediamine / PANI / HRP and Au/ poly-phenylenediamine / PANI / HRP microelectrode arrays.

1.3.3.1 Electrochemical analysis

1.3.3.2 Reusability of modified electrodes



ศูนย์วิจัยทรัพยากร
จุฬาลงกรณ์มหาวิทยาลัย

CHAPTER II

THEORETICAL BACKGROUND

Since this research focus on a sonochemical fabrication of HRP microelectrode arrays for phenol detection, this chapter will include various theoretical topics involved. Chapter starts with the introduction about biosensor. Moreover, enzyme immobilisations as another core technology employed in this study along with its influential parameters are also focus in this chapter. Finally, the fabrication methods for microelectrode arrays are also detailed in this chapter.

2.1 Biosensor

Biosensors have been defined in many ways and have been described by Turner (1987): 'A biosensor is a device incorporating a biological sensing element either intimately connected to or integrated within a transducer'. The main components of a biosensor are the biological compartment, transducer, and signal processor, as shown in Figure 2.1. The biological compartment is the partition which an interaction between the biological component and the substrate such as enzymes, antibodies and nucleic acid etc. The detection device is called transducer, which observes change into a measurable signal. And the signal process usually converted to a digital signal and passed to a microprocessor stage where the data is processed, converted to concentration units and output to a display device or data store.

The important characteristics of a biosensor are selective, sensitive, and fast response. These requirements may depend mainly on bioreceptor which should contain excess amount of active enzyme. Thus, essential features of desired carrier are: large surface areas and high pore volume to obtain high enzyme loading, small size that can be put in electrode easily, and biocompatible to achieve high activity and stability of enzyme without the maintain problem. Further, carriers should facilitate substrate to immobilised enzyme and electron transfer to transducer with fewer barriers to the analyst solution.

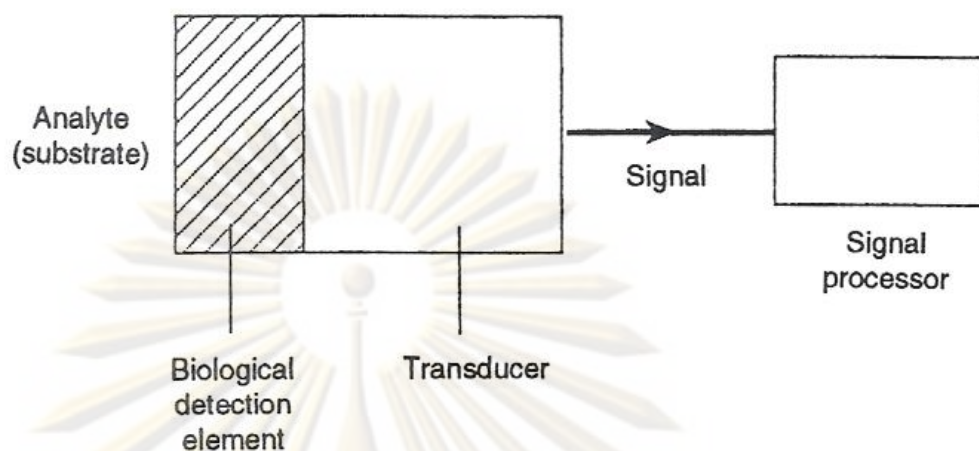


Figure 2.1 Schematic layout of a biosensor (Eggins, 1999).

2.2 Electrochemical method

An electrochemical is the method in which either current or potential is measured during an electrochemical reaction. This method the gas or liquid containing the trace impurity to be analyzed is sent through an electrochemical cell containing a liquid or solid electrolyte and in which an electrochemical reaction specific to the impurity takes place. There are four main types of electrochemical methods, potentiometry, voltammetry, coulometry, and conductimetry detection method. Firstly, the principles of electrochemistry are briefly informed.

2.2.1 Potentiometry detection method

This method is a detection method in which the potential of a cell is related to the concentration (activity) of a reactant which is a component of the cell fluid. The signal is measured as the potential difference (voltage) between the working electrode and the reference electrode. The working electrode's potential must depend on the concentration of the analyte in the gas or solution phase. Furthermore, the reference electrode is needed to provide a defined reference potential.

2.2.2 Voltammetry detection method

The common characteristic of all voltammetric techniques is that they involve the application of a potential (E) to an electrode and the monitoring of the resulting current (i) flowing through the electrochemical cell. The uniqueness of each rests on subtle differences in the manner and timing in which the potential is applied and the current measured. These differences can also provide very diverse chemical, electrochemical, and physical information, such as highly quantitative analyses, rate constants for chemical reactions, electrons involved on redox reactions, and diffusion constants.

Cyclic voltammetry (CV) has become an important and widely used electroanalytical technique in many areas of chemistry. It is rarely used for quantitative determinations, but it is widely used for the study of redox processes, for understanding reaction intermediates, and for obtaining stability of reaction products. This technique is based on varying the applied potential at a working electrode in both forward and reverse directions (at some scan rate) while monitoring the current. For example, the initial scan could be in the negative direction to the switching potential. At that point the scan would be reversed and run in the positive direction can be performed. The response obtained from a CV can be very simple, as shown in Figure 2.2. Cyclic voltammogram shows the anodic peak potential (E_{pa}), anodic peak current (i_{pa}) or oxidation current because the potential is scanned positively, anodic current occurs when the electrode becomes a sufficiently strong oxidant. When the scan direction is switched to negative for reverse scan, the electrode becomes a sufficiently strong reductant. This causes the cathodic peak potential (E_{pc}), the cathodic peak current (i_{pc}) or reduction current occurs. This oxidation peak will usually have a similar shape to the reduction peak.

Furthermore, the linear sweep is another voltammetric method where the current at the working electrode is measured while the potential is swept linearly in time. Oxidation or reduction specie is registered as a peak or trough in the current signal at the potential that species begin to be oxidized or reduced. The potential sweep profile of which can be seen in Figure 2.3.

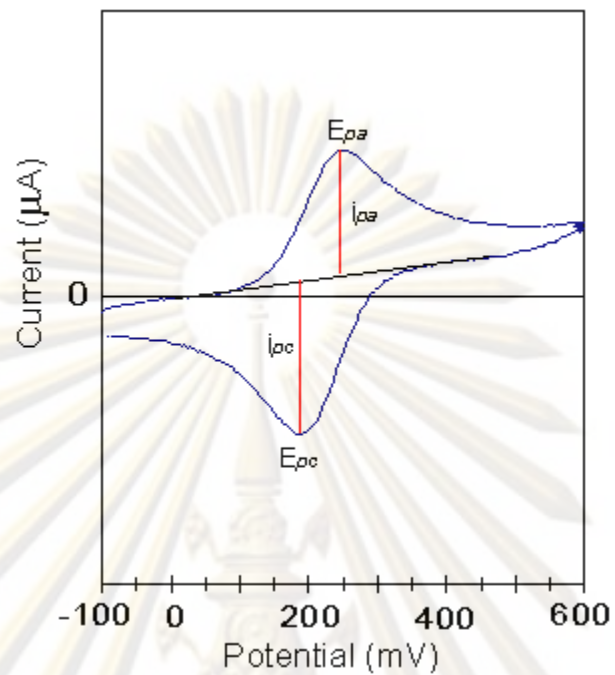


Figure 2.2 current-potential plot for cyclic voltammetry ([http://www-biol.paisley.ac.uk/marco/enzyme electrode/chapter1/cv.gif](http://www-biol.paisley.ac.uk/marco/enzyme%20electrode/chapter1/cv.gif))

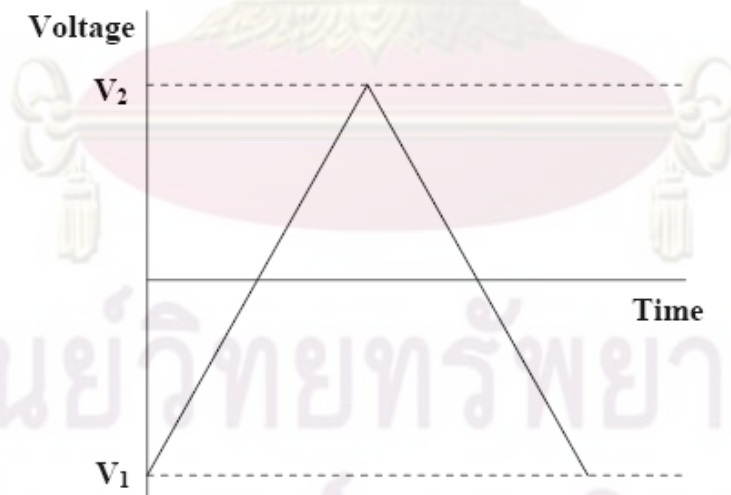


Figure 2.3 potential-time plot for cyclic voltammetry (<http://www.bath.ac.uk/~chsacf/solartron/Electro/html/dl.ht>)

2.2.3 Coulometry detection method

Coulometric method determines the amount of matter transformed during an electrolysis reaction by measuring the amount of electricity (in coulombs) consumed or produced. There are two basic categories of coulometric techniques. Potentiostatic coulometry involves holding the electric potential constant during the reaction using a potentiostat. The other, called coulometric titration or amperostatic coulometry, keeps the current (measured in amperes) constant using an amperostat.

2.2.4 Conductimetry detection method

The method use for measure conductance of a solution, using inert electrode, alternating current, and electrical null circuit thereby ensure no net current flow and no electrolysis. The concentration of ions in the solution is estimated from the conductance.

2.2.5 Mass transport

The transport of species between the electrode and solution is described the movement of a reactant or the product formed during an electrochemical reaction to and from an electrode surface. This transport can describe by three following significant processes which are diffusion, convection or migration (Wang, 2006).

Convection is the physical movement in the solution this may occurred via stirring or hydrodynamic transport (Selkirk, 1997). It consists of both natural and forced convection. Natural convection is caused by thermal and/or density gradients and becomes significant at macro electrodes after approximately 10 s. Forced convection can take the form of stirring, pumping or bubbling gas through the solution and can be applied to swamp contributions from natural convection to make experiments over 10 s long more reproducible.

Migration is known as the movement of a charged body under the influence of an electrical field (Brett & Brett, 1986). The mobility of the charged body is dependent on its charge and size, as well as the viscosity of the solution. Migration

effects on the analyt of interest are usually lowered by adding electrolytes, the small ions of opposing charge which have the same relative mobility.

Diffusion is described as the movement of species under the influence of a gradient of chemical potential, that is the concentration distribution (Brett & Brett, 1986). If linear diffusion towards a planar surface is considered, then the movement, or flux (j), that a certain amount of material (C) undergoes through a unit distance (x) in one second can be described by Fick's first law,

$$J = -D_0 \frac{\partial [C]}{\partial x} \quad (2.1)$$

where D_0 , is a characteristic diffusion function of the material involved. In practice, it is more useful to consider the variation of concentration at a point as a function of time. This can predicted by use Fick's second law,

$$\frac{\partial [C]}{\partial t} = D_0 \frac{\partial^2 [C]}{\partial x^2} \quad (2.2)$$

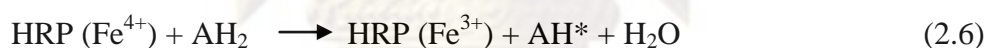
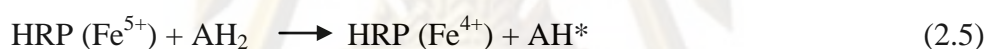
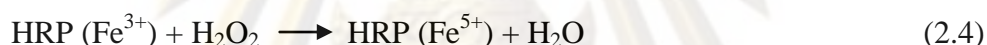
where $\frac{\partial [C]}{\partial t}$ is the concentration in terms of position and time, and $\frac{\partial^2 [C]}{\partial x^2}$ is the concentration gradient.

However, to use these equations, the experimental conditions need to be defined. The Cottrell equation is easily used and defines the current density i , at a planar electrode containing excess electrolyte at constant temperature. This is shown in equation 2.3, where n is the number of electrons, F is the Faraday constant, D is the diffusion coefficient of species C , A is the electrode area, $[C]_{\infty}$ is the concentration of C in the bulk solution and t is the time.

$$i = nFAJ = \frac{nFAD^{1/2}[C]_{\infty}}{(\pi t)^{1/2}} \quad (2.3)$$

2.3 Horseradish peroxidase for phenol detection

Horseradish peroxidase is a monomeric glycoprotein with a molecular mass of 44 kDa, purified from horseradish roots (*Amoracia rusticana*). It is a typical member of the plant peroxidases that catalyses the oxidation of a number of organic and inorganic compounds (the second substrate) with hydrogen peroxide or alkyl peroxide (the first substrate) (Sato et al., 1995). Horseradish peroxidase is of great importance for the determination of phenolic compounds in environmental control, protection and health benefits due to their toxicity and persistency in the environment (Yang et al., 2006). Other applications of HRP include polymer synthesis especially for phenolic resin synthesis, diagnostic assays, nucleic acid analysis, biosensors, bioremediations, and other biotechnological processes (Liu et al. 2006). Reactions of the enzyme can be shown as follows (Rosatto et al., 1999):



The first Eq. (a) represents a two-electron oxidation of the heme prosthetic group of the native peroxidase by H_2O_2 . This reaction results in the formation of an intermediate, $\text{HRP (Fe}^{5+})$ (oxidation state +5). In the next Eq. (b), $\text{HRP (Fe}^{5+})$ loses one oxidizing equivalent upon one-electron reduction by the electron donor AH_2 and forms $\text{HRP (Fe}^{4+})$ (oxidation state +4). In the third step (c), $\text{HRP (Fe}^{4+})$ accepts and 4 additional electrons from the electron donor molecule AH_2 and the enzyme are returned to their native state (Ruzgas et al., 1996).

2.4 Enzyme immobilisation

There are many methods for enzyme immobilisation. The immobilisation method used has mark influences on the properties of immobilised enzyme: for example, activity, stability, deactivation, and regeneration. Thus, the selection of enzyme immobilisation strategy should be considered carefully. Various strategies

have been employed including physical adsorption, covalent binding, physical entrapment, and affinity methods (Andreescu, et al., 2008). Figure 2.4 illustrates the general approaches of several enzyme immobilisation methods.

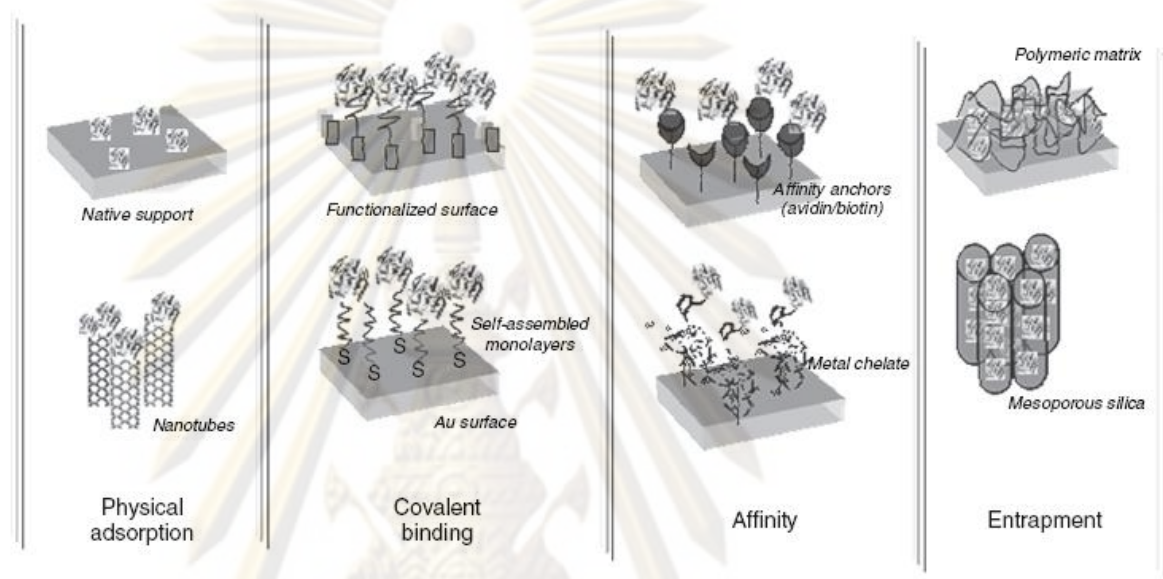


Figure 2.4 schematic representations of various enzyme (E) immobilisation strategies (Andreescu, et al., 2008)

2.4.1 Physical adsorption

Generally, physical adsorption is the easiest, inexpensive and the least denaturing immobilisation method. The procedure consists of simple deposition of the enzyme onto the support or electrode material. It does not involve additional reagents, sequential steps or enzyme modifications that could affect its activity. However, due to the fact that the binding forces involved are weak, the enzyme immobilised in this way is susceptible to pH, temperature, solvent and ionic strengths changes and does not provide increased enzyme activity and long-term operational and storage stability.

2.4.2 Covalent bonding

The attachment of an enzyme by covalent linkage consists of two steps. The first step involves activation of the material to provide useful chemical reactivity for subsequent binding of the biomolecule. Typically, this is achieved with bifunctional groups or spacers such as glutaraldehyde, carbodiimide/succinimide, self-assembled monolayers or multilayers (SAM) and aminopropyltriethoxysilanes. The second step consists of binding the enzyme to a chemically activated support. The chemistry involved in the immobilisation process depends upon the type of material used and its surface characteristics. This procedure has some advantages such as the increased stability of the enzyme due to the strong chemical binding, but has poor reproducibility, requires the use of large amounts of enzyme and the immobilised enzyme has relatively low activity due to the fact that the process can involve groups that are essential for its activity.

2.4.3 Affinity Immobilisation

Increasing efforts have been focused on the development of new and innovative techniques which can ensure controlled spatial orientation/conformation, without loss of enzyme activity during the immobilisation procedure. A recent trend is to create (bio) affinity bonds between an activated support and a specific group of the protein sequence. When these groups are not present in the native enzyme, they can be engineered at a specific location which does not affect the activity or the folding of the protein. The method is usually reversible facilitating the reuse of support matrix and provides stable enzyme attachment. In addition, it provides a basis for controlled and oriented immobilisation of the enzyme on different supports, opening the way for new approaches to enzyme immobilisation.

2.4.4 Entrapment

One of the most convenient methods of enzyme immobilisation is by physical entrapment in an inert material. This method has some advantages over the other procedures such as mild conditions, easy one-step fabrication, low cost and high stability of encapsulated enzyme. The limitations of the method are diffusional barriers of the transport of substrate and/or product resulting in long response times, difficulties in controlling the pores dimensions and possible enzyme leaching.

In some cases, the activity of the enzyme can be affected by the physical and chemical properties of the immobilisation matrix. The process, however, can be considered as general applicable for all enzymes. Examples of materials used for encapsulation include photopolymerisable polymers, chemically generated polymers (i.e., alginate, latex), electrochemically generated polymers (polypyrrole, polyaniline, polyacetylene, polythiophene, polyindole), inorganic clays and sol-gels. In this process, enzymes can be immobilised together with activators or artificial mediators such as ferrocene, quinoline derivatives, tetrathiafulvalene and organic salts that facilitate the transport of the electrons from the redox center of the enzyme to the surface of the electrode. This feature is particularly important for biosensing.

2.5 Microelectrode arrays

In case of the geometric dimensions of an amperometric electrode become progressively smaller, the behavior of the electrode begins to change from a large electrode which can be approximated by an electrode of infinite dimension. These differences are caused by changing conditions of the mass transport from the bulk of solution towards the electrode and have several important practical implications, such as a decreased ohmic drop of potential, fast establishment of a steady-state signal, a current increase due to enhanced mass transport at the electrode boundary, and increased signal-to-noise ratio. These effects make the small electrodes advantageous in many areas of electroanalytical chemistry. The application of small-size electrodes was further enhanced by increasing demands from analytical chemistry (e.g., the need for electrodes in miniature cells in detection for high-performance separations or in

electrochemical sensors) and biochemistry (*in situ* electroanalytical measurements on living organisms).

These small-size electrodes have been called microelectrodes. The radius of microelectrodes are smaller than 50 μm different from conventional sized electrode (radius 1 mm or greater) (Zoski, G.,2007). In addition to single electrodes, microelectrode arrays have been prepared and used. Both experimental and theoretical works have demonstrated the advantages of such electrode assemblies, which result from specific mass transport of electroactive materials or diffusion regimes taking place at their interface such as, the microelectrodes in the arrays do not interact with each other. Arrays of microelectrodes exhibit higher signal-to-noise ratios than macroelectrodes. Lower current detection limits can be achieved. In this part, a basic discussion in fabrication microelectrode array is presented in the follow.

2.5.1 Diffusion at microelectrode

Diffusion at the macro-electrode surfaces can be a major problem with electrochemical sensors. This is due to the diffusion occurs at a much slower rate than convection (in the order of a million times slower). If a solution is stirred outside of a macroelectrode sensor, the measurable signal will fluctuate due to these variable convection rates. This problem can be overcome if the rate of diffusion is larger than the rate of convection. At microelectrodes the predominant mode of mass transport is also diffusion, but now the flux as a result of diffusion is very large. This is because the mass transport of electroactive species is varied from the normal linear diffusion that procures at large or planar electrodes, to a three-dimensional diffusion (hemispherical diffusion profile), and therefore the effects of convection tend to be less apparent than electrodes of conventional size. Figure 2.5 illustrates the diffusion profile to the surface of a hemispherical microelectrode compared to that of a planar electrode.

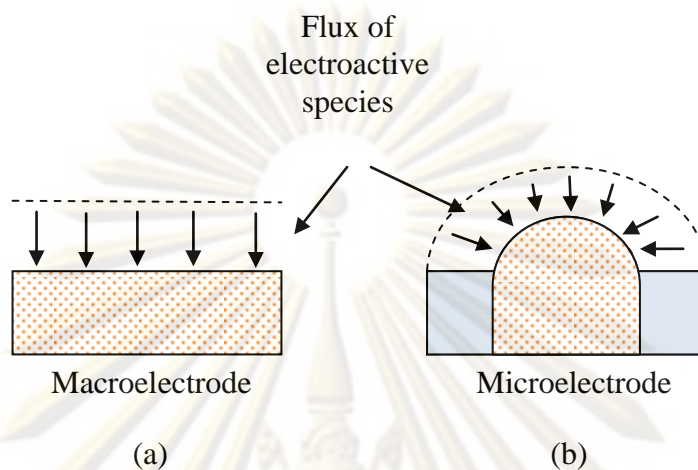


Figure 2.5 Diffusion profile to a macroelectrode (a) and a hemispherical microelectrode (b)

It can be seen that the diffusion gradient to the surface of the macroelectrode follows linear profile. In the case of a hemisphere of diameter, using the same boundary conditions as for linear diffusion, Cottrell has calculated the expression for the variation of current with time for a spherical electrode as in equation 2.7

$$i = nFAJ = nFAD[C]_{\infty} \left[\frac{1}{(\pi Dt)^{1/2}} + \frac{1}{r} \right] \quad (2.7)$$

where r is the electrode radius. At the time of experiment is short, the planar diffusion is observed. The dependency of the current flow at hemispherical microelectrodes with time is greatly reduced at the longer time due to the small value of r .

$$r = \left[\frac{(\pi Dt)^{1/2}}{10} \right] \quad (2.8)$$

This is presented the smaller the radius of the hemispherical microelectrode (r), the more rapidly the effect of time (t) decreases and steady-state current is obtained much sooner. Therefore, in the case of microelectrode the equation 2.7 becomes equation 2.9.

$$i = \frac{nFAD[C]_{\infty}}{r} = 2\pi nrFD[C]_{\infty} \quad (2.9)$$

As a consequence of their small size and enhanced diffusion, microelectrode exhibits a modified form of the cyclic voltammogram as shown in Figure 2.6. The resulting current due to reduction or oxidation of an electroactive species exhibits a sigmoidal-shaped response. This sigmoidal shape is characteristic of a microelectrode observed under entirely quiescent conditions. The steady-state limiting current observed (at the microelectrode plateau region in the curve) may be directly related to the concentration of the electroactive species, making it extremely useful for determining the concentration of analytes in liquid, solid, and even gas phases.

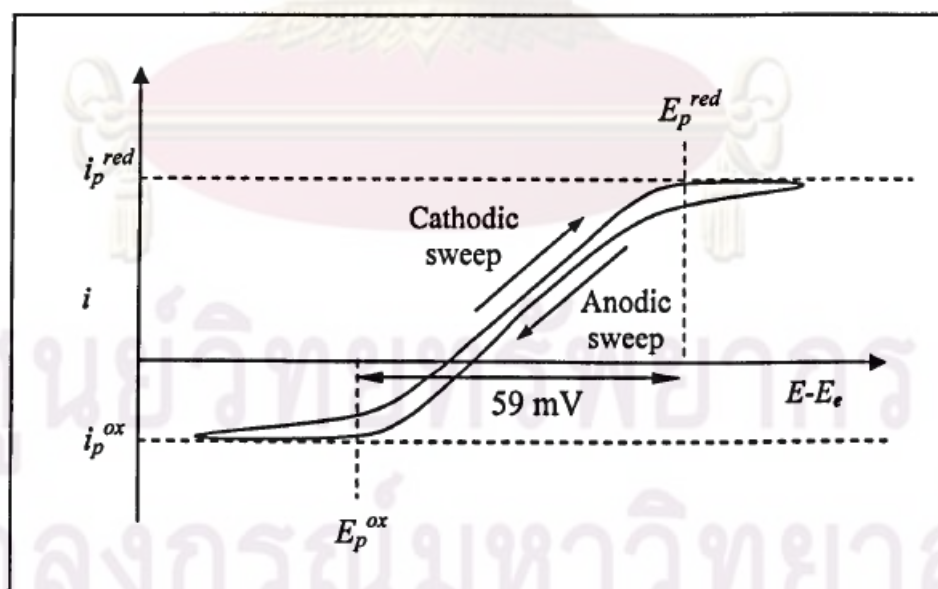


Figure 2.6 Characteristic sigmoidal shaped cyclic voltammogram for a reversible electron transfer reaction at a microelectrode.

For microelectrode array, the total measured current can be increased whilst retaining the particular properties of single microelectrodes with respect to high concentration gradients. The total response of this array of electrodes will depend on the spacing between the individual elements of the array. If the elements are spaced sufficiently far apart, the total response will be the sum of the responses of the individual electrodes (Aoki & Osteryoung, 1981, Caudill et al., 1982). However, if the spacing is sufficiently small such that the diffusion layers overlap as steady-state is approached, the total response will be less than that predicted by the sum for each. The diffusion profile of microelectrode arrays is displayed in Figure 2.7. To obtain optimum properties, well defined diffusion characteristics have to be established, depending on the electrode radius, their spacing and geometrical arrangement. In the case where electrodes are closer together, the system will initially behave in the same way as it would with larger spacing. However, as the diffusion layers begin to move towards equilibrium, the individual diffusion shells begin to overlap and cause a reduction in the hemispherical diffusion of material to the electrode surfaces. This effect is dependent on electrode size, density and distribution and in extreme cases may result in the sensor array behaving like a macroelectrode electrode of the same area (Zoski, 2007).

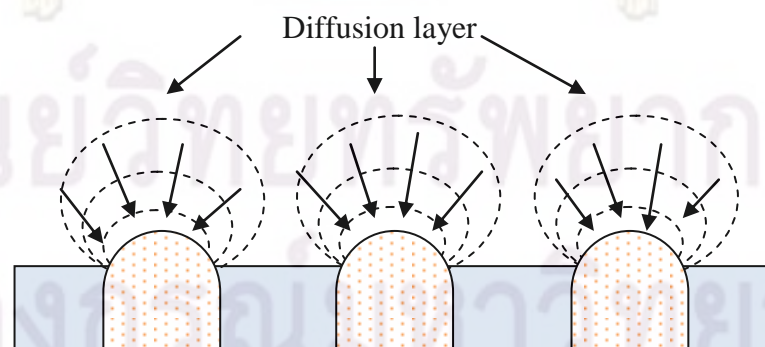


Figure 2.7 Schematic representation of diffusion at a microelectrode array.

2.5.2 Fabrication of microelectrode arrays

The method for fabrication microelectrode arrays have been divided which depending on the type of array required (Zoski, 2007). Four different fabrication methods for microelectrode array are detailed in this part which is template, etching, lithographic and mechanical methods.

2.5.2.1 Template approaches

The template method entails within the cylindrical and monodisperse pores of membrane or other porous material. One of the applications of the template method is electrochemical plating method. The gold nanorods were synthesized using template-growth electrochemical deposition method and deposited on a flat Au-coated stainless steel plate as the working electrode for cyclic voltammetry (Lin, et al., 2008). Gold nanorod arrays were grown inside commercial polycarbonate (PC) membrane templates (100 nm pore channel size) with the assistance of an electric field according to the electrochemical deposition method (ECD). Moreover, Foyet et al. (2007) prepared Zn-Ni alloy nanorods by using anodic aluminium oxide and the hexagonal phase of lyotropic liquid crystals containing zinc and nickel ions. The combination of the hexagonal phase of a liquid crystal and the alumina membrane (double template deposition) leads to the reduction of size of the nanorod. Figure 2.8 shows the structures of zinc–nickel alloy nanomaterials prepared by double template method.

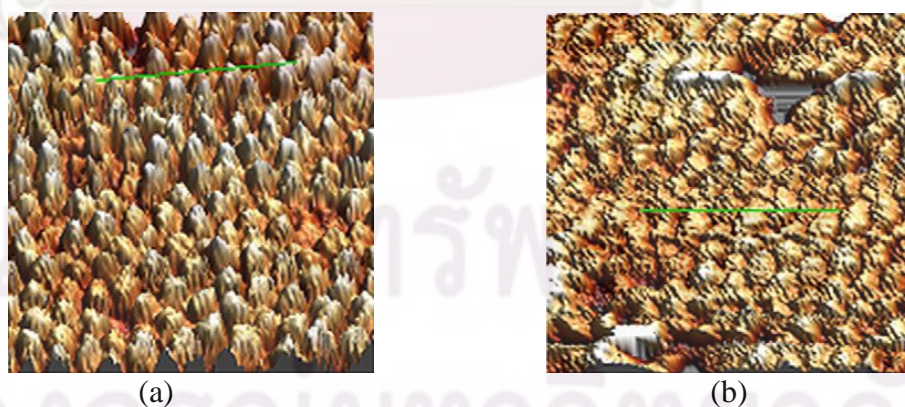


Figure 2.8 The 3D AFM micrograph of anodic aluminum oxide (AAO) membrane (a) and Zn–Ni alloy nanorods obtained from aqueous bath (b) (Foyet, et al., 2007)

2.5.2.2 Etching technique

This method is the subtractive and/or additive processes, where material is removed/added to a selective manner. The way of removing material for construction of microelectrode array is through etching. The subtractive etching techniques are wet etching, electrochemical etching, laser machining, ultrasonic drilling and mechanical method (Zoski, G.,2007). Microelectrode arrays can be fabricated using a chemical etching technique originally developed for sharpening tips of optical fibers in near-field optical microscopy. The chemical sharpening process, termed meniscus etching, utilizes surface tension force at the glass-etchant interface. The process is schematically illustrated in Figure 2.9. Glass probes are immersed into HF-based etchant. An organic layer, such as vegetable oil, is added on top of the etchant to modify contact angle at the glass etchant interface. The etchant wets the surface of the probes and gradually reduces their dimensions. The surface tension force at the glass-etchant interface reduces with the diminishing dimensions, forcing the height of the meniscus to decrease with time until the etching front reaches the center of the probe and a sharp tip is formed. The process is self-terminating. The balance of the two opposing forces, the surface tension and the weight of the etchant, determines the final tip geometry. Probe spacing and organic layer composition can modify the contact angle at the glass-etchant interface, and consequently the final tip geometry(Lee, et al., 2006).

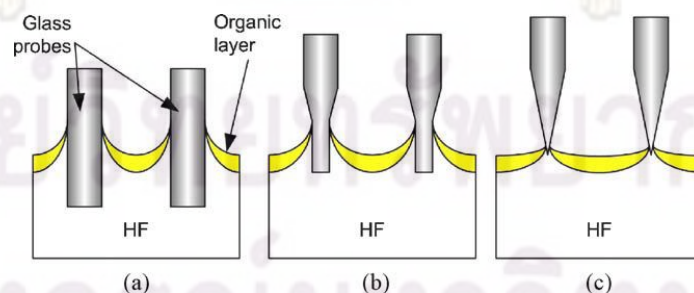


Figure 2.9 Fabrication of microelectrode array tips using meniscus etching. The etchant wets of the probes the surface (a) and (b) gradually reduces their dimensions (c) the etching front reaches the center of the probe and a sharp tip is formed.

2.5.2.3 Lithographic method

Lithographic method has the advantage of being highly controllable and reproducible over mechanical and template approaches. Fabrication of highly sophisticated electrode geometries is a possibility that has been utilized only to a limited extent so far. Lithography is a technique that transfers a copy of a master pattern onto the surface of a solid material, such as a silicon wafer.

Microelectrode arrays which are prepared in a very simple way by dispersing sufficiently small particles of a conductive material (usually a very fine graphite powder) in an insulator are poorly defined microelectrode array. The well-defined arrays are now almost exclusively prepared by photolithography. Konry et al. (2008) fabricated a micro-patterned structure of conductive polymer, poly(pyrrole-benzophenone), on indium tin oxide (ITO) glass chips for the subsequent photo-immobilisation of various bioreceptor antigens. From this method showed homogeneous and compact structures of the polymer (Figure 2.10) application.

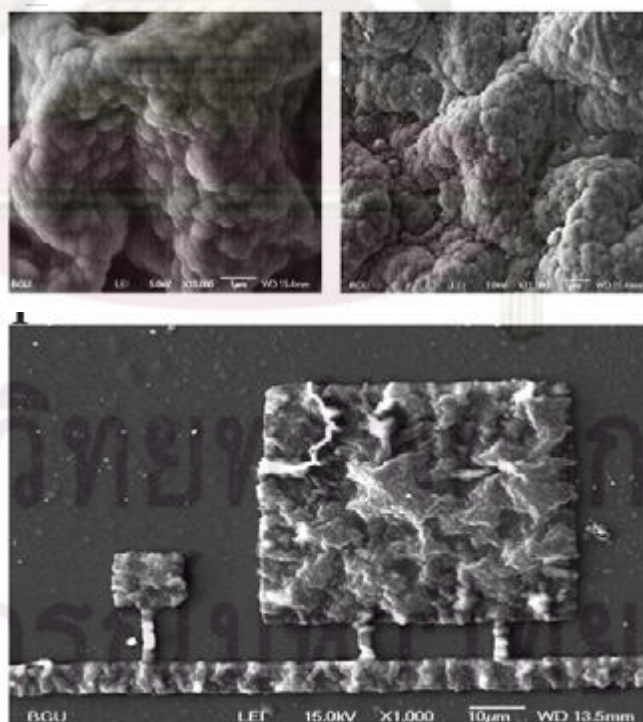


Figure 2.10 The SEM analysis of the array film of conductive polymer, poly(pyrrole-benzophenone), on indium tin oxide ITO (Konry et al. 2008)

2.5.2.4 Mechanical methods

The variety techniques have been used for fabrication microelectrode array by mechanical method. Such as, wire technique, sandwich method, the formation of composition and sonochemical fabrication. In this research is focused on sonochemical method. There are many researches described the sonochemical method for microelectrode arrays fabrication. Barton et al. (2004) described a novel sonochemical fabrication approach for the production of microelectrodes, which lends itself to the mass production of sensor arrays. A novel and patented procedure was described for the sonochemical fabrication of a new class of microelectrode array based sensor with electrode element populations of up to $2 \times 10^5 \text{ cm}^{-2}$. Biosensors formed by sonochemical approach offer unrivalled sensitivity and impart stir independence to sensor responses. Furthermore, the modified electrode was studied by Myler et al. (2005). Upon coating the working electrode with the insulating polymer polydiaminobenzene, microelectrode arrays were fabricated via a sonochemical fabrication; these arrays again displayed true stir-independent responses. The sonochemical fabrication method has been extensively reported with glucose oxidase (Myler, et al., 2004), alcohol oxidase (Myler et al. 2005), and acetylcholinesterase (Pritchard, et al., 2004). This research represented high microelectrode population density and low limits of detection (Law et al., 2005).

In this research, the sonochemically fabrication method is used for HRP microelectrode arrays. Even this method make poorly defined microelectrode arrays, and less reproducibility, it is easy to fabrication and widely used for enzyme immobilisation.

2.5.3 Sonochemistry

The properties of ultrasound offer great potential to a wide range of applications. Most modern ultrasonic devices rely on transducers, composed of piezoelectric material, which respond to the application of an electrical potential with a change in dimension (the inverse of the piezoelectric effect). If the potential is alternated at high enough frequencies, the vibration of the transducer will generate sound in the ultrasonic frequency range.

2.5.3.1 Applications of ultrasound

Cavitation phenomena created by the application of ultrasound to a liquid medium have been exploited for cleaning purposes, the most widely used application of ultrasound. Ultrasonic cleaning is particularly efficient in removing surface contaminants such as dirt or bacteria. Large crates used in the food industry and surgical equipment are typical objects cleaned in this way (Kuttruff, 1991). In the food industry, ultrasound can be used for mixing, tenderizing, ageing emulsifying, cutting and even thawing. Sterilisation of milk can be achieved by the action of sound waves on micro-organisms found in it while the emulsion bases for sauces such as ketchup and mayonnaise can be prepared using ultrasound.

Ultrasound is used in the medical field for other purposes other than cleaning. For example, sound waves can be used for the diagnosis of a number of heart defects, fetal monitoring within pregnancy and also medical imaging of tumours. For such purposes high frequency ultrasonic waves are applied so as to minimise damage to tissues and organs. Lower frequency waves have been shown to remove kidney stones by cavitation (Leroy, 1994), as well as cancer cells (Shuqun *et al*, 2000) and blood clots (Shlamovitz *et al*, 2003), in the new field of medicine termed therapeutic ultrasound. Finally, gene therapy can be carried out with the use of ultrasound since under certain conditions the latter can cause a transient permeability of cell membranes thus allowing large molecules to enter the cell (Miller, 1999).

Sonochemistry itself incorporates many specific uses of ultrasound. These include environmental protection (Yim *et al*, 2002, Theron *et al*, 2001), materials science (Xia *et al*, 2001; Ding *et al*, 2002) including new catalytic materials, improved extraction, crystallisation, and new methods in polymer technology, electrochemistry (Walton & Phull, 1996; Klima *et al*, 1994) providing improvements in plating electrosynthesis, electroanalysis, and biotechnology such as the modification of enzyme and whole-cell activities (Sasaki *et al*, 2001).

2.5.3.2 The principles of ultrasound

In solid materials, atoms can vibrate in any direction creating transverse waves, perpendicular to the direction of travel. When the frequency and amplitude of the longitudinal wave becomes sufficiently high, the rarefaction stage causes the molecules of a liquid (such as water) to cavitate to form a bubble. This cavity will grow in size over a few cycles taking in some of the vapor or gas from the medium. The bubble growth will continue until an equilibrium size is reached which matches the frequency of the bubble resonance, a parameter controlled by the applied frequency of sound (Figure 2.11). However, the acoustic field experienced by an individual bubble is not stable because of the interference caused by other bubbles forming and resonating around it. The result is that some bubbles suffer sudden expansion to an unstable size and collapse violently. The violent collapse of these bubbles generates large shear forces, which can be used for mixing and particle dispersion. In the collapsing bubble itself, high energies and pressures are generated. Many theories exist to explain the energy release involved in cavitation, but the most understandable in a qualitative sense is the 'hot-spot' approach (Suslick et al., 1986) which explains that heat is generated from the rapid compression of gases and vapours.

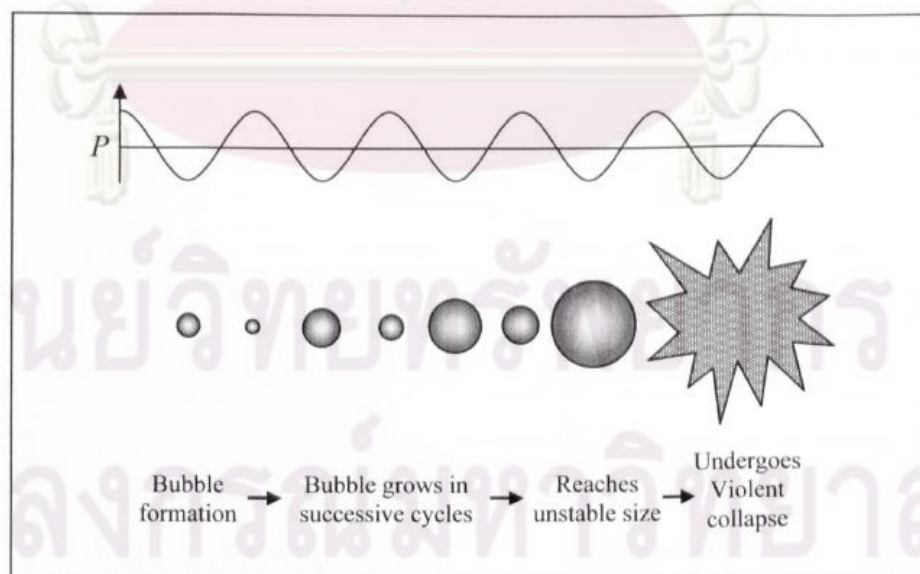


Figure 2.11 The development and collapse of cavitation bubbles

The dynamics of cavity growth and collapse is very different in the cavitation near a solid-liquid interface. When a bubble collapses near a surface, bubble collapse is no longer symmetrical. The presence of a solid surface hinders the movement of liquid from that side, and so the majority of the liquid enters the bubble from the opposite side (Figure 2.12). The result is that a jet of liquid is effectively targeted towards the solid surface at speeds in excess of 100 m/s (Leighton, 1998).

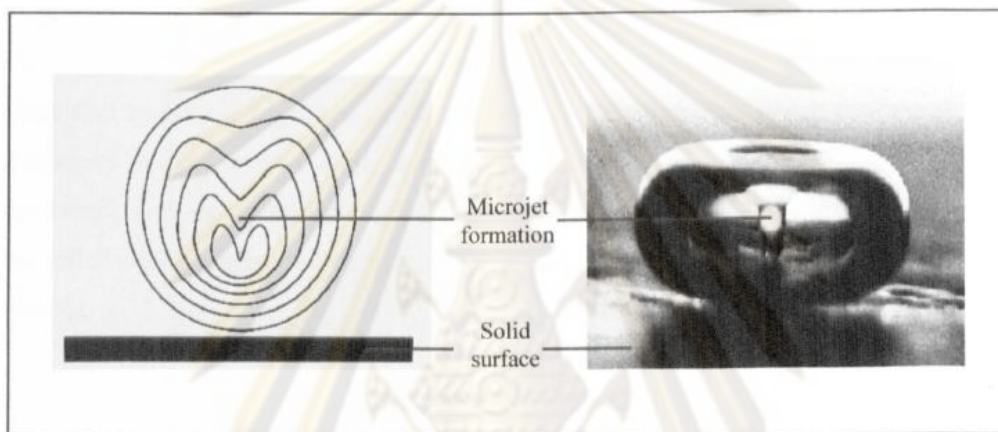


Figure 2.12 Cavitation bubble collapse near a solid surface

ศูนย์วิทยทรัพยากร
จุฬาลงกรณ์มหาวิทยาลัย

CHAPTER III

LITERATURE REVIEW

The development of enzyme biosensors has been extensively studied due to its broad application in industrial, pharmaceutical, food and environmental analysis. In case of the determination of phenolic compound, electrochemical techniques especially amperometric biosensors have been considered advantageous due to their high sensitivity, simplicity, and easy to be miniaturization. In this chapter, literature concerning the horseradish peroxidase (HRP) based biosensor is demonstrated in the first part. Moreover, the study of microelectrode array for enzyme biosensor was detailed in the second part.

3.1 Horseradish peroxidase (HRP) enzyme biosensors

Horseradish peroxidase (HRP) proved to be suitable for many practical applications such as the determination of phenol, which is often involved in the elimination of phenolic compounds (Mello et al., 2003, Munteanu et al., 1998, Munteanu et al., 1998). Furthermore, HRP affinity for hydrogen peroxide allowed the development of many electrodes or amperometric biosensors for the detection of hydrogen peroxide, either using direct or mediated electron transfers (Zhang et al., 1996, Cosnier et al., 1995). In this research modified HRP based microelectrode arrays by using the phenol as the model reaction. Hence, the phenol detection mechanism should be briefly described.

The HRP enzyme mechanisms for phenol detection are mediator electron transfer and direct electron transfer. Rosatto et al., (1999) studied immobilization of HRP on silica gel modified with titanium oxide for phenol detection. They found that the enzymatic mechanism involved in peroxidase based biosensor for phenol detection consists in the oxidation of native HRP (Fe^{3+}) by hydrogen peroxide (Figure 3.1) and become HRP (Fe^{5+}). Then HRP (Fe^{5+}) accepts one-electron from the electron donor which is phenol or M_{red} and forms HRP (Fe^{4+}). Then HRP (Fe^{4+}) accepts one-electron from the electron donor or M_{red} again and forms native HRP (Fe^{3+}). In each step of HRP (Fe^{5+}) changing to HRP (Fe^{3+}), M_{red} get one-electron each from an

electrode. In this step, the reduction current is occurring and proportional to the phenol concentration in the solution (Ruzgas et al., 1995). Nevertheless, peroxidase can also do the direct electron transfer (Figure 3.2) between the enzyme itself and the electrode. Direct electron transfer is similar to mediator electron transfer, but in this case HRP (Fe^{5+}) accepts directly two electrons from the electrode

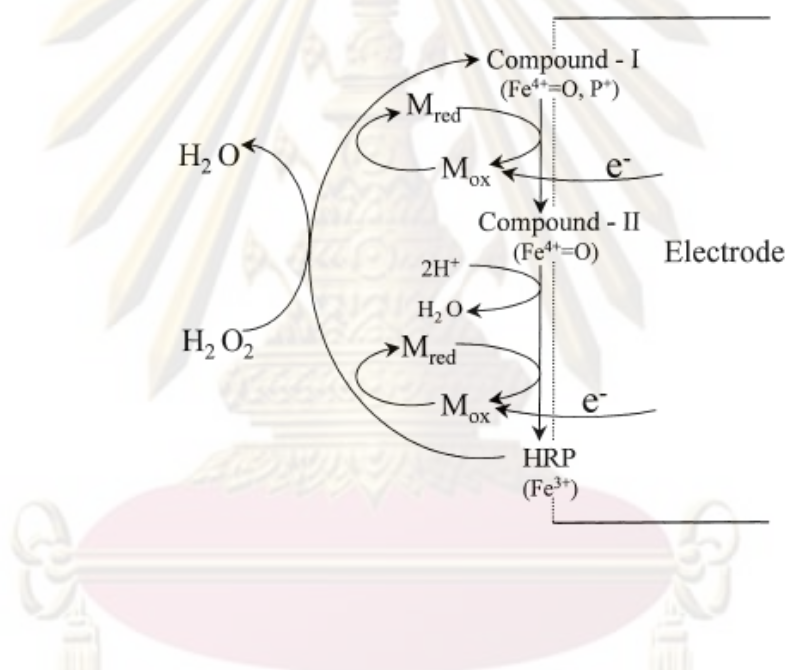


Figure 3.1 Mechanism of mediated electron transfer at HRP modified carbon paste electrode. M_{ox} and M_{red} are the oxidised and reduced forms of the mediator, respectively (Rosatto et al., 1999).

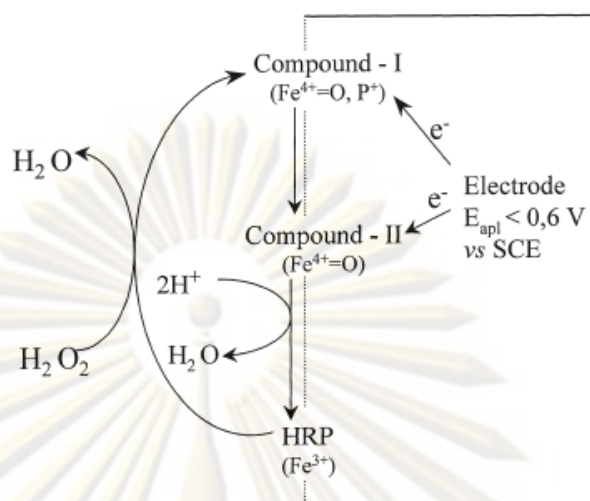


Figure 3.2 Mechanism of the direct electron transfer between HRP and base electrode (Rosatto et al., 1999).

3.1.1 HRP immobilization method for biosensor application

The immobilization method has significant influence on the properties of immobilized enzyme such as, activity, stability, deactivation, and regeneration. There are different methods to immobilize HRP such as covalent immobilization, (Jun Chen et al., 2006) entrapment (Li et al., 2008), and cross-linking (Rosatto et al., 1999) method. Furthermore, to improve sensitivity and compatibility of biosensors, the immobilization of enzymes on nanomaterial is very promising concept. Example of nanoparticles used for enzyme immobilization include carbon nanotubes (Rivas et al., 2007), gold (Yi et al., 2000), and silver nanoparticles (Kim et al., 2004). In the following section, the HRP enzyme immobilization comprehends with polymer and nanoparticle has been reported.

3.1.1.1 Physical Adsorption

This technique is very simple and minimal preparation rarely research describes about this method. In the case of HRP biosensors, Ruzgas et al. (1995) studied the modified electrode with HRP on graphite electrode. The population of adsorbed HRP molecules and/or the graphite surface structure could not be treated as homogeneous. It was found that 42% of the total amounts of HRP molecules adsorbed on the electrode were accessible for direct unmediated electron transfer from the graphite electrode. This method is only suitable for work over a short time span and sensitive in changing pH, temperature, and ionic strength.

3.1.1.2 Covalent bonding

This technique is the formation of covalent bonds between the enzyme and the support matrix. Enzyme and support surfaces bind together with the chemical linkers containing functional groups, such as amino, carboxyl, or sulfhydryl. Caramori et al. (2004) immobilized HRP on poly(ethylene terephthalate)–poly(aniline) composite. The composite was synthesized by submitting polyethylene terephthalate (PET) plates to hydrazinolysis treatment, followed by polyaniline (PANI) synthesis over the PET surface. The treatment was revealed reactive groups on the PET and resulting in different reactive groups for HRP bonding. Hwa-Jung et al. (2008) immobilized HRP on the surface of poly(Th-co-EpoxyTh) by covalent bonding. Even though this method demonstrated a high sensitivity, its stability has yet to be improved. Furthermore, the covalent bonding immobilization method is usually performed under mild conditions such as low temperature and low ionic strength. These cause of limitation of biosensor application.

3.1.1.3 Entrapment

In this method, the enzyme is mixed with a monomer solution, which is then polymerized to a gel matrix. The most common polymers used to form the gels can be either natural organic polymers or synthetic polymers such as the immobilization of HRP, into Poly3,4-ethylenedioxy thiophene (PEDT) which are a conductive polymer films (Jun Chen et al., 2006). This immobilization process described a great

potential to achieve high density enzyme containing polymers for the development of stable biosensors. In addition, Li et al. (2008) experimented for fabrication of hydrogen peroxide biosensor, which had been developed by entrapping HRP enzyme in chitosan/silica sol-gel hybrid membrane. But this method created large barriers, and inhibiting the diffusion of substrate. There was also a loss of enzyme activity through the pores of the gel.

3.1.1.4 Cross-linking

In this method, Enzymes can be immobilized by cross-linking among themselves to form particles. The most popular cross-linking reagents used are glutaraldehyde (Rosatto et al., 1999, Wang et.al, 2009), dimethyladipimidate (Besselink et al 2003), and dimethyl suberimidate (Bouvrette et al., 1997)). For example, the HRP enzyme was immobilized on modified silica gel surface by adsorption together with cross-linking using glutaraldehyde by using modified carbon paste electrode (Rosatto et al., 1999). Furthermore, Rosatto et al. (2002) repeated their study in the HRP immobilization by cross-linking method which used $\text{SiO}_2/\text{Nb}_2\text{O}_5$ as an immobilization support. It was found that, immobilization was possible without glutaraldehyde addition but with its present, the system noise was lower. Wang et al. (2009) investigated hydrogen peroxide biosensor, which was constructed by cross-linking between HRP and polyaniline using glutaraldehyde as a cross-linking agent. Wang et al. (2005) developed the HRP biosensor by sandwich configuration: ferrocene-chitosan: HRP: chitosan-glyoxal. The biosensor surface was cross linked with glyoxol (Figure 3.3). The fabrication procedure was systematically optimized to improve the biosensor performance. The biosensor had a fast response of less than 10 s to H_2O_2 , with a linear range of 3.5×10^{-5} to 1.1×10^{-3} M, and a detection limit of 8.0×10^{-6} M. Even though this method is useful for stabilizing adsorbed biomaterial, it causes damage to enzyme, limits diffusion of substrate, and poor rigidity (Brian, 1996).

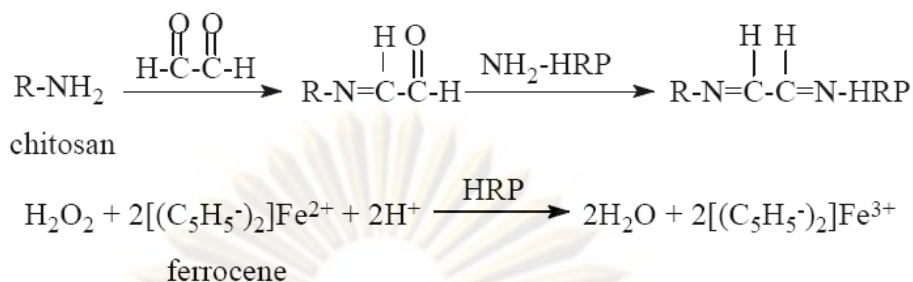


Figure 3.3 The chitosan film cross-linked with glyoxal diagram (Wang et al., 2005)

3.1.2 Polymer for HRP biosensor

In order to immobilize enzymes on electrode surfaces, polymer film are needed. Both conducting and non-conducting polymers have been widely studied for enzyme immobilization for sensor applications. In this part, polymers which are used for HRP biosensor will be detailed.

3.1.2.1 Conductive polymer

The electro-polymerization of the conducting monomers has been studied extensively for the construction of biosensors, because the prepared conducting polymers have excellent electrocatalytic properties and rapid electron transfer ability. Also, the conducting polymers permit the transfer of charges to produce electrochemical signals between the electrode and the incorporated biomolecules. For biosensor applications, the conducting polymers are often functionalized with carboxyl, amino, aldehyde, or succinimidyl carbonate groups, or conjugated directly with various electronic mediators or bio-recognizable molecules to facilitate immobilization (Guimard et al., 2007).

Abundant researches proposed various types of conductive polymers for HRP biosensors. Thanachasai et al. (2002) fabricated HRP into poly(pyrrole-co-[4-(3-pyrrolyl)butanesulfonate]) (Py-PS) copolymer film deposited on an SnO₂ electrode surface by electropolymerisation. In this study, the comparison between the HRP/Py-PS electrode and HRP-incorporated polypyrrol (PPy) electrodes which were prepared under similar condition were determined. The HRP/Py-PS electrode retained 60% of

initial response (100%), while the HRP/PPy electrode almost completely lost activity. Moreover, the HRP was incorporated into the carbon nanotube (CNT)/ polypyrrole (PPy) nanocomposite matrix (Korkut et al. 2008). The eighteen phenolic compounds were detected by CNT/PPy/HRP nanobiocomposite film electrode in this case. The biosensor exhibited low detection limit with short response time for testing.

Not only polypyrrole that was used for HRP biosensor, the synthesis of the polythiophene with carboxylic acid groups in order to immobilize HRP via the copolymerization of thiophene and 3-thiopheneacetic acid in acetonitrile was researched (Kim et al., 2007). In this study, the amounts of HRP on the surface of polythiophene electrode with carboxylic acid groups are very low. Afterward, Kim, et al., 2008 describe the utility of film of poly(thiophene-co-epoxythiophene) (poly(Th-co-EpoxyTh)) immobilized with HRP through covalent bonding as sensor electrode. The HRP-immobilized poly(Th-co-EpoxyTh) electrode showed linearity from 0.1 to 30 mM H₂O₂, good reproducibility, and long life time. In addition, the electroactive polymer, polyaniline (PANI), which undergoes redox cycling, and can couple electrons directly from the enzyme active site, to the electrode surface. The HRP was immobilized onto the carbon paste electrode modified with a layer electrodeposited PANI (Morrin et al., 2003). Mathebe et al. (2004) prepared an amperometric biosensor by the deposition of HRP enzyme on PANI doped platinum disk electrode. The PANI film was electrochemically deposited on the electrode. Furthermore, the hydrogen peroxide biosensor was composed by cross-linking between HRP and PANI. The PANI synthesized in a solution containing ionic liquid, 1-ethyl-3-methylimidazolium ethyl sulfate, was an electroactive polymer at pH over 6. From these researches, numerous conductive polymers were presented. The electrodeposition polymerization of polymers was popularly used. Furthermore, others conductive polymers which used for HRP biosensor and the polymerization methods are shown in Table 3.1.

Table 3.1 Examples of polymer for HRP immobilization biosensor

Type of polymer	Polymer	Polymerization method	Reference
conductive polymer	Poly{pyrrole-co-[4-(3-pyrrolyl)butanesulfonate]}(Py-PS)	Electropolymerisation	Thanachasai et al. (2002)
	Polyaniline (PANI)	Electropolymerisation	Mathebe et al. (2004) Morrin et al. (2003)
	Polypyrrole (PPy)	Electropolymerisation	Li, G. et al. (2007) Korkut et al. (2008)
	Polythiophene	Electropolymerisation	Kin et al. (2007)
	Poly(thiophene-co-epoxythiophene)	Electropolymerisation	Kim et al.(2008)
	Poly(l-lysine)	Chemical polymerization	Ngamna O. et al.(2005)
	Poly(3,4-ethylene-dioxythiophene)-poly(styrene sulfonate)	Colloidal dispersion	Asberg P. et al. (2003)
	1-butyl-3methyl-imidazolium tetrafluorobonate	Entrapment	Lu X., et al. (2006)
non-conductive polymer	3-aminophenol	Electropolymerisation	Nakabayashi et al. (2000)
	Chitosan	Cross-linking	Xu et al. (2006) Li (2008)
		Entrapment	Lu X., et al.(2006)

Since described before that polyaniline or PANI is one of the most widely used, this research would applied the polyaniline for enzyme microelectrode arrays. The chemical structure of aniline is displayed in Figure 3.4.

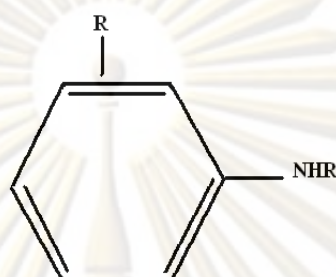


Figure 3.4 The chemical structure of aniline

3.1.2.2 Non-conductive polymer

In this part, the researches which described non-conductive polymers for HRP biosensor are detailed. Nakabayashi et al., (2000) reported the used of non-conductive polymer, 3-aminophenol for HRP immobilization. In this case, ferrocene was used as an electron-transfer mediator, which was coated with electropolymerized film of 3-aminophenol. The growth of non-conductive polymer is self-limiting, and consequently the films tend to be very thin (10-100 nm.). Furthermore, Chitosan which is biopolymer have been used for HRP enzyme biosensor. Chitosan has been found to be an interesting biopolymer for immobilization of desired biomolecules because of excellent film-forming ability, high permeability, mechanical strength, nontoxicity, biocompatibility, low cost, and easy availability. With its attractive properties, chitosan has received much attention as the material for design of modified electrodes. In the study of Xu et al. (2006), the results exhibited the presence O-carboxymethyl chitosa in silica sol-gel for HRP immobilization. The film would not crack. When there was no CMCS, the response time for analytic substrate became longer and no more enzyme activity was retained. Therefore, the presence of CMCS provided friendly surroundings for the immobilization of enzymes. Additionally,

chitosan was used for co-immobilizing mediator and enzyme (Li et al., 2008). The biosensor which used chitosan for enzyme immobilization exhibited high stability, lower detection limit and better reproducibility and stability.

3.1.3 Particles for HRP biosensors

The development of nanostructured materials for biosensor is currently becoming an emerging area of research (Andreescu et al., 2008). The uniqueness of these materials is due to their electrical, optical, and magnetic properties which offer distinctive prospects for designing powerful biocatalytic systems. Electrochemical biosensors have been fabricated from mostly metallic nanoparticles which are capable to provide better analytical characteristics in terms of sensitivity, selectivity, reliability, ease of fabrication and use and lowcost. Metal nanoparticles based electroanalysis has been reviewed by Santos D et al., 2002. The nanoparticles such as gold (Yi et al., 2000, Lin et al., 2007, Xu et al., 2007), silver (Welch et al., 2005, Wu, et al., 2006), and carbon nanotube (Rivas et al., 2007) were used for HRP enzyme biosensors are illustrated below.

3.1.3.1 Gold nanoparticles

The ability of gold (Au) nanoparticles to provide a stable immobilization of biomolecules is a major advantage for the preparation of biosensors. Furthermore, gold nanoparticles permit direct electron transfer between redox proteins and bulk electrode materials, thus allowing electrochemical sensing to be performed with no need for electron transfer mediators (Pingarron et al., 2008). In the terms of HRP biosensors, gold nanoparticles were rarely reported.

Peroxidase biosensors based on self-assembled monolayer (SAM) modified electrodes have been reported to be fabricated using gold nanoparticles. For example, The Au colloids on a cysteamine monolayer on the gold electrode surface were used to study the direct electron transfer of immobilized HRP. This biosensor exhibited an excellent electrocatalytic response to the reduction of H_2O_2 without the need of an electron mediator (Yi et al., 2000). Recently, a disposable pseudomediatorless

amperometric biosensor was fabricated for H₂O₂ determination by modification of an indium–tin oxide (ITO) electrode with (3-mercaptopropyl) trimethoxysilane. The stable nano-Au-SH monolayer was prepared through covalent linking of gold nanoparticles and thiol groups on the ITO surface. HRP and tetramethyl benzidine, as the electron transfer mediator, were finally coentrapped by colloidal gold nanoparticles. The results showed that the AuS monolayer not only could steadily immobilize HRP but also efficiently retain HRP bioactivity (Lin et al., 2007). Gold nanoparticles have also been self-assembled to hollowporous thiol-functionalized poly(divinylbenzene-*co*-acrylic acid) nanospheres. An HRP biosensor was prepared by chemisorbing gold nanoparticles onto the thiol groups of nanospheres and enzyme immobilization on the gold nanoparticles surface (Xu et al., 2007).

3.1.3.2 Silver nanoparticle

Silver nanoparticles have advantageous properties to improve the character of the biosensor, such as the metallic properties, which can enhance the electron conductivity and adsorb the enzyme by the interaction between the enzymes and silver nanoparticles. Furthermore, silver nanoparticles may facilitate more efficient electron transfer than gold nanoparticle in biosensor (Xu et al, 2004). However, there were a few reports for HRP biosensor which incorporated with silver nanoparticle.

The examples of silver modified electrodes are electrochemical detection of hydrogen peroxide using an edge-plane pyrolytic-graphite electrode (EPPG), a glassy carbon (GC) electrode, and a silver nanoparticle-modified GC electrode (Welch, et al., 2005). The limit of detection for this modified nanosilver electrode was 2.0×10^{-6} mol L⁻¹ for hydrogen peroxide in phosphate buffer (0.05 mol L⁻¹, pH 7.4) with a sensitivity which is five times higher than that observed at a silver macroelectrode. Xu et al. (2004) reported the horseradish peroxidase (HRP), mediator methylene blue (MB), nanosized silver particles and sol–gel solution are mixed and coated on the surface of glass carbon (GC) electrode to get the biosensor. The silver nanoparticles in the sol–gel film can adsorb the enzyme molecules and improve the sol–gel film conductivity. The biosensor has a high sensitivity, quick response to H₂O₂ and good stability. Furthermore, the Silver–DNA hybrid nanoparticles with controlled

dimension were reported by Wu et al. (2006). The hybrid nanoparticles showed a narrow size distribution and a favorable catalytic ability to reduction of hydrogen peroxide and dissolved oxygen, which were related to the DNA concentration in deposition solution and the deposition time. The modified electrode obtained showed a linear response to hydrogen peroxide concentration.

3.1.3.3 Carbon nanotube

The nature of the electrode is very important for the electrochemical transduction process. In this sense, CNTs represent an important alternative for the transduction event due to their excellent electronic properties. In fact, in recent years we have witnessed the development of highly sensitive and selective electrochemical biosensors based on the use of carbon nanotubes (Rivas et al., 2007).

A highly sensitive biosensor for phenols and catechols was obtained by incorporation of polyphenol oxidase within carbon nanotubes paste electrodes (CNTPE). The response for dopamine was 12-fold more sensitive than at polyphenol oxidase (PPO) within carbon paste electrode (CPE-PPO) (Rubianes et al., 2005). Qian and Yang (2006) proposed a hydrogen peroxide biosensor obtained by cross-linking of HRP on a multiwalled carbon nanotubes-chitosan (MWCNT-CHIT) composite film modified glassy carbon electrode (GCE). Furthermore, they reported the sensitive and selective determination of hydrogen peroxide based on the use of a GCE modified with a MWCNT/chitosan dispersion cross-linked with horseradish peroxidase by glutaraldehyde. Another strategy reported by Lin et al. (2006) was the development of a novel nanobiocomposite material through the immobilization of multiwall carbon nanotube (MWCNT), nafion and heme proteins on a choline-modified GCE. The immobilized proteins present activity of peroxidase working on the electrocatalytic reduction of oxygen, hydrogen peroxide, nitric oxide, among others. Chen and Lu (2007) proposed a hydrogen peroxide biosensor through the encapsulation of hemoglobin in a composite film of previously oxidized CNT.

3.2 Microelectrode arrays

Microelectrode arrays (MEAs) have been used for the last three decades in the field of cellular biology as tools for probing electrophysiologic activity either *in vitro* or *in vivo*. The availability and development of microelectromechanical systems (MEMS) techniques has made possible the fabrication of three dimensional structures which add spatial resolution and cell development control arrays of microelectrodes exhibit higher signal-to-noise ratios than macroelectrodes and lower current detection limits can be achieved. This part describes about the different types of microelectrode arrays (random, ordered, and three dimensional) is shown.

3.2.1 Classification of microelectrode arrays

The individual electrode in an array may have different designs such as random or ordered arrangement. There exists in the literature a variety of methods of fabricating arrays of metal nanoelectrodes on electrode surfaces, such as electrochemical or electroless deposition of metal nanoparticles onto a suitable electrode substrate (Xiao et al., 2008). These methods produce random arrays of nanoparticles on the electrode surface such that the array rarely, if ever, is diffusionally independent on most practical experimental timescales. Lithographic techniques of fabricating ordered micrometer and nanometer sized metal arrays are progressing, but this technique is limited in that it can only produce nanoelectrodes with diameters of the order of 100 nm, whilst a significant fraction of the individual electrodes in the array are not in electrical contact with the substrate, forming “dead” electrodes (Zoski, G.,2007). The different types of microelectrode array are described in this part.

3.2.1.1 Random microelectrode arrays

The main advantage of this type of array is the comfort for fabrication. The disadvantage is that they are geometrically badly defined. The badly defined spacing between conducting surfaces can lead to overlapping diffusion layers. Xiao et al., 2008 reported the random array of boron doped diamond (BDD) nano-disc electrodes (RAN BDD), formed by a simple three step method. First molybdenum (IV) dioxide

nanoparticles are electrodeposited onto a BDD substrate. Second the electrode surface is covered in an insulating polymer film by the electropolymerisation of a 4-nitrophenyldiazonium salt. Third the molybdenum dioxide nanoparticles are dissolved from the BDD surface using dilute hydrochloric acid to expose nano-discs of BDD for removing the polymer layer directly. The various microelectrodes were produced by this method with similar distribution of microelectrode size and number density, confirming that this is a reliable and reproducible method. The appearance of this microelectrode arrays is shown in Figure 3.5. Furthermore, Ordeig et al. (2006) studied the quantitative analysis of voltammetric data measured at randomly micro-disc electrode arrays. Theory and experiment are found to be consistent and it is demonstrated that the former allows the number of 'dead' electrodes in the array to be counted. In particular it is concluded by voltammetric means that only ca. 30% of the carbon fibers emerging at the surface are electrochemically active. However this type of microelectrode is applicable to manufacturer (Ordeig et al., 2006).

3.2.1.2 Ordered microelectrode arrays

The design of microelectrode arrays with well defined geometry is preferred to electrochemical proposes. The advantage of ordered arrays is their ability to be fabricated by lithographic method which fit bulk fabrication. There are high reproducibility and disposability. On the other hand, high quality ordered microelectrode arrays are not easy to be fabricated. The example of ordered microelectrode array is a microlithographically fabricated iridium ultramicroelectrode array was used to provide a disk array for formation of mercury microhemispheres (Samuel et al., 1994). The array, made up of 19 interconnected 10- μm -diameter microelectrode arrays, provides a multiplication of the signal current proportional to the number of microelectrodes in the array, without any indications of overlap of the diffusion fields.

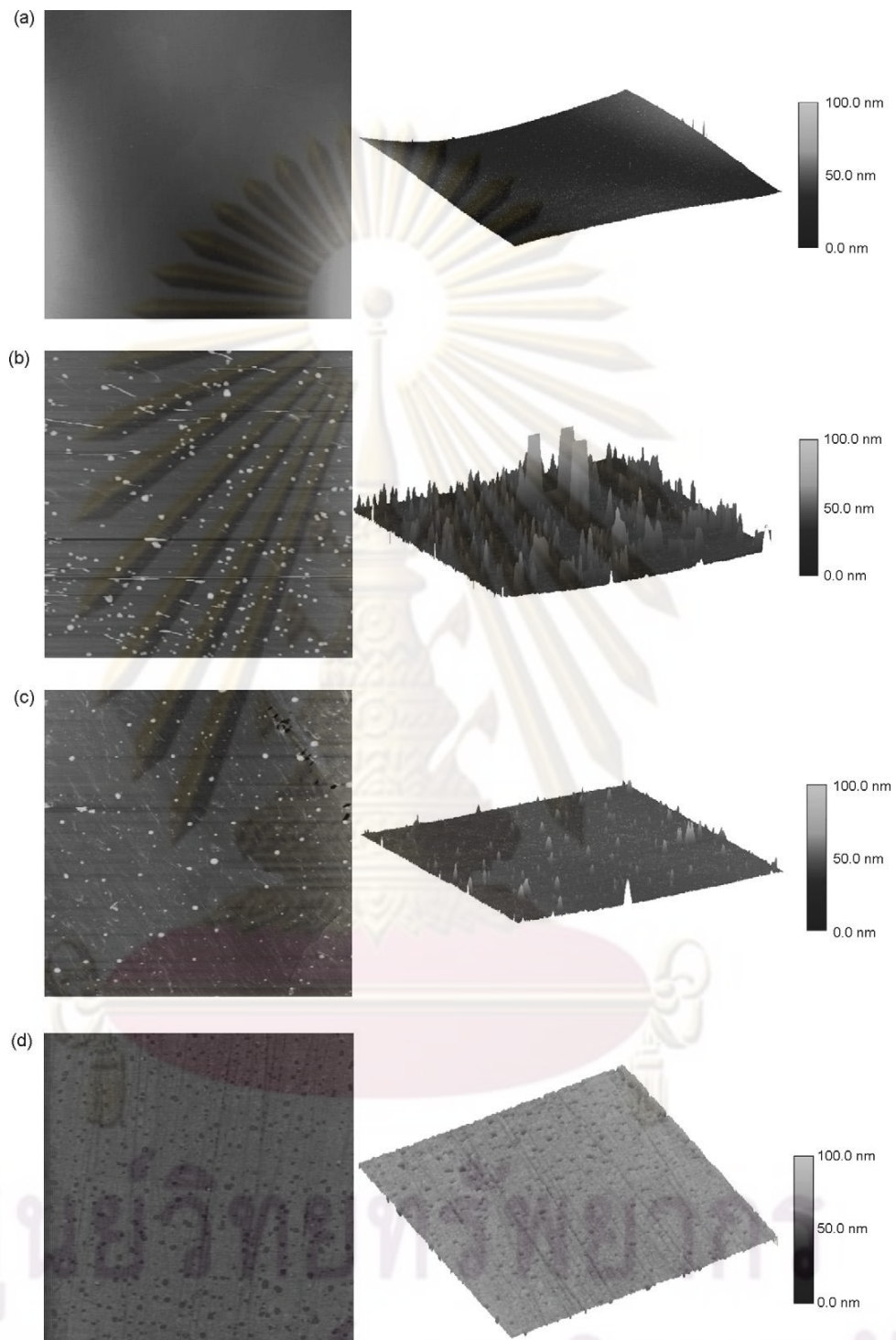


Figure 3.5 AFM images showing the 2D (left) and 3D (right) surfaces of: (a) the bare BDD electrode; (b) the MoO₂ nanoparticle modified electrode; (c) the polymer film covered electrode (d) the RAN BDD electrode (Xiao et al., 2008).

3.2.2 Particle in microelectrode arrays

In recent years microelectrode arrays have been shown to significantly enhance the sensitivity of electrochemically based analytical determination method. However, the use of nanoparticles for enhancing the properties of enzyme microelectrode array as in macroelectrode was rarely reported. Lin et al. (2008) reported cyclic voltammetry by using 1-D gold nanorods. The ordered 1-D gold nanorod-modified electrodes exhibit more enhanced CV signals than that of disordered gold nanorod-modified electrodes (Figure 3.6). Moreover, Simm et al. (2005) studied the simple preparation of random silver micro and nano-electrode arrays by mechanically attaching particles from suspension of metal colloid. These arrays were compared with arrays formed by the electro-deposition of silver on a glassy carbon substrate, with the silver being partially stripped off, leaving a stable micro and nanoparticle array on the surface. Although the arrays produced mechanically achieved larger particle sizes than those grown electrochemically, the result for the reduction of halothane were similar.

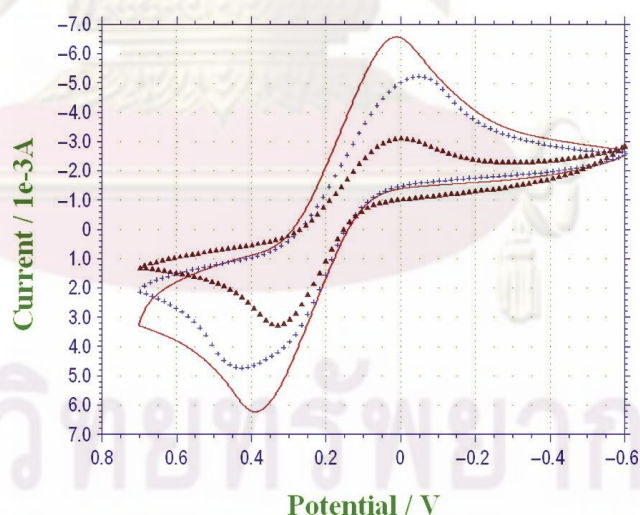


Figure 3.6 Cyclic voltammetry experiments show the performances of three working electrodes. i.e. the 1-D arrayed gold nanorods modified working electrode which enhance most the performance (ordered) (-). Disordered gold nanorods modified working electrode (*) and flat electrodes (Δ) exhibit smaller peak height. Lin et. al (2008)

3.2.3 Polymer electrodeposition in microelectrode array

The electrochemical polymerisation of a polymer directly onto an electrode is widely used for both macro- and microelectrode application. This method can offer a more suitable method of modification, providing complete coverage of the electrode surface on a molecular level (Castanón et al., 1997). Electropolymerisation has many advantages compared with other deposition or polymerisation methods. By using different electropolymerising conditions, including monomer concentration, solvent conductivity, pH value, scanning potential range, and applied scanning cycle, different characteristics and functions of the films can be obtained (Imisides et al., 1991). These differences have been found to include thickness, surface topography, pH response, electron transfer kinetics (Martinusz et al., 1994), and protection against metal corrosion (Marsh et al., 2001).

Electropolymerised films are generally formed by the oxidation of a monomer, conducting or insulating polymer films that coat the electrode surface (Emr & Yacynych, 1995). Conducting polymers are capable of transducing energy arising from certain chemical interferences into electrical signals which are easily monitored. The three most common monomers of conducting polymers are pyrrole (Zuo et al., 2008, Hui et al., 2009), aniline (Barton et al., 2004, Law et al., 2005 Myler et al., 2005) and thiophene (Kim et al., 2007). The main disadvantages with these types of films is that they are not very reproducible due to the deposition process, and anions present in the solution or solution pH can influence the conductivity of the film (Curulli et al., 1998). Non-conducting (insulating) polymer films, by contrast, form self-regulating films which have a uniform thickness and cover the surface completely with few defects or pinholes. The most common non-conducting polymer is phenylenediamines (PPD) (Prichard et al., 2004, Myler et al., 1997, Barton et al., 2004) which used in this project.

3.2.3.1 Electrodeposition of poly-phenylenediamine (PPD)

The *o*-phenylenediamine monomer is an aromatic diamine which can be synthesized by nitration and reduction processes involving benzene as show in Figure 3.7.

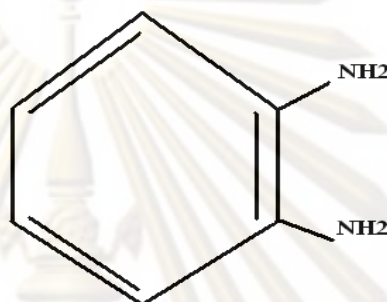
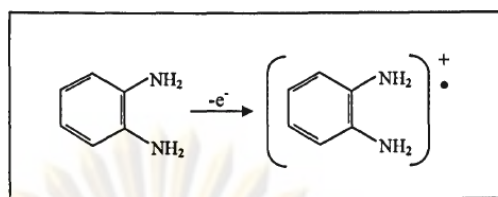
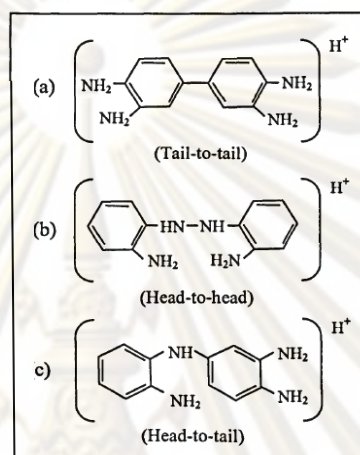


Figure 3.7 The chemical structure of *o*-phenylenediamine.

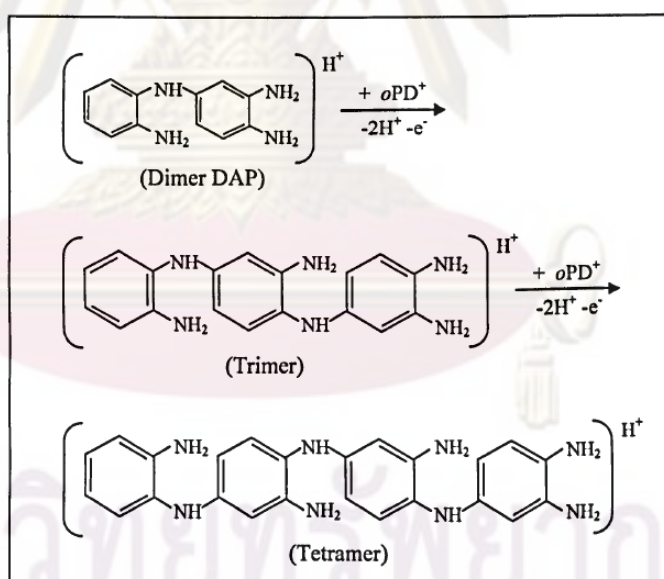
Electropolymerisation of *o*PD offers the advantage of producing a very thin (<100 nm) (Mill 2005) and self-insulating film that can be coated on any conducting, three dimensional surface. Myler et al., (1997) describe the development of enzyme electrodes for the detection of glucose in whole blood, based on ultra thin *o*-phenylenediamine composite membranes. The electrodpolymerization which Myler et al., (1997) used was applied in this research. The polyphenylenediamine (PPD) was grown at the pH 7.4 in phosphate buffer, the extent of conjugation is progressively decreased as suggested by the increasing amount of free NH₂ groups at the surface (Losito et al., 2001). The oxidation of *o*PD monomer was first taken placed by applied the potential in the initial cycle of electrodeposition to form a radical monocation (Figure 3.8a). Then, the monocation species immediately combines via radical coupling to form one of three possible dimmers (Figure 3.8b). As C-N coupling has been shown to be dominant for the anodic oxidation of aromatic amines in aqueous solution (Mill 2005), the 'head-to-tail' dimer configuration is formed preferentially (Figure 3.8c). This structure is suitable for propagation, and the molecule can undergo further elongation to produce longer chain and results in a conjugated polymer structure (Figure 3.9).



(a)



(b)



(c)

Figure 3.8 Initial oxidation of the *o*PD monomer to form a radical monocation (a), the dimerization following the oxidation of *o*PD (b), and the chain propagation (c) (Mill, 2005).

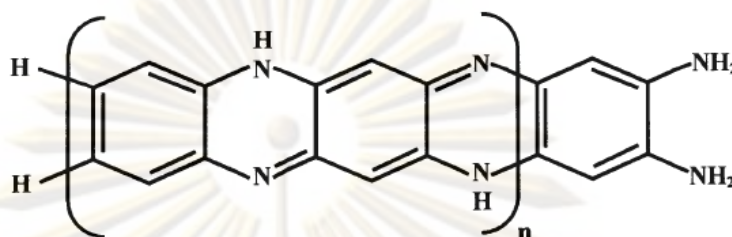


Figure 3.9 Proposed structure of poly(o-phenylenediamine) (Li et al, 2002).

3.2.3.2 Electropolymerisation of aniline

Polyaniline (PANI) which used in this research is the polymer of choice here due to its ease of polymerisation, low cost, high conductivity depending on the film forming conditions (Jaewang et al., 2007), and particularly, its high chemical durability against oxygen and moisture. Furthermore, it is thermodynamically possible that dissolved polyaniline film. This means that the film may behave as an electron-transfer mediating catalyst. The mechanism of growth and attachment of polyaniline is known to vary with substrate (Rodriguez et al., 1987). The polymerisation is initiated in acidic medium by the formation of an aniline radical cation, whose charge is localised mainly on the nitrogen atom (Figure 3.10). The monomer units are then connected by C-N bonds in para positions (head to tail couplings), to form leucoemeraldine, which is essentially non-conducting in both the base and protonised form. Strong oxidation of leucoemeraldine base leads to a non-conductive semi-quinone form, pernigraniline base.

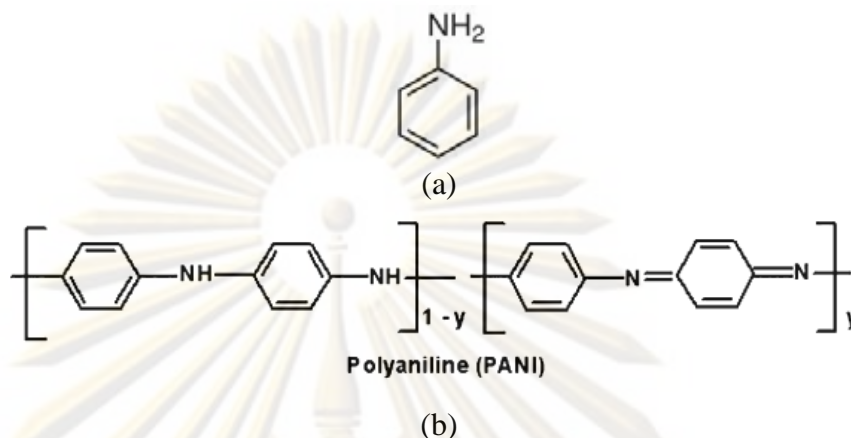


Figure 3.10 The structure of aniline (a), and polyaniline (b)

3.2.4 Applications of microelectrode arrays

Microelectrodes have numerous advantageous properties compared to electrodes of conventional dimensions, which have led to their widespread adoption in recent years. Their small size provides important practical characteristics such as a decreased ohmic potential drop (so that experiments are possible with much reduced supporting electrolyte concentrations), fast establishment of a steady-state signal, a current increase due to enhanced mass transport at the electrode boundary, and increased signal-to-noise ratio (Morf & de Rooij, 1997). These effects make sufficiently small electrodes advantageous in many areas of electroanalytical chemistry (Karel Stulik & Kutner, 2000). However, one major disadvantage of microelectrode is that the current output is very low for microelectrodes because of their extremely reduced size. Furthermore, another significant problem occurs if the single microelectrode in a sensor becomes damaged or fouled in any way, leading to the failure of the sensing device to register a signal. However, these problems can be overcome by replacing an individual microelectrode with a number of microelectrodes acting in parallel and forming an array of microelectrodes (Morf & de Rooij, 1997; Zoski et al., 2004). The arrays of microelectrodes increase the current for electrochemical measurements without losing the special features of a single

microelectrode such as high mass flux, steady-state current. Furthermore, the microelectrode arrays ensure redundancy in a sensing device if one, or several, of the individual microelectrodes failed to work. The use of microelectrode arrays has now produced a major impact in the area of electrochemical sensors and biosensors (Zhu et al., 2007).

Anjos et al. (2008) propose an electrochemical sensor strategy for the simultaneous calculation of oxygen and carbon dioxide in solvent using propylene carbonate (PC) as the electrolyte. It was demonstrated that short voltage pulses and gold microelectrode arrays can be successfully used in the electrochemical reduction of both oxygen and carbon dioxide individually, and measure their concentrations in tertiary gas mixtures. Some research presented significant results about microelectrode array for biological cell culture studies and gas sensors based on nanostructured materials such as porous silicon (PS) (Ramirez-Fernandez, 2006). In the case of the developed microelectrode array for biological culture, the signal recording and stimulation achieved that the charge injection limit can be lowered to less than 100 nC/cm^2 . The microelectrode array biosensor is an ideal in vitro system to monitor both acute and chronic effects of drugs and toxins and to perform functional studies under physiological or induced pathophysiological conditions that mimic in vivo damages. By recording the electrical response of various locations on a tissue, a spatial map of drug effects at different sites can be generated, providing important clues about a drug's specificity (Stett et al., 2003).

For enzyme microelectrode arrays, a few researches have been investigated. Burmeister et al. (2003) studied enzyme-based microelectrode array for real time measurement for neurotransmission in vivo by used of Ceramic-based multisite microelectrode arrays. Moreover, microelectrode array for glucose detection was studied by (Liu, et al., 2008). The glucose oxidase was entrapped into polypyrrole (PPy) nanofiber. This electrode demonstrated a good biocatalytic activity with glucose and occurred the response time of about 15 s. For glucose determination, Myler et al. (2004) similarly reported the sonochemically fabricated microelectrode arrays for glucose analysis by glucose oxidase. With this microelectrode array achieved the linearising sensor response between 0 – 60 mM glucose concentration. Moreover, the same research group (Myler et al., 2005) continuing studied the

similarly microelectrode arrays fabrication for alcohol oxidase. In the application of monitoring pesticides, Pritchard et al. (2004) developed the sonochemically fabricated microelectrode arrays based acetylcholinesterase for pesticides determination. The enzyme response in this case achieved the concentration determination down to $1 \times 10^{-17} \text{M}$. with similarly result in the organophosphate pesticides by Law et al. (2005). Which the determination concentration of dichlorvos, parathion and azinphos were $1 \times 10^{-17} \text{M}$, $1 \times 10^{-16} \text{M}$, and $1 \times 10^{-16} \text{M}$, respectively.

The use of microelectrodes and the assisted diffusional mass transport associated with the hemispherical diffusional profiles achieved the small signals associated with the enzyme as detailed before. However, the application of microelectrode arrays in HRP for phenol detection has not been report. For phenol detection, the sonochemically fabrication method for HRP microelectrode array is the interesting method for improve the phenol determination method due to this technique improve the response, lower detection limit and maybe improved the leakage problem of HRP immobilization in macroelectrode.



ศูนย์วิทยทรัพยากร
จุฬาลงกรณ์มหาวิทยาลัย

CHAPTER IV

MATERIAL AND METHOD

4.1 Reagents

The Aniline hydrochloride, ferrocenemonocarboxylic acid, gold (III) chloride trihydrate (ACS reagent; $\geq 49.0\%$ Au basis), hexaammineruthenium (III) chloride, *o*-phenylenediamine dihydrochloride, potassium ferricyanide, potassium ferrioxalate (all 'Analytical Reagent' grade), and horseradish peroxidase (HRP; E.C. 1.11.1.7; 167 purpurogallin units mg^{-1} ; one purpurogallin unit is defined as a production of 1.0 mg purpurogallin from pyrogallol in 20 s at pH 6.0 and 20 °C.) were purchased from Sigma-Aldrich (Gillingham, Dorset, UK).

Acetic acid, orthophosphoric acid and sodium hypochlorite solution (all GPR7 grade), disodium hydrogen orthophosphate 12-hydrate, sodium chloride, phenol, and sodium dihydrogen orthophosphate 1-hydrate (all 'AnalaR®' grade) were purchased from BDH (Lutterworth, Leicestershire, UK).

4.2 Equipments

A Sycopel Analytical Electrochemical Workstation Model AEW2 potentiostat (Sycopel Scientific Ltd, Washington, Tyne & Wear, UK) controlled by a PC equipped with an ECProg3 software program was used for all lab-scale electrochemical studies (Figure 4.1)



Figure 4.1 Sycopel AEW2 potentiostat

A Transsonic T460, 35 kHz, 30W ultrasound tank (Fisher Scientific, Loughborough, Leicestershire, UK) was used for the sonochemical ablation of microelectrode arrays and for cleaning of electrode surface bubbles prior to the electropolymerisation of carbon electrodes, to ensure a homogenous polymer layer.

For microscopy characterization, the scanning electron microscopy (SEM; Joel JSM-6480LV, Japan) was used.

The working electrode used in this research is glassy carbon electrode. Furthermore, the Ag/AgCl and Pt electrode were applied as reference and counter electrode in all experiment (Figure 4.2).



(a) GC electrode



(b) Pt electrode



(c) Ag/AgCl electrode

Figure 4.2 GC electrode (a), Pt electrode (b), and Ag/AgCl electrode were used as working, counter and reference electrode, respectively in this research

4.3 Buffer and Solutions

The phosphate buffered saline (PBS) at pH 7.4 stock solution prepared by using 0.13 mM sodium di-hydrogen orthophosphate NaH_2PO_4 , 0.528 mM di-sodium hydrogen orthophosphate Na_2HPO_4 and 0.51 mM sodium chloride NaCl .

Acetate buffer pH 5.5 prepared by using 0.0011 M acetic acid, 0.0088 M sodium acetate and 0.51 mM sodium chloride NaCl .

The three redox couples were used in this research are, 5 mM ferrocenecarboxylic acid (FCA) solution, 5 mM hexaammineruthenium (III) chloride solution, and 5 mM Ferri/Ferro cyanide was prepared from 4.22 M potassium hexacyanoferrate and 3.3 M potassium ferricyanide. The all three redox couples were prepared in pH 7.4 PBS.

4.4 Experimental procedure

4.4.1 The electrode pretreatment

The glassy carbon electrode (GCE) was first gently polished consecutively using 0.3 and 0.05 μm alumina powders. The polished GCE was then cleaned in ethanol and distilled water respectively by a sonicate bath at 35 kHz for 5 mins each. An electrode was dried under room temperature after the sonication before use.

4.4.2 An ultra thin poly-phenylenediamine film polymerization

The solution of 5 mM *o*-phenylenediamine dihydrochloride was prepared in phosphate buffer (pH 7.4) and was sonicated for 20 mins for deoxygenation. The prepared solution was then electropolymerized on GCE by potential sweep between 0 and 1000 mV versus Ag/AgCl at 20 mVs^{-1} for 50 cycles using Pt as a counter electrode. All electrodes were connected with a Sycopel Scientific AEW2 portable electrochemical workstation to a PC running ECProg3 software. Then, the polydiaminobenzene (PDB) coated electrode was dried for 2 hours at room

temperature and rinsed with deionised water for removal of unpolymerised molecules. (Myler et al., 2005)

4.4.3 Sonochemically ablation for polymer thin film

The modified GCE obtained in section 2.2 was immersed into a distilled water contained sonicated bath in the middle of the tank measured from all dimensions, and was clamped to a metal rod stand throughout the experiments. An effect of sonication time was studied by varying duration times at 16, 17.30, 18, and 19 mins each at a fixed frequency of 35 kHz. Subsequently, the sonicated modified electrode was dried at room temperature for 1 hr, and cyclic voltammetry was performed in 5 mM ferrocenecarboxylic acid (FCA) between -400 and +800 mV at 20 mVs⁻¹. Additionally, the amperometric responses were investigated at varied FCA concentrations to test the performance of the modified electrode. For another redox couples were applied for cyclic voltammogram in this research, the apply potential between -1000 to 1000 mV for 5 mM Ferri/Ferro cyanide, and the potential between 200 to -400 mV for 5 mM hexaamineruthenium (III) chloride.

4.4.4 The electropolymerization of PPD/HRP/PANI and PPD/HRP/Au/PANI microelectrode arrays

For the fabrication of PPD/HRP/PANI microelectrodes, the sonochemically prepared microelectrodes (as in Section 4.4.3) were submerged in aniline/HRP acetate buffer solution (0.5 mM aniline, and 300 unit/ml HRP) (pH 5.5) for co-electropolymerisation by sequentially cycling the working electrode between -200 and +800 mV versus Ag/AgCl for 20 cycles at 50 mVs⁻¹ (Barton et al., 2004). Immediately following polymerisation, the working electrode was submerged in pH 7.4 phosphate buffers to prevent enzyme denaturation and stored at 4 °C prior to use.

Fabrication of PPD/HRP/Au/PANI microelectrode arrays was carried out similarly to the preparation of PPD/HRP/PANI microelectrodes, however, electrodeposition of Au nanoparticle was achieved prior to HRP/PANI co-deposition. A solution of 0.3 mM HAuCl₄.3H₂O in distilled water was electrodeposited onto the sonochemically fabricated microelectrode at -200 mV for 30 s which resulted in Au

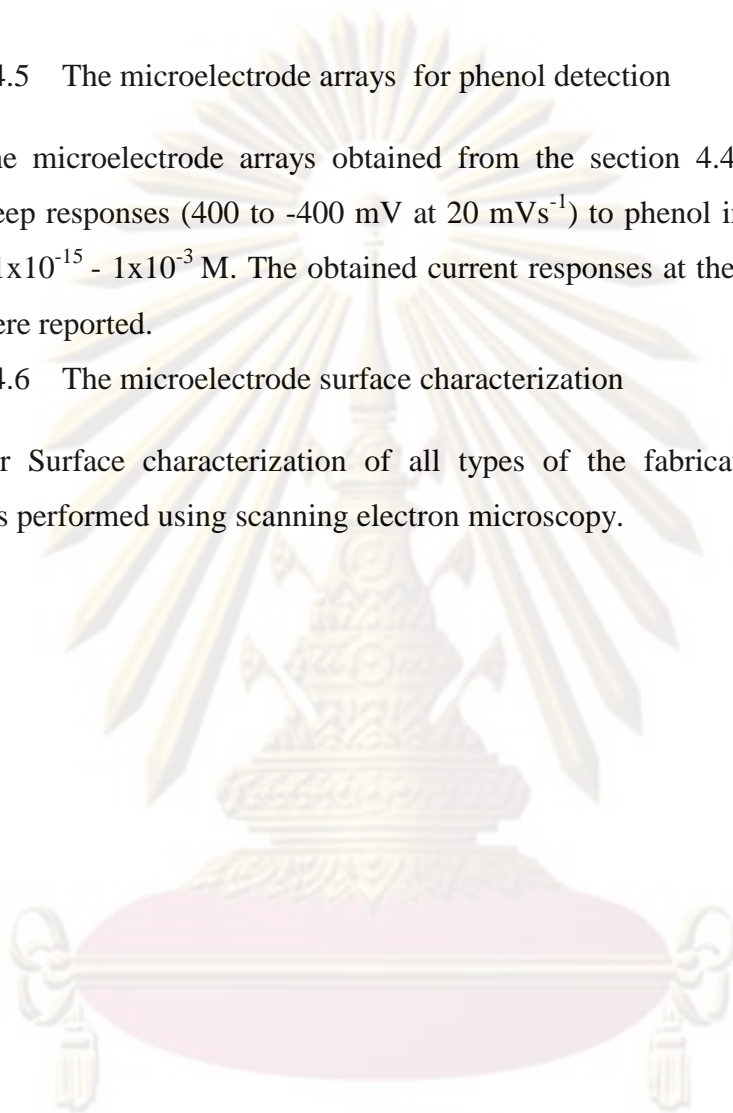
nanoparticles deposition onto microelectrode surfaces. HRP/PANI co-deposition was finally followed using the method mentioned above.

4.4.5 The microelectrode arrays for phenol detection

The microelectrode arrays obtained from the section 4.4.4 were tested for linear sweep responses (400 to -400 mV at 20 mVs^{-1}) to phenol in the concentration range of 1×10^{-15} - 1×10^{-3} M. The obtained current responses at the applied voltage of 50 mV were reported.

4.4.6 The microelectrode surface characterization

For Surface characterization of all types of the fabricated microelectrode arrays was performed using scanning electron microscopy.



ศูนย์วิทยทรัพยากร
จุฬาลงกรณ์มหาวิทยาลัย

CHAPTER V

RESULTS AND DISCUSSION

This research covers an investigation of microelectrode arrays fabrication for HRP based biosensors using a son chemical technique. The three major attempts were carefully explored. Firstly, the PPD/HRP/PANI microelectrode arrays assemblage was especially developed. The micro arrays ablation conditions were studied in the first period. Next, enzyme microelectrode arrays were produced. Secondly, Au particles were introduced in the microelectrode arrays aiming at increasing response currents. Finally, the comparisons between two types of microelectrode arrays were elaborated. Additionally, kinetic study of the concerned reaction is included in comparison to that of free enzymes.

5.1 Microelectrode arrays fabrication

The *o*-phenylenediamine dihydrochloride (*o*PD) was firstly electrodeposited on the glassy carbon electrode (GC). The suitable conditions for the poly-*o*PD or poly(*o*-phenylenediamine) (PPD) thin film production was investigated (Appendix A). In this part, sonochemical ablation of PPD film on GCE is the main focus. Furthermore, the HRP based microelectrode arrays were examined. To analyse the formation of microelectrode arrays, cyclic voltammetry was applied, and SEM was used to determine surface characteristics of the ablated PPD film.

5.1.1 Electropolymerisation of *o*-phenylenediamine dihydrochloride (*o*PD)

5.1.1.1 Mechanism of *o*PD electropolymerisation

The 5 mM *o*PD was electrodeposited on GC electrode for 50 cycles at a fixed scan rate of 20 mVs⁻¹, and this is shown schematically in Figure 5.1. The cyclic voltammetry for the electropolymerisation of the insulating PPD film is shown in Figure 5.2. The diversity of PPD macromolecular structures obtained was resulted from the differing polymerization conditions. It is suggested (Losito et al., 2003) that under acidic polymerisation conditions (pH<5), PPD possessing a phenazine-like

structure, which amino groups of an *o*PD unit are condensed with the benzene ring of the closed unit along the polymer chain, although free primary amino groups have been seen to be still present, at least at the surface (Losito et al., 2001). At higher pH > 5, the extent of conjugation is progressively decreased, since there is an increasing amount of free amino groups at the surface. These structures also show some agreement with the properties of PPD synthesized at the particular pH values, for example, the better electroactivity exhibited by the polymer obtained at low pH (Losito et al., 2001). The different structures of PPD can thus be attributed to the peculiar mechanisms of the oxidative polymerisation at different conditions which is proposed by Losito et al., (2003) (Figure 5.3).

In the first stage of polymerisation, the oxidization of monomer to the corresponding free radical cation in any pH condition (as shown in (1) reaction in Figure 5.3) is occurred during the forward scan from 0 to 1000 mV, the relevant peak potential is presented according to the oxidisation (Figure 5.2). Furthermore, no reduction peak is found in the reverse scan, suggesting that the oxidized *o*PD was involved in further chemical process which led to non-reducible species in the potential range adopted. From the free radical cation, radical coupling (tail-to-tail, head-to-head, head-to-tail) of these radicals give three possible different dimers (A1, A2 and A3, respectively) that can be further oxidised by a two electron-two H⁺ process forming another species (B) which is mostly obtained from the dimer A3 (head-to-tail). The fully reduced dimer A3 may be involved in three different and competitive processes: oxidation to the B1 dimer (2), internal coupling (intramolecular oxidation followed by cyclisation) leading to the intermediate species B2 (3) which rapidly evolves into its fully oxidised form, 2,3-diaminophenazine (2,3-DAP) or further radical coupling (i.e. chain propagation) (4) to form a trimer, B3. The fully reduced trimer, B3, then plays a role similar to that of the A dimer, leading to either fully (D) or partially (E) oxidised trimers or to the fully reduced tetramer (F).

Then, the key point in the polymerisation mechanism seems to be the competition between oxidative coupling, leading to chain propagation, and intramolecular oxidation processes leading to the formation of (i) phenazine, (ii) 1,4-benzoquinonediimine units or (iii) both. For instance, 2,3-DAP and D arise from

phenazine-forming processes, whereas B and E arise from 1,4-benzoquinonediimine forming processes.

In summary, the insulating film may be formed via the polymerisation of the *o*PD di-cation formed on disproportionation, or the monocation radical oxidising at a conducting film surface rather than the electrode surface, yielding an insulating film which results in decreasing the oxidation current during potential cycling (Figure 5.2). The following significantly decreasing anodic peak in successive scans (Figure 5.2), indicated a low efficiency of *o*PD oxidation on the PPD film as compared to the bare electrode. This result can be attributed to the film resistivity, thus hindering further monomer oxidation and subsequently polymer deposition. Hence, the electrode became progressively insulated by the polymer film during the polymerisation. In this research, the anodic irreversible peak current decreased to nearly the background level on the 50th cycle, indicating that the electrode became totally insulated and therefore could not be coated with any further polymer (Sayyah et al., 2009).



ศูนย์วิจัยทรัพยากร
จุฬาลงกรณ์มหาวิทยาลัย

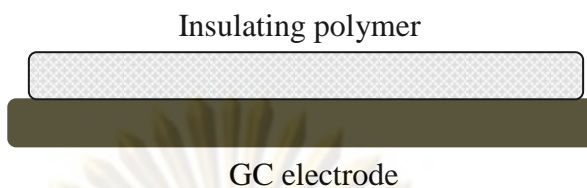


Figure 5.1 The schematic of polymer (PPD) to form an insulating film on GC electrode

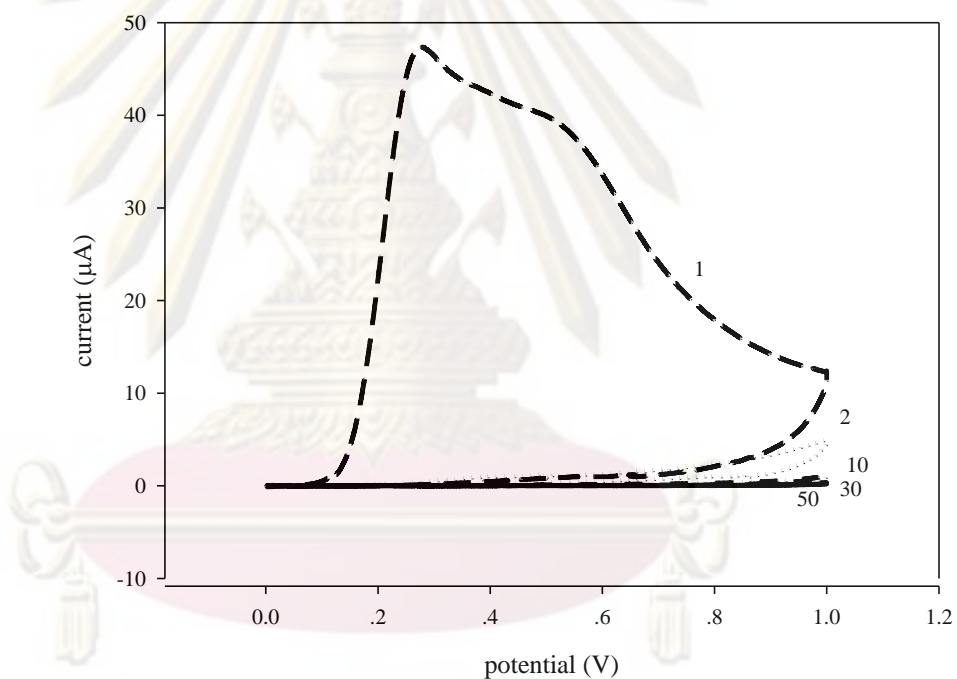


Figure 5.2 Cyclic voltammograms for the electropolymerisation of 5 mM *o*PD at a potential scan rate 20 mVs^{-1} vs Ag/AgCl.

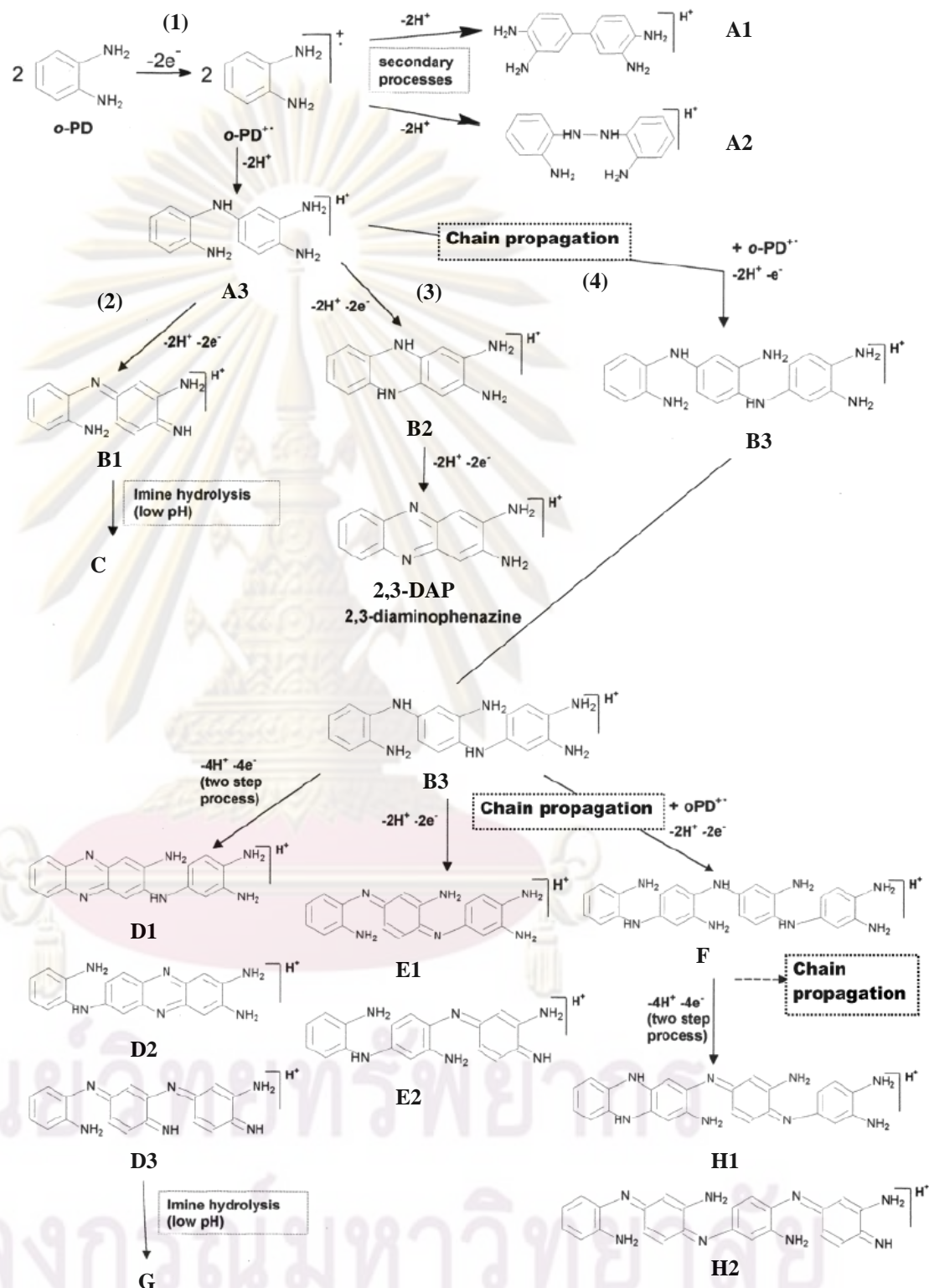


Figure 5.3 Schematic representation of the *o*PD polymerisation mechanism proposed by Losito et al. (2003).

5.1.1.2 The electrochemical characterisation of PPD film

Electroactivity of the electrochemically deposited PPD films grown on GC electrode was initially tested by cyclic voltammetry in pH 7.8 phosphate buffer at a scan rate of 20 mVs^{-1} using three different redox couples. Figure 5.4, 5.5 and 5.6 display cyclic voltammograms of 5 mM ferri/ferro cyanide $[\text{Fe}(\text{CN})_6^{3-/4-}]$, 5 mM hexaammineruthenium (III) chloride $[\text{Ru}(\text{NH}_3)_6^{3+/2+}]$, and 5 mM ferrocenecarboxylic acid $[\text{Fc}(\text{CO}_2\text{H})^{3+/2+}]$, respectively for both bare GC electrode(a) and PPD coated electrode(b). The reactions of these redox couples are indicated in following equations

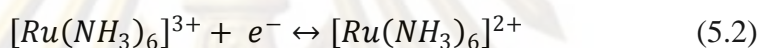
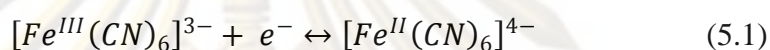


Figure 5.5a illustrates the cyclic voltammogram obtained which the initial sweep is in the cathodic direction reducing Fe^{3+} to Fe^{2+} . The cyclic voltammogram yields the magnitude ratio of the two peak currents closed to 1, which the i_{pa} and i_{pc} are 66.47 and -65.3 μA , respectively since the solution consisted mainly of ferricyanide, the reaction product from the cathodic sweep (ferrocyanide) experiences a diffusion gradient away from the electrode, causing it to move out of the diffusion layer and resulting in a charge bias in favour of reduction. Furthermore, a peak separation of approximately 220 mV which is much higher than the value of 59 mV expected for a reversible, diffusion-controlled single electron transfer reaction (Adrian, 1999). Contrastingly, a very little voltammetric response is observed for the PPD coated electrode confirming that the electrode surface was mostly insulated by the film. The absence of $[\text{Fe}(\text{CN})_6^{3-/4-}]$ peaks on the voltammogram corresponding to the PPD covered electrode (Figure 5.5b) agreed with the previous results experimented under similar pH values for PPD grown on gold electrode (Barton et al., 2004) and screen printed electrode (Myler et al., 2004).

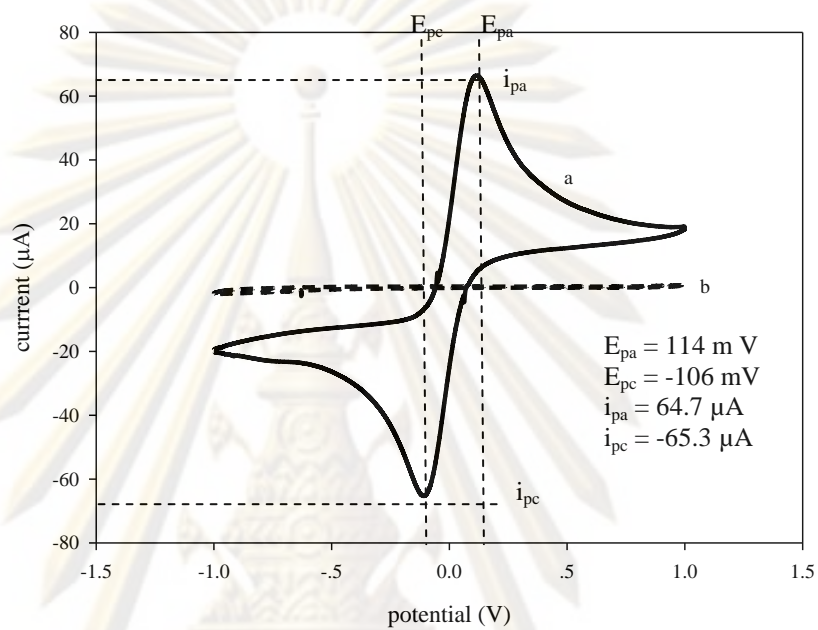


Figure 5.4 Cyclic voltammetry of 5 mM ferri/ferro cyanide at (a) a bare GC electrode and (b) a similar electrode coated by an electrodeposited film of PPD at scan rate 20 mVs^{-1} .

ศูนย์วิทยทรัพยากร
จุฬาลงกรณ์มหาวิทยาลัย

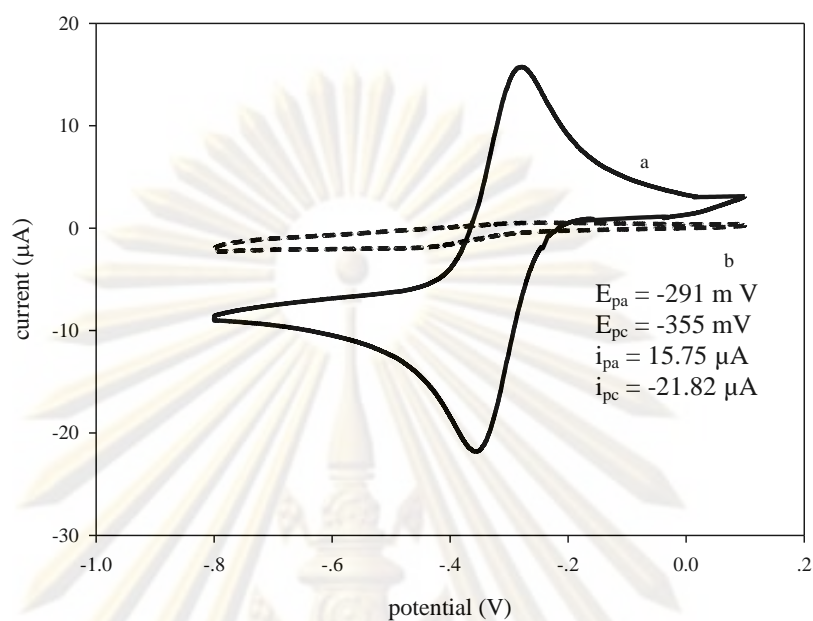


Figure 5.5 Cyclic voltammetry of 5 mM hexaammineruthenium(III) chloride at (a) a bare GC electrode and (b) a similar electrode coated by an electrodeposited film of PPD at scan rate 20 mVs^{-1} .

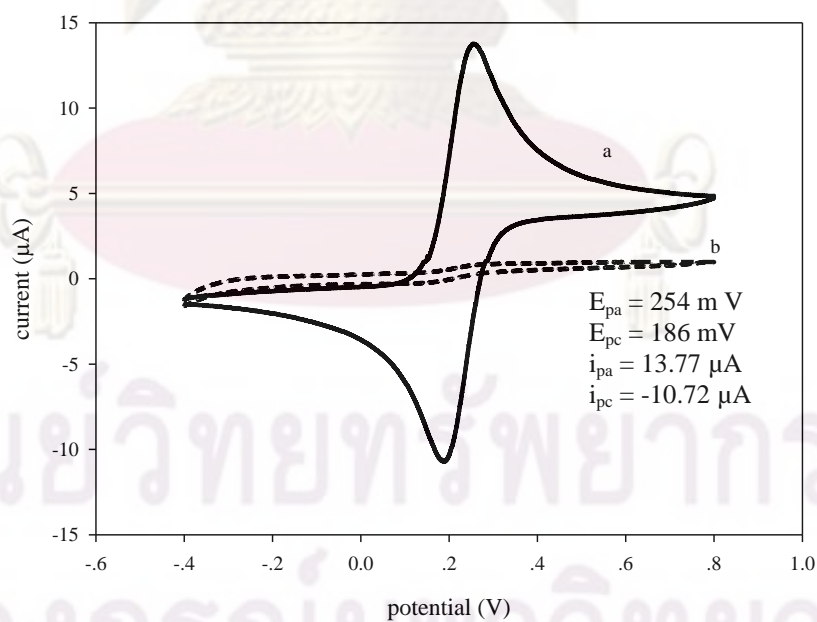


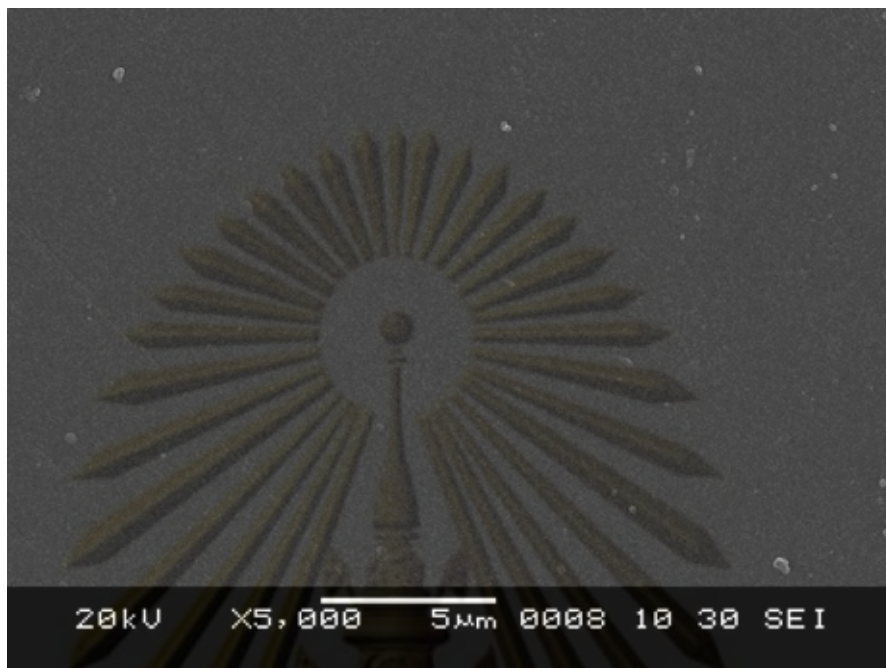
Figure 5.6 Cyclic voltammetry of 5 mM ferrocenecarboxylic acid at (a) a bare GC electrode and (b) a similar electrode coated by an electrodeposited film of PPD at scan rate 20 mVs^{-1} .

In the case of $[\text{Ru}(\text{NH}_3)_6]^{3+/2+}$ and $[\text{Fc}(\text{CO}_2\text{H})]^{3+/2+}$ redox couples were, the reversible electron transfers similar to the $[\text{Fe}(\text{CN})_6]^{3-/4-}$ redox couple were observed. The $[\text{Ru}(\text{NH}_3)_6]^{3+/2+}$ system exhibited slightly greater reversibility in terms of peak separation (ΔE_p) than the $[\text{Fc}(\text{CO}_2\text{H})]^{3+/2+}$ system (peak separation of 64 and 68 mV). However, the cyclic voltammograms using the three redox couples did exhibit clear redox peaks. The near Nernstian behaviour of the redox couples should be attributed to a good electron transfer at the surface of GC electrode.

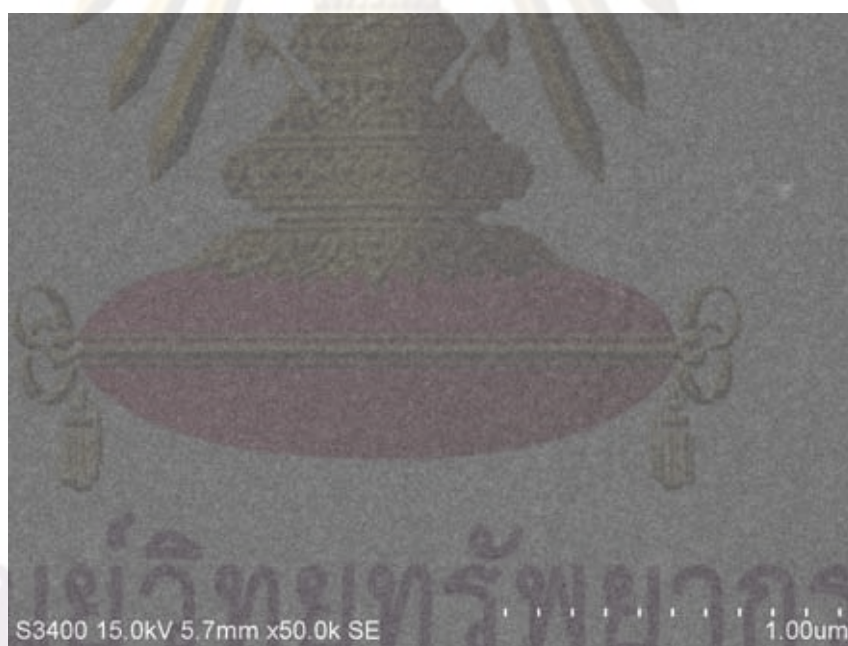
The cyclic voltammogram obtained from PPD coated electrode using $[\text{Ru}(\text{NH}_3)_6]^{3+/2+}$ and $[\text{Fc}(\text{CO}_2\text{H})]^{3+/2+}$ as redox couples displayed similar results with $[\text{Fe}(\text{CN})_6]^{3-/4-}$. A very small value of the peak currents obtained in these two redox couple confirmed the insulating behaviour of PPD thin film coated on GC electrode.

5.1.1.3 The microscopic characterization of PPD film

The scanning electron microscopy of PPD coated on GC electrode (Figure 5.7a) compared with the bare GC electrode (Figure 5.7b) confirms that the GC was fully coated by an insulating PPD film. The AFM image also confirms that the PPD film was very rough (Figure 5.7c). Furthermore, the AFM image would suggest that the PPD film thickness was about 27 – 31 nm using 3 positions of section analysis which was represented in the three vertical distances. This was in agreement with Barton et al. (2004) which gold coated glass slides were used as a working electrode, the 30-40 nm thickness of the PPD thin film was found. For the gold spotter-coated glass slide electrode presented by Myler et al.(1997), the film thickness obtained was of similar range (~35 nm).



(a)



(b)

ศูนย์วิทยาศาสตร์สุขภาพ
จุฬาลงกรณ์มหาวิทยาลัย

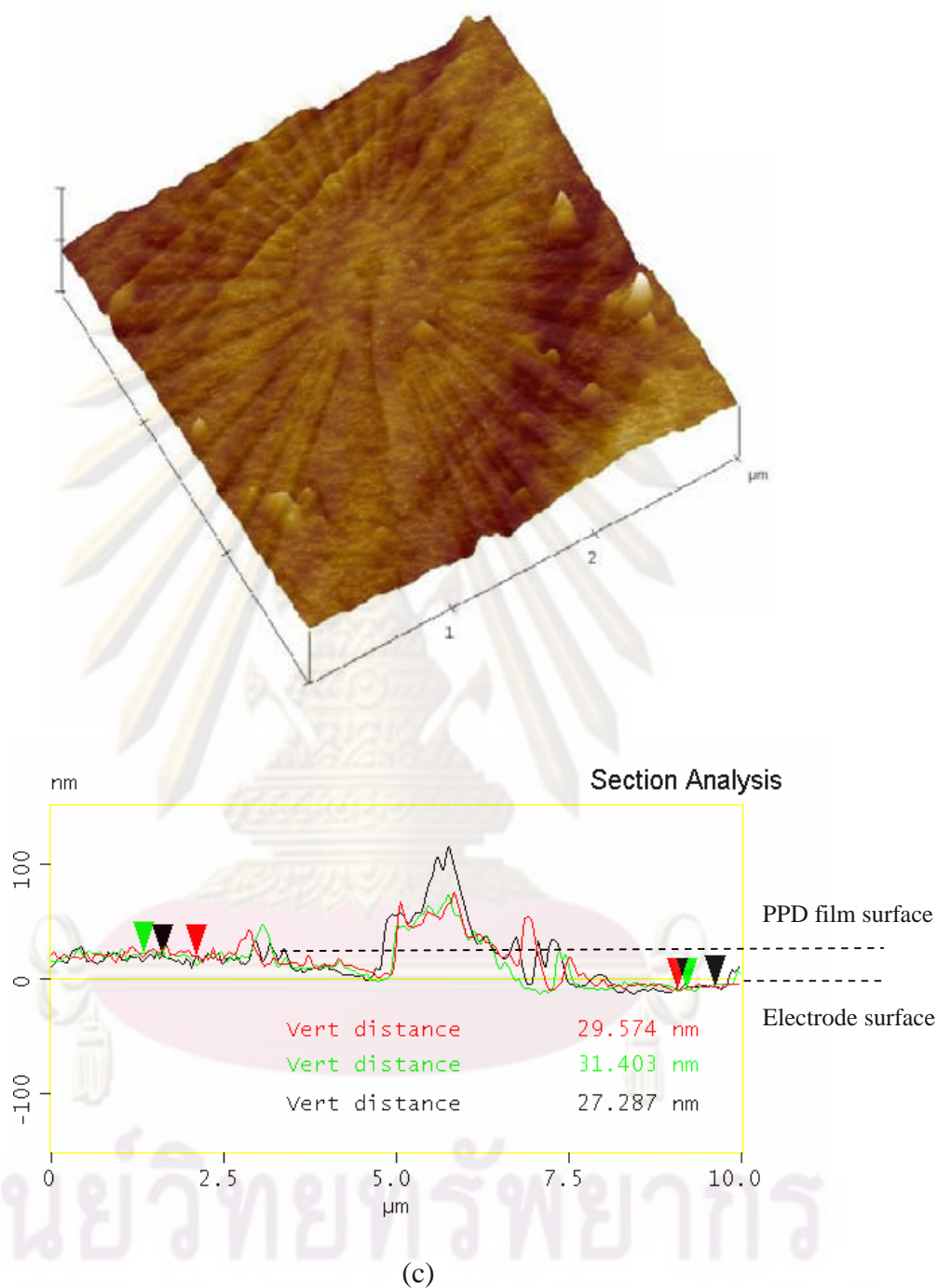


Figure 5.7 Electron micrographs of PPD insulated (a), bare GC electrode (b), and AFM image for PPD coated GC electrode (c), the 5 mM *o*PD electropolymerisation for 50 cycles at a scan rate 20 mVs^{-1} between 0 to 1000 mV.

5.1.2 Sonochemically for microelectrode arrays fabrication and Characterisation

The fabrication of microelectrode arrays has been discussed before that the most common techniques for fabrication was photolithography because of its reproducibility, conversely the cost prohibitive for the mass production of disposable sensor. However, a novel approach for the fabrication of microelectrode arrays that lends itself to mass production is sonochemical fabrication due to the simplicity and inexpensiveness of the approach. The method takes advantage of acoustic cavitation due to the passage of an ultrasonic wave through the medium which is absolutely a simple method.

5.1.2.1 An ultrasonic ablation mechanism

It has previously been shown that α PD may be electropolymerised on conductive electrode surfaces to form essentially insulating polymer films of less than 100 nm (Myler et al., 1997) thicknesses. In this research, the film thickness obtained was determined around 27-31 nm on the GC electrode. The film was found to be perfectly insulated since cyclic voltammetry for the electrodeposition of the film presented diminishing peak currents as reported earlier.

For fabrication of microelectrodes on the polymer thin film, ultrasonic have been utilised in a novel approach for the fabrication of microelectrodes by means of ultrasonic ablation of thin polymer films. As describe before in Chapter 2, an ultrasound (in a kHz range) passes through a solvent such as water and induces cavitation, whereby localised hotspots of up to several thousand degrees Kelvin are created in the form of super-heated vapour bubbles (Suslick, 1990). The surrounding medium, which is of ambient temperature, very rapidly cools the vapour bubbles, and causes them to collapse upon themselves. When these events occur close to a solid surface, the movement of water is hindered by the presence of the object and so the majority of the liquid enters the bubble from the opposite side (Figure 2.11). This resulted in an asymmetric bubble collapse, which produces a high velocity jet of liquid targeted towards the solid surface. The velocity of these microjets (hundreds of

metres per second) may cause the shattering of hard, brittle solids, and for more ductile materials receive surface ablation from the impact of such jets (Suslick, 1990).

In the case of soft, ultrathin polymer films, such as poly(o-phenylenediamine), the extent of this surface ablation is sufficient to cause perforation through to the harder underlying conductive surface, as depicted in Figure 5.8.

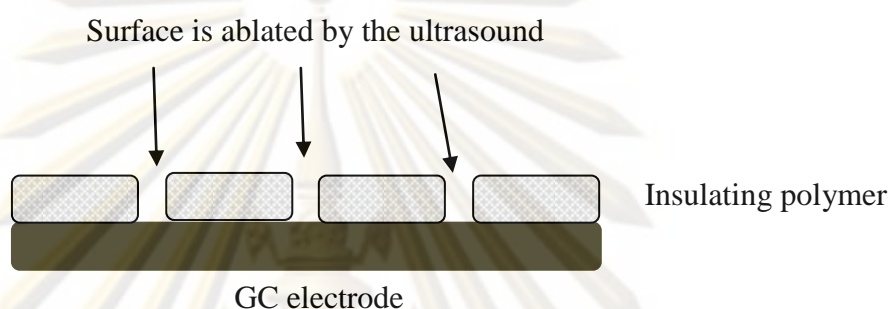


Figure 5.8 The schematic diagram of sonochemical ablation forming microelectrode arrays

5.1.2.2 Ultrasonic cavitation mapping study

For this research, the bench top ultrasonic baths such as the Camlab Transsonic T460 possesses a single ultrasonic transducer was used for microelectrode arrays formation with the fixed position of electrode is shown in Figure 5.9. Consequently, the degree of acoustic cavitation experienced when multiple sensors are sonicated simultaneously varies considerably at differing positions within the tank (Gornall, 2004). Conversely, for a single sensor in a small ultrasonic bath with a single transducer, this is a simple task since the electrode should be located vertically above the transducer. The effective electrode position was investigated using the same ultrasonic bath. The four different positions for microelectrode arrays ablation were tested as demonstrated in Figure 5.10.

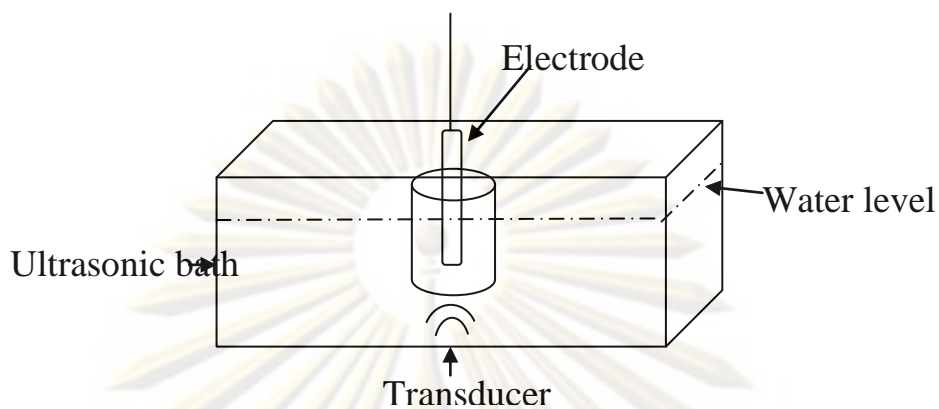


Figure 5.9 Laboratory-scale microelectrode arrays fabrication via ultrasonic ablation

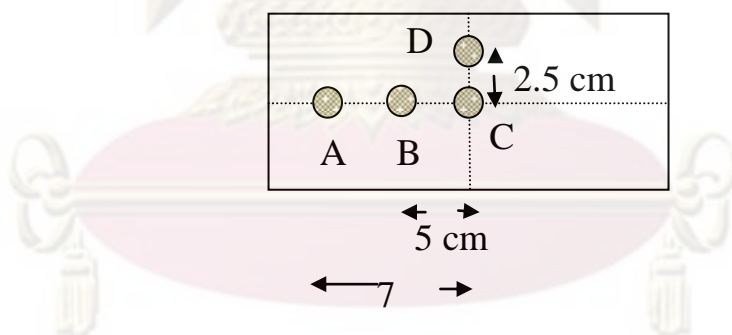


Figure 5.10 Positioning of electrode during ultrasonication (A, B, C, and D)

ศูนย์วิทยทรัพยากร
จุฬาลงกรณ์มหาวิทยาลัย

In a fixed transducer ultrasonic tank (such as the prototype above) an ultrasonic standing wave field is generated inside the liquid (Hepher et al, 2000), (Yasui et al, 2005 m). As the wave propagates through the medium, some regions experience high amplitude pressure variation (antinode) and others experience very little pressure change (node). Nodal positions correlate to multiples of the wavelength (λ) of the ultrasonic wave, while antinodal positions relate to multiples of half wavelength ($\lambda/2$), as illustrated in Figure 5.11. Two classes of cavitation exist by the liquid tear apart around antinode, known as stable and transient cavitation (Mills, 2005). Stable cavitation refers to bubbles generated at lower acoustic pressures (or higher frequencies) and which exist over many acoustic cycles. The stable cavitation bubble oscillates with the surrounding pressure field. The radius of the bubble increases in size results from a lower internal vapour pressure when compared to the surrounding medium. The dissolved gases diffuse across the interface into the bubble cavity during this stage. At the compression period, the surface area of the oscillating stable cavitation bubble is smaller than the rarefaction phase and the dissolved gas tends to diffuse into the bubble at a faster rate than diffuse out during compression. At some point, for example, the interaction with a neighbouring bubble, results in the collapse of the bubble. The presence of non-condensable gas which has diffused across the interface from the surrounding medium cushions the collapse. Consequently, the energy released is greatly reduced, preventing a significant contribution to the process of ultrasonic ablation caused by the microjets of water (Chapter 2).

For transient cavitation, refers to those cavities which exist at the much shorter time scale (1-3 cycles), this cavity size expands too many times of its equilibrium size. Since the bubble only exists for an extremely short time (typically only one cycle), there is no time for heat exchange or the diffusion of dissolved gases into the cavity. The cavity contains some vapour from the surrounding medium, but the vapour remains at or near its equilibrium pressure and can evaporate or condense freely at the cavity wall. The result is that in the absence of cushioning residual permanent gas when the cavity collapses. The collapse of transient cavities is extremely energetic, generating temperatures of several thousand degrees Kelvin, pressures of around 1000 atm, and generating the powerful microjets of fluid

associated with asymmetrical bubble collapse near a solid surface (Tuziuti et al, 2005). These microjet fluids are responsible for the mechanical effects of ultrasonic cavitation and are required for the perforation PPD films in the fabrication of microelectrode array constructions.

The formation of cavitation bubble at position transducer ultrasound tanks, where standing waves create the localised pressure fields termed nodes and antinodes (Figure 5.11). Instead of being homogeneous, cavitation bubbles will form clusters consisting of streams of bubbles (streamer) moving towards to the focal pressure antinode to form a dense cloud containing cavitating bubbles (Figure 5.11). The bubbles are moved by acoustic pressure gradients couple with bubble oscillations to produce a translational force (Mills, 2005).

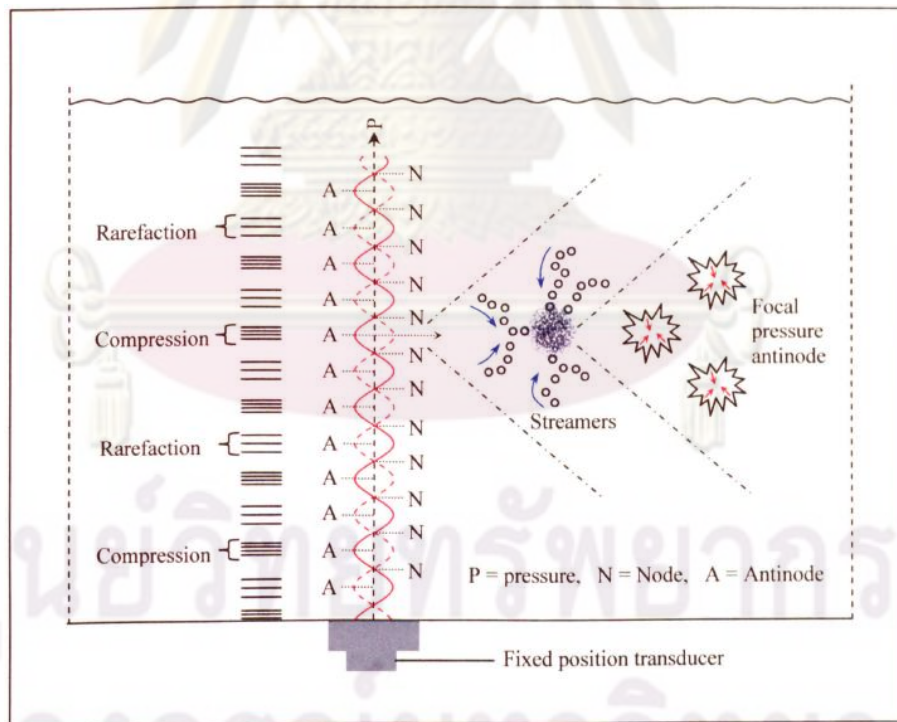


Figure 5.11 Schematic representation of ultrasonic wave propagation and acoustic cavitation (Mills, 2005)

The position of electrode in the fix transducer ultrasonic bath should be located vertically above the transducer (Mason, 1999) which may achieve the enough energy for perforation. Furthermore, the production of reproducible microelectrode arrays is only immersing the electrode in the water and applying an ultrasonic pulse. The construction of the tank and the distribution of the ultrasonic intensity within this vessel must be firstly considered in order to correct positions of the electrode Thus, correlations between the electrochemical behaviour of the individual electrodes at different positions in the sheet can be made.

In order to elucidate the effect of the locations of the electrode in the tank, the cyclic voltammogram of 5 mM ferri/ferro cyanide was determined, and the peak current at 100 mV at different position and sonication time is plotted in Figure 5.12. It is thought that the most intense regions of power are expected to be found directly above a transducer (Mason et al, 1989). Therefore, one would expect that the most ablation on the polymer surface would be observed on the electrode that is located in the middle of the tank directly above the transducer since the most create power localised at the transducer. However, the plot shown in Figure 5.12 exhibit the effect, with the most ablation being present from the middle of the tank with the high current at 100 mV in 5 mM ferri/ferro cyanide. This referred that the electrode was placed over the transducer which was in the middle of the tank.

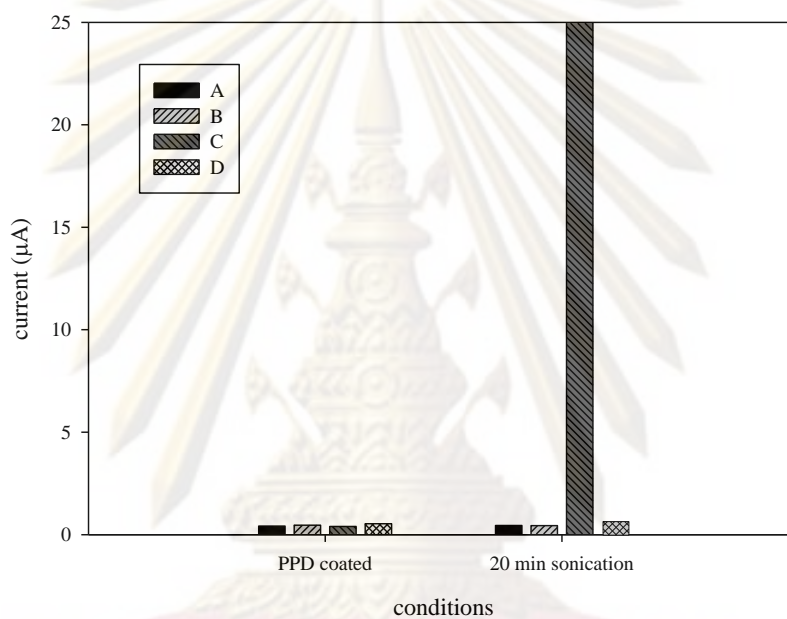


Figure 5.12 The current responses at 100 mV from cyclic voltammogram for 5 mM ferri/ferro cyanide at a scan rate of 20 mVs^{-1} of the sonochemically ablation of electrodeposited film of PPD at different electrode positions.

ศูนย์วิทยทรัพยากร
จุฬาลงกรณ์มหาวิทยาลัย

5.1.2.3 The electrochemical characterisation of microelectrode arrays

To obtain optimum microelectrode properties, suitable diffusion characteristics have to be established. These characteristics depend on radius, spacing, and geometrical arrangement of the electrodes in the arrays. The beneficial microelectrode array characteristics for the sonochemically fabricated microelectrode arrays are their pore sizes and distribution. The pore radius should be smaller than the distance between the pores to demonstrate the microelectrode arrays (Wang, 2006). Thus, to achieve the optimum properties, sonication time for microelectrode array formation is a significant parameter. Furthermore, the scanning electron microscopy was used to image the sonicated electrode surfaces.

Cyclic voltammetry is a simple diagnostic tool that can be used to determine if microelectrode are sufficiently distributed so that microelectrode arrays are formed. Since microelectrodes are known to exhibit sigmoidal shaped cyclic voltammograms for reversible solution bound redox species (Huang, et al., 2009) so that it exhibits microelectrode behaviour. Conversely, the characteristic peak shaped voltammograms are expected at a planar of the macroelectrode surfaces or indeed arrays in which the microelectrodes are too closely packed together.

According to the section 5.1.1.2, the hexaammineruthenium (III) chloride $[\text{Ru}(\text{NH}_3)_6^{3+/2+}]$ and ferrocenecarboxylic acid $[\text{Fc}(\text{CO}_2\text{H})^{3+/2+}]$ seemed to obtain greater electron transfer than ferri/ferro cyanide redox couple for GC electrode was used as working electrode in this research. The cyclic voltammograms recorded in 5 mM $[\text{Ru}(\text{NH}_3)_6^{3+/2+}]$ and 5mM $[\text{Fc}(\text{CO}_2\text{H})^{3+/2+}]$ solutions were applied at the different sonication time for microelectrode arrays ablation in this and further experiments (Figure 5.13 and 5.14, respectively). The voltammograms corresponding to the microelectrode behaviour was achieved at the 17.30 min of sonication time due to the sigmoidal shaped is clearly demonstrated. Since the diffusion layer thickness is much bigger than the size of electrode at 17.30 min of sonication (d/r ratio is large, according to Chapter 2, section 2.5.1), the sigmoidal shape is appeared at this time. The sigmoidal shaped has been reported for the microelectrode arrays fabrication using a similar insulating film on screen printed surface at 20 sec of sonication (Barton et al., 2004). The increasing sonication time gave the slightly increasing in

signal current in both of redox couples. However, at longer sonication times (18 and 19 min) complete sigmoidal response currents indicating that electrode sizes are bigger which caused the planar diffusion characteristics. At the short sonication time (16 min), arrays behaved like each individual electrodes and no interference from overlapping diffusion occurred and showed the planar diffusion. Cyclic voltammograms obtained by using the ferrocenecarboxylic acid as a redox couple showed similar results as of hexaammineruthenium (III) chloride

It is clearly seen that the sigmoidal shaped curves in Figure 5.15 shows the voltammetry of the $[\text{Fc}(\text{CO}_2\text{H})^{3+/2+}]$ at a 17.30 min of sonochemically produced microelectrode arrays compared with the bare GC electrode and PPD coated electrode at the same conditions. The voltammograms corresponding to the bare GC electrodes (Figure 5.15a) indicates a Nernstian peak separation of approximately 64 mV, as would be expected for a reversible, diffusion controlled single electron transfer process. In contrast, very little faradaic response is observed for the PPD coated electrode, confirming the presence of an insulating polymeric layer (Figure 5.15b). Interrogation of the ultrasonically ablated microelectrode array sensors revealed a sigmoidal response, suggesting a hemispherical diffusion profile typically associated with microelectrode constructions (Zoski, 2007). Theory predicts that for an ideal microelectrode, the oxidative and reductive sweeps will overlay perfectly, however it can be seen that in Figure 5.15c, there is some separation of the forward and reverse sweeps. This is a consequence of the chaotic nature of the cavitation process, whereby microelectrode pores are positioned randomly across a sensor surface.

ศูนย์วิจัยทรัพยากร

จุฬาลงกรณ์มหาวิทยาลัย

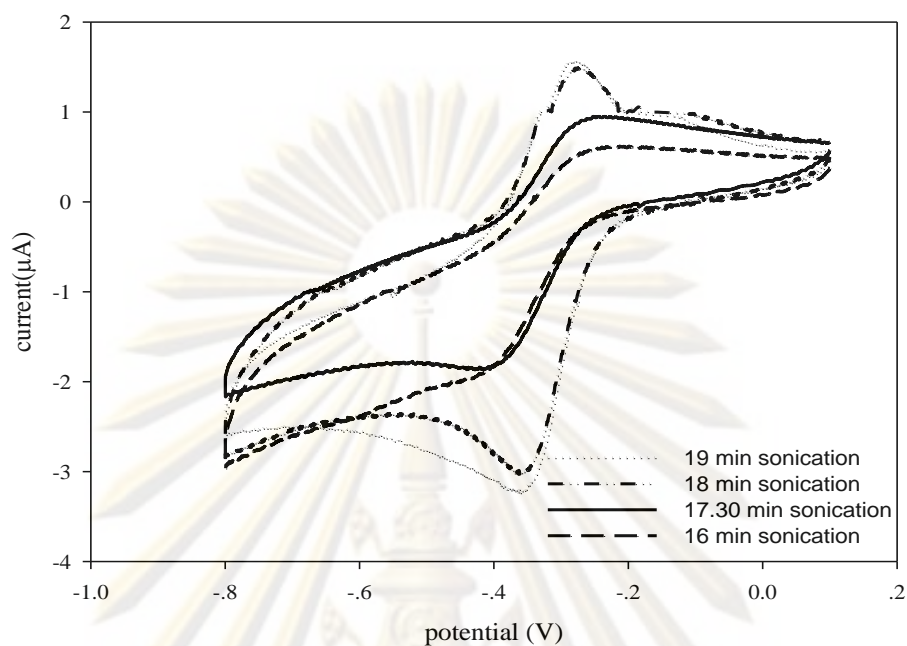


Figure 5.13 Cyclic voltammetry of 5 mM hexaammineruthenium(III)chloride of the sonochemically ablation PPD coated GC electrode at various sonication time at scan rate 20 mVs^{-1} .

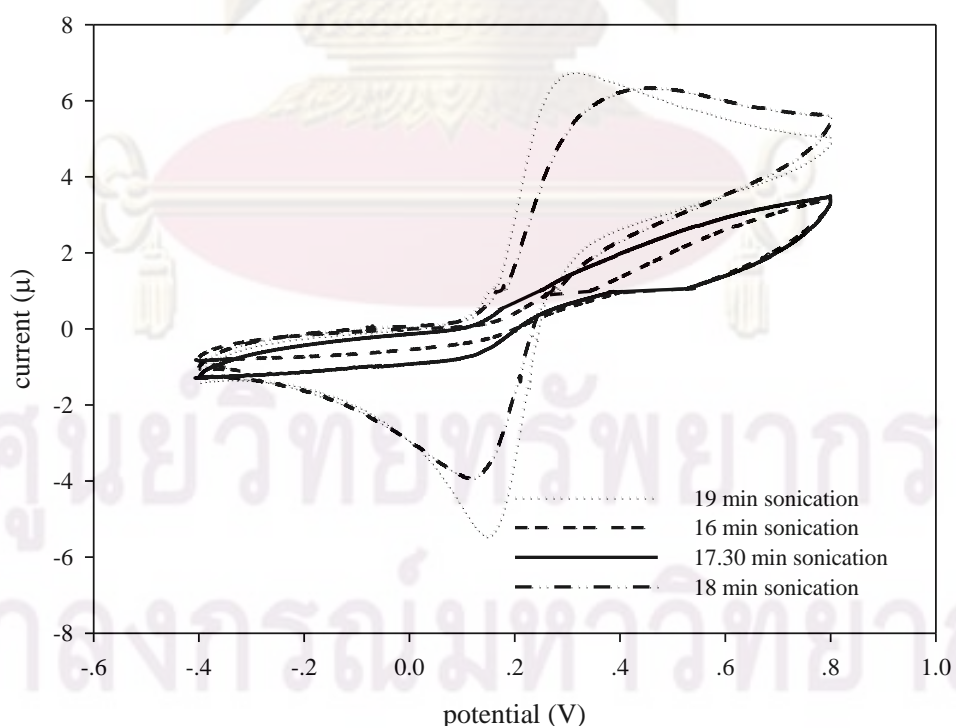


Figure 5.14 Cyclic voltammetry of 5 mM ferrocenecarboxylic acid of the sonochemically ablation PPD coated GC electrode at various sonication time at scan rate 20 mVs^{-1} .

Particularly for $[\text{Fc}(\text{CO}_2\text{H})^{3+/2+}]$ species, the shape of the voltammograms achieved at 17.30 min could be described as near to a sigmoidal shape since there appears to be only one plateau in the anodic region (Figure 5.16). However, this does not necessarily directly relates to whether the array exhibits true microelectrode behaviour or not. The presence or lack of a reverse plateau is a function of the rate of regeneration of the redox couple with respect to its consumption. This is dependent on the balance between factors such as the electrode kinetics, the thickness (and geometry) of the diffusion layer, and the scan rate, and possibly other influences including localised concentrations of both the reduced and oxidised species within the sonochemically formed microelectrode (Gornall, 2004). Since a plateau (in either region) is indicative of lack of diffusion control, kinetics acting as the rate limiting step in either the cathodic or anodic transient sweep can be considered an appropriate indicator for microelectrode behavior.

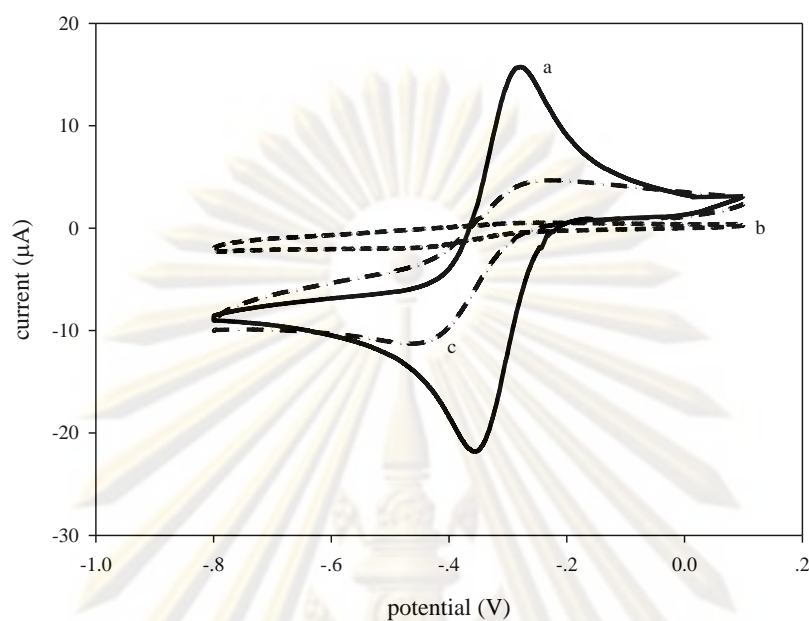


Figure 5.15 Cyclic voltammetry of 5 mM hexaammineruthenium (III) chloride at (a) a bare GC electrode (b) a PPD coated GC electrode and (c) a PPD coated electrode subsequently sonicated for 17.30 min at scan rate 20 mVs^{-1} .

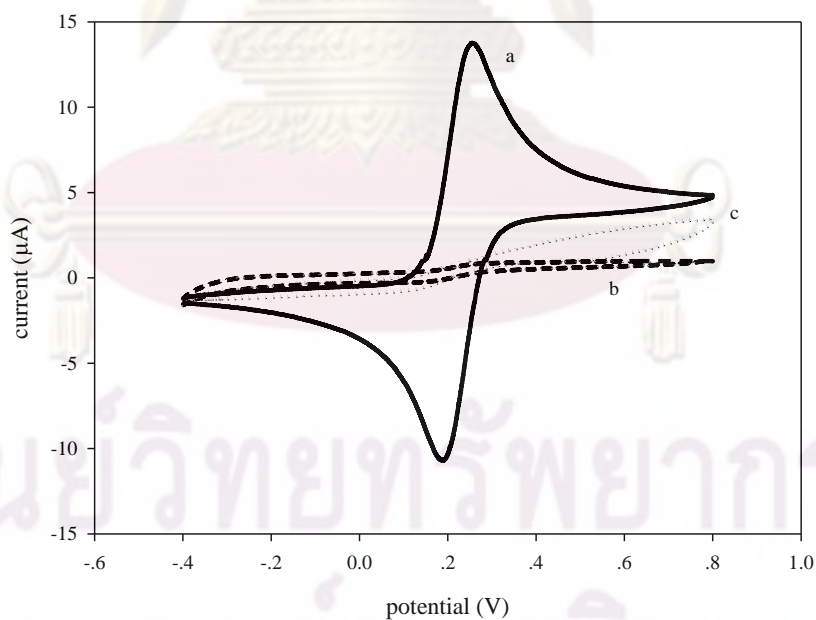


Figure 5.16 Cyclic voltammetry of 5 mM ferrocenecarboxylic acid at (a) a bare GC electrode (b) a PPD coated GC electrode and (c) a PPD coated electrode subsequently sonicated for 17.30 min at scan rate 20 mVs^{-1} .

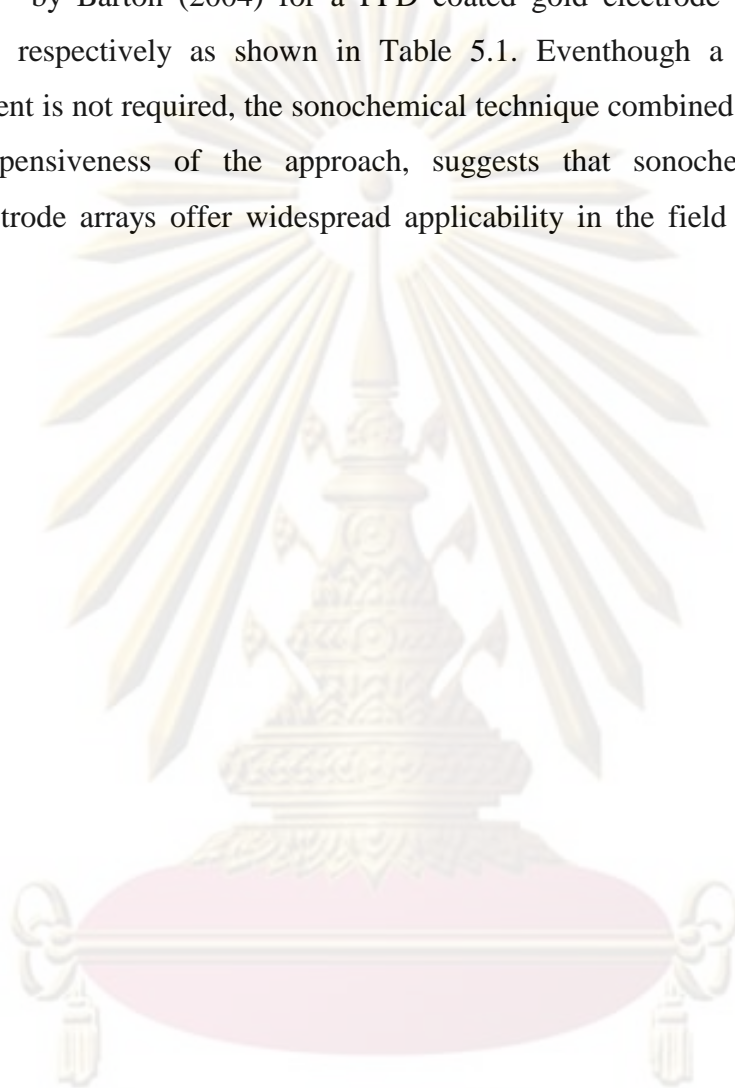
5.1.2.4 Microscopic characterization of microelectrode arrays

The scanning electron micrograph was also applied for microelectrode arrays surface characterization for the different sonochemical ablation times (Figure 5.17). By comparison with the PPD coated GC electrode (Figure 5.7a), the micro-sized pores may clearly be seen within the surface of the polymer film in all ranges of the sonication time. The distribution of pores is random since ultrasonic cavitation is a chaotic process. There appeared to get larger and higher in density of pores at longer sonication time, confirming the voltammogram in Figure 5.13 and 5.14, which the higher responses were obtained at the longer sonochemical ablation time

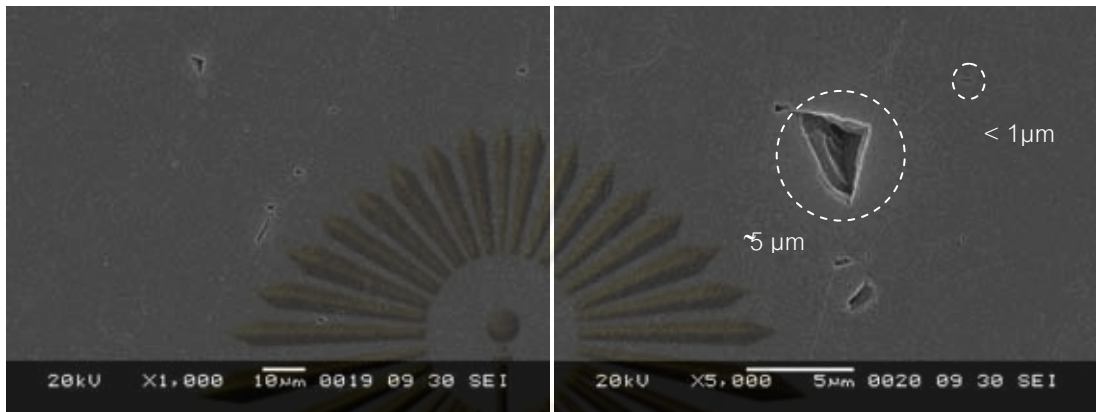
It also appeared that most of the cavities were of bimodal sizes, possessing either micron diameters μm (around 4-5 μm) or sub- μm (around 0.5 μm) structures found at 16 and 17.30 min of sonication times. There was little evidence of cavities with diameters falling in between this range. It is likely that the smallest of the cavities observed were formed by the initial impact of the micro-jets of fluid which were expelled following the collapse of vapour bubbles within the water (Suslick, 1990). These initial cavities were known to act as nucleation sites for the formation of further bubbles (Suslick, 1990). The cavity would then grow as new bubbles implode within the confines of the original cavity, giving rise to an enlargement in the diameter of the cavity. Moreover, the large pore size (around 10 μm) is presented at higher sonication time (18 and 19 min), it is suggested that pores can continue being the nucleation site for further cavitation. In contrast to other reports (Myler et al., 2000, Barton et al. 2004), round-edged pores were not achieved in our case. Instead, sharp-edged geometric forms were detected which possibly indicated the more brittle PPD film obtained on glassy carbon surface in comparison to those of others. However, further investigation is needed before any solid conclusion could be drawn.

The pore density was estimated from the SEM image to be about 5×10^4 pores cm^{-2} in 16 min of sonication for estimated micron size (around 5 μm). The companion size at 17.30 min, 18 min, and 19 min of sonication are expounded the approximate population density 7×10^4 , 6×10^4 , and 21×10^4 pore cm^{-2} . For the sub-micron size at different sonication times 16, 17, 18, and 19 min were presented in 14×10^4 , 17×10^4 , 15×10^4 , and 37×10^4 pores cm^{-2} , respectively. Furthermore, appraised 10 μm

pore sizes are acquired at 18 and 19 min of sonication. This is in good agreement to the population density of 8×10^4 pores cm^{-2} calculated by Myler (2000) and 7×10^4 pores cm^{-2} by Barton (2004) for a PPD coated gold electrode and screen printed electrode, respectively as shown in Table 5.1. Eventhough a defined geometric arrangement is not required, the sonochemical technique combined with the simplicity and inexpensiveness of the approach, suggests that sonochemically fabricated microelectrode arrays offer widespread applicability in the field of electrochemical sensors.



ศูนย์วิจัยทรัพยากร
จุฬาลงกรณ์มหาวิทยาลัย

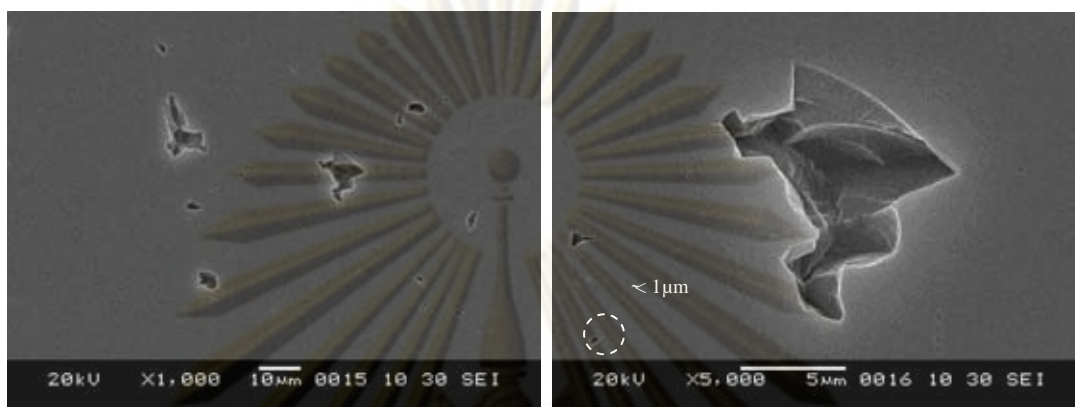


(a) 16 min

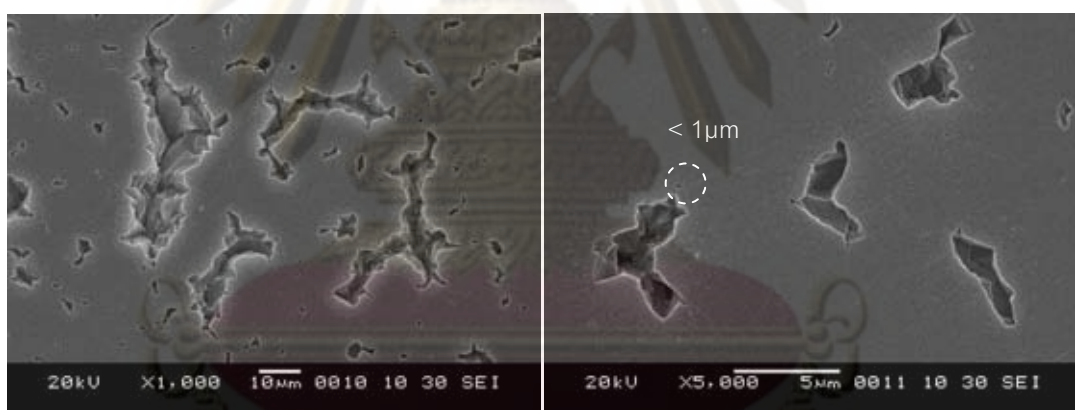


(b) 17.30 min

ศูนย์วิทยทรัพยากร
จุฬาลงกรณ์มหาวิทยาลัย



(c) 18 min



(d) 19 min

Figure 5.17 Scanning electron micrographs of GC electrode coated with PPD at (a) 16 min, (b) 17.30 min, (c) 18 min, and (d) 19 min of sonication in water at 35 kHz.

จุฬาลงกรณ์มหาวิทยาลัย

Table 5.1 Summary of the effect of sonication time

	Sonication time (min)	Pore size (μm)	Density (pore cm^{-2})
This work (GC)	16	< 1	14×10^4
		~5	5×10^4
	17.30	< 1	17×10^4
		~5	7×10^4
	18	< 1	15×10^4
		~5	6×10^4
		~10	NA
	19	< 1	37×10^4
		~5	21×10^4
~10		NA	
Myler et al., 2000 (Gold coated glass slide)	1	~3 - 4	7×10^4
Barton et al., 2004 (Gold coated glass slide)	1	~3 - 4	7×10^4
Prichard et al., 2004 (Screen printed)	20 (sec)	~4	2×10^4

ศูนย์วิทยทรัพยากร
จุฬาลงกรณ์มหาวิทยาลัย

5.1.2.5 Characterization and reproducibility

This research investigated the microelectrode arrays by using GC electrode which has never been reported elsewhere. PPD films of about 30 nm thickness were formed on the surfaces of GC electrodes via the electropolymerisation of *o*-phenylenediamine. The microelectrode arrays were then formed by sonochemical ablation of the PPD films to expose microscopic areas of the underlying conductive substrates. Five electrodes were selected for the reusability investigation. Calibration curves for hexaammineruthenium(III) chloride and ferrocenecarboxylic acid plotted using final current value is presented by amperometric response in Figures 5.19 and 5.20, respectively, error bars are also shown with these plots. These calibration curve represented good microelectrode behavior (Gornall, 2004). For example, for a concentration of 5 mM hexaammineruthenium(III) chloride (the concentration at which maximum error occurs), these microelectrode arrays showed the reproducibility of 3.15% relative standard deviation (RSD) (Figure 5.21). For the same concentration of ferrocenecarboxylic acid the reproducibility was determined at 7.87% RSD. The similar result was obtained from the Barton et al. (2004) report, which achieved 6.8% RSD by using the same technique. This showed good reproducibility can be obtained by using sonochemically fabrication technique to produce microelectrode arrays.

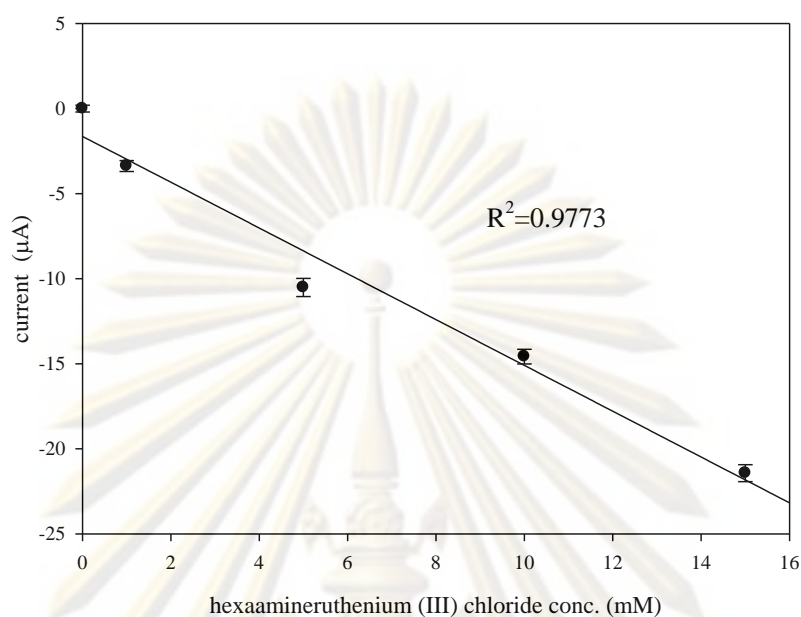


Figure 5.18 Calibration curves of current resulting from the amperometric reduction of hexaammineruthenium (III) chloride at sonochemically fabricated microelectrode arrays 17.30 min at the potential -40 mV

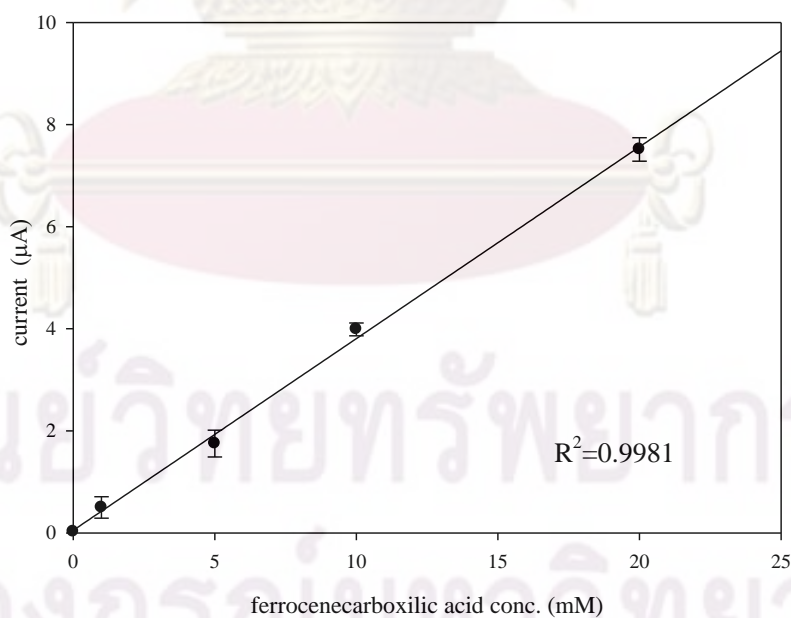


Figure 5.19 Calibration curves of current resulting from the amperometric reduction of ferrocenecarboxylic acid at sonochemically fabricated microelectrode arrays 17.30 min at the potential 35 mV

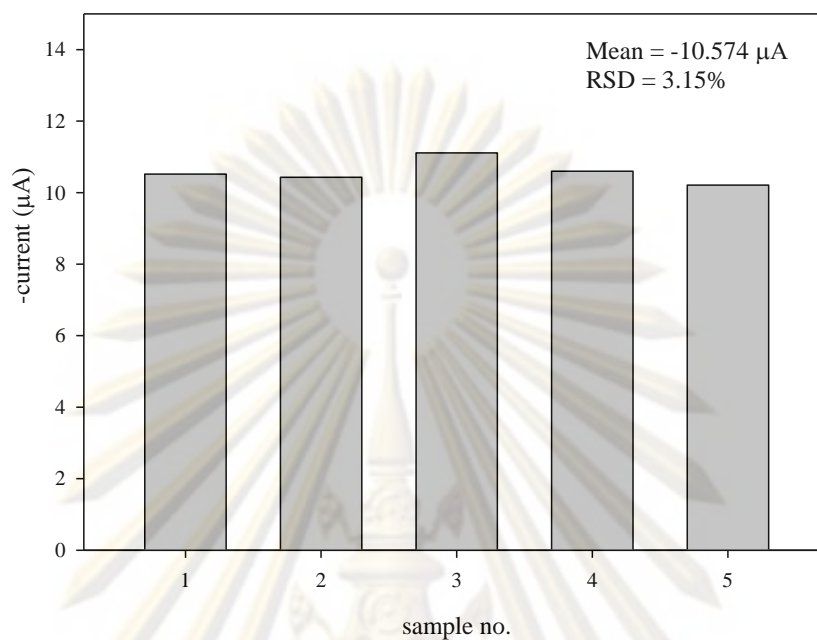


Figure 5.20 Comparison of the negative current in 5 mM hexaammineruthenium (III) chloride for different 17.30 min of sonochemically ablation on PPD modified electrode at -40 mV

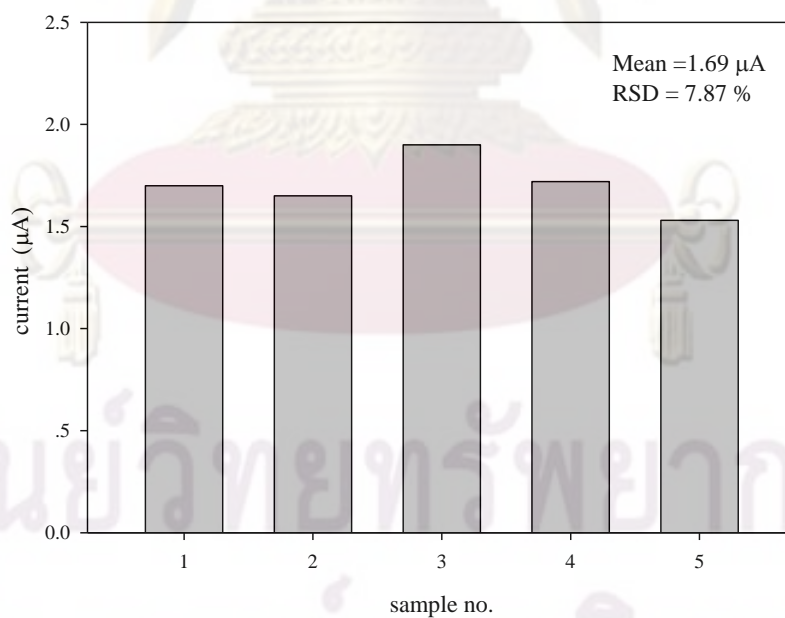


Figure 5.21 Comparison of the negative current in 5 mM ferrocenecarboxylic acid for different 17.30 min of sonochemically ablation on PPD modified electrode at 50 mV

From these result, the excellent reproducibility can be obtained for microelectrode arrays production by the sonochemical fabrication approach. Furthermore, there is the various technique for improve the reproducibility of microelectrode arrays. For sonochemically fabrication method to produced microelectrode array, theory suggests that increased homogeneity of ultrasonic power intensity is also entirely achievable. For example, Mason (1999) has reported that the homogeneity in an ultrasound tank may be improved by the addition of 1 or 2% surfactant. This may reduce the surface tension of the water and permit more cavitation.

5.2 PANI/HRP microelectrode arrays

5.2.1 Planar electrode

The electropolymerisation conditions and sonochemical technique for microelectrode arrays have already been optimized. Using the optimal conditions for PPD coated and microelectrode array fabrication by sonochemically technique from the previous sections would suggest a perfectly microelectrode arrays for enzyme microelectrode arrays formation.

Horseradish peroxidase (HRP) has been widely studied for the construction of hydrogen peroxide biosensor (Seo, et al., 2007) and phenol biosensors (Ruzgas et al., 1995, Mello et al., 2003, Kafi et al., 2009). There are a few reports available on preparation of modified electrode attending with the immobilization of HRP and conducting polymer. As the poly-aniline (PANI) is the one of the promising conducting polymer since its electrochromic behaviour. PANI has been extensively applied for microelectrode arrays for pesticides biosensors (Pritchard et al., 2004) and glucose oxidase biosensors (Myler et al., 2004). The custom built PANI and HRP microelectrode arrays are specially modified onto the microelectrode arrays based with the assuming diagram as show the schematically in Figure 5.22. This based on the nature of horseradish peroxidase ($pI = 7.2$) and aniline radical which would present the positive charge in the solution (acetate buffer pH 5.5), HRP and aniline

radical may electrodeposited together during scanning potential sweep, the HRP possibly scatter in the polymer film.

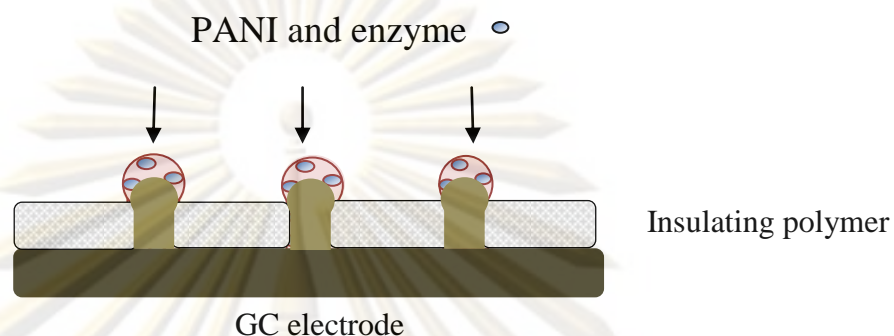


Figure 5.22 The schematic of sonochemical ablation formation of microelectrode arrays

5.2.1.1 Electropolymerisation of aniline

In this work, poly-aniline solution containing HRP enzyme pH 5.5 was firstly electrodeposited onto GC electrode surfaces by 20 cycles between -0.2 V and +0.8 V (Barton et al., 2004). Perversely optimum pH for HRP activity is 5.5 (Panwittayakool, 2008), the appropriate pH 5.5 used for the polymer and HRP electropolymerisation in this work. Previous works have indicated that optimal conditions for poly-aniline deposition with acidic solution. An electroconductive aniline is finest electrodeposited when the process is obtained under strongly acidic condition pH 1 (Barton et al., 2004). Previous works have indicated that optimal conditions for poly-aniline deposition include a potential between -0.2 V and 0.7 to 1.2 V along with acidic solution pH and ensured electroconductivity of the final polymer as poly-aniline is not electroconductive if prepared at neutral or basic pH (Pritchard et al., 2004). Garifallou et al.(2007) had reported the pH range used varied from pH 3.7 down to pH 1 and it was found that electroconductive aniline was best when obtained at pH 1.

Deng and Berkel (1999) have proposed the electropolymerisation mechanism of aniline (Figure 5.24). The aniline oligomers are formed via a series of oxidation/addition reactions starting with the oxidation of aniline to the radical cation

followed by monomer radical coupling to form the head-to-tail (C), tail-to-tail (D), and/or the head-to-head (E) which are the same mechanism in the polymerization of aromatic amine. The dimers in turn are oxidized (to form (C1), (D1), and (E1), respectively) and grow to larger n -mers via addition of aniline to form the trimer (F and F1) or addition of another dimer molecule to form the tetramer (G and G1). However, it has been shown that the proportion of the three dimers formed depends on a number of experimental conditions including aniline concentration and, in particular, pH. Note that polymer growth in Figure 5.23 is most often reported as the major dimeric product of aniline electropolymerisation in acidic aqueous solution.

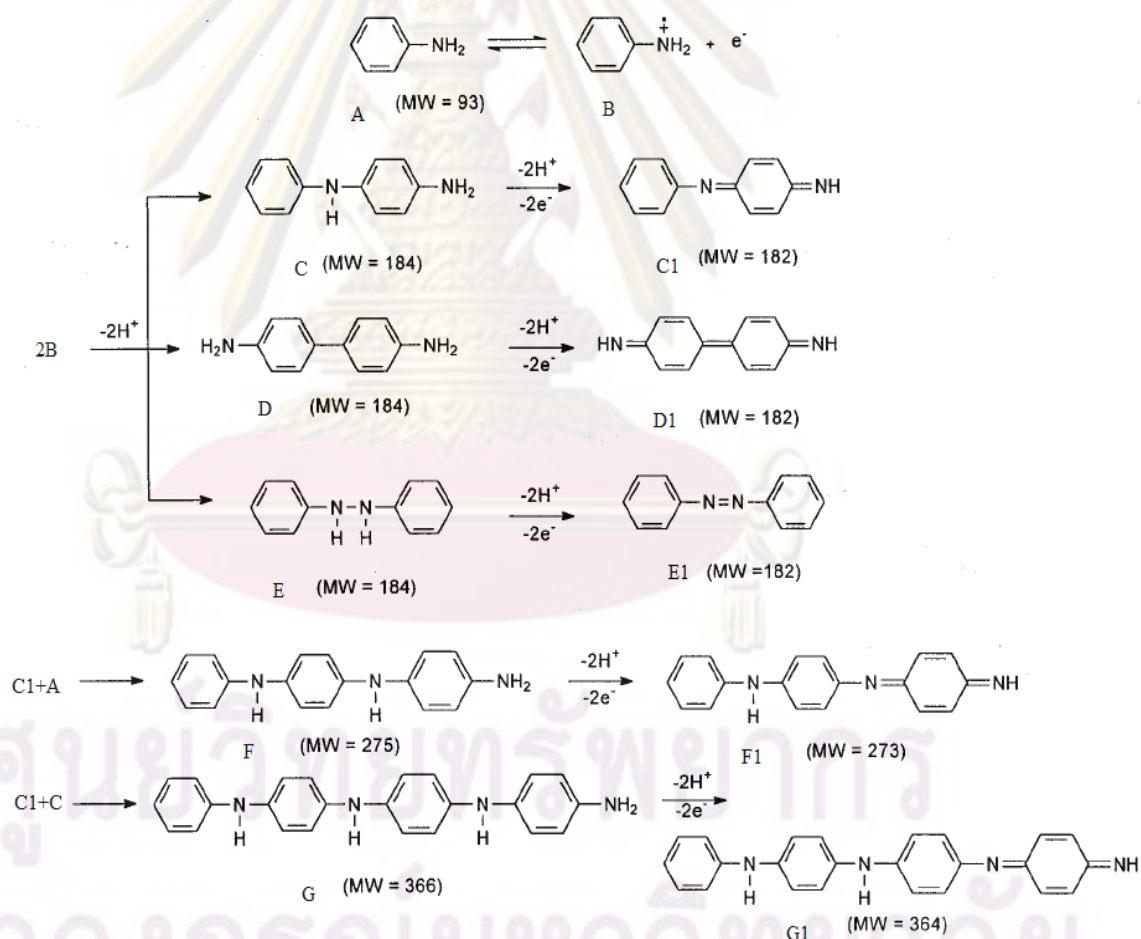


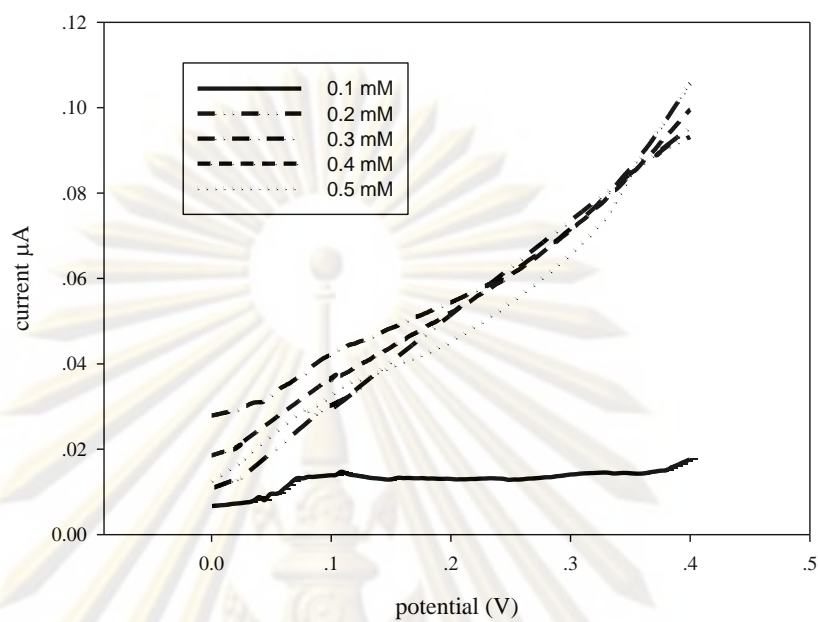
Figure 5.23 Schematic representation of the aniline polymerisation mechanism proposed by Deng and Berkel (1999)

5.2.1.2 The effect of aniline concentration for the HRP/PANI electropolymerization

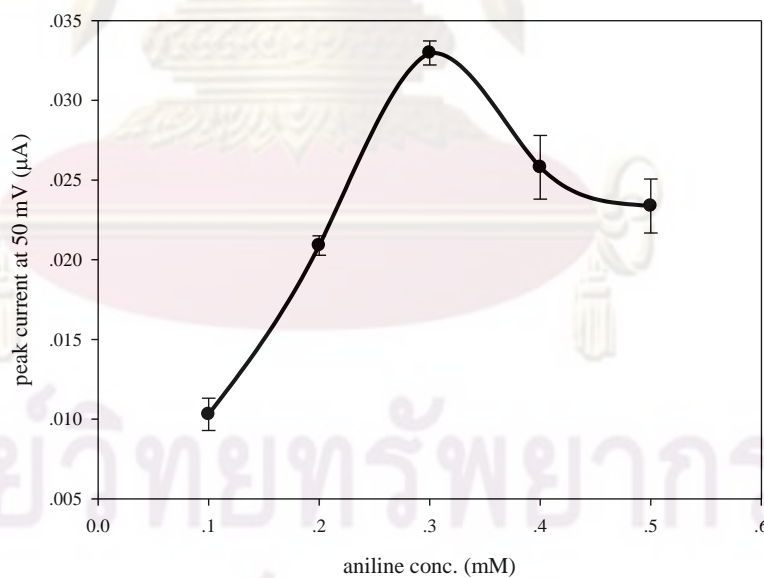
Since none of previous reports circumstantiated an electrodeposition of HRP/PANI, the optimum condition for electrodeposition of HRP/PANI compound were firstly studied on bare GC electrode between -200 to 800 mV of potential sweep scan rate 20 mVs^{-1} for 20 cycle (Barton et al., 2004). The various aniline concentrations (0.1-0.5 mM) pH 5.5 acetate buffer were determined by fixing HRP concentration at 500 Uml^{-1} . The linear sweep at different aniline concentration in the presence of H_2O_2 and phenol at H:P ratio 0.7 (Rosatto et al., 1000) is shown in Figure 5.24a. Furthermore, the current exhibition at 50 mV presented in Figures 5.24b suggest the 0.3 mM aniline is achieved the high current at 50 mV $0.033 \mu\text{A}$. At the low monomer concentrations (0.1mM) did not allow sufficient polymer formation and HRP entrapment onto the electrode surface to give a response in the phenol concentration studied. Higher monomer concentrations may affect the mass transfer due to the lower flexibility. Furthermore, the monomer can be precipitated which not sufficient to polymerised since the high monomer concentration.

5.2.1.3 Effect of HRP concentration

The HRP concentration is an important condition for the microelectrode arrays optimization. From the former research found the lower sensitivity might be attributed to the high biocomponent loading in the electropolymerized solution, since severe problems with polymer formation (poor adhesion, poor monomer polymerization yield) occur in the presence of high protein (HRP) concentration (Schuhmann et al., 1997). The chosen concentration range ($100\text{-}1000 \text{ U ml}^{-1}$) was carefully studied on bare GC electrode with 0.3 mM aniline. Figure 5.25a displayed the linear sweep of modified electrode in hydrogen peroxide and phenol solution. Similarly, the 50 mV current is presented in Figure 5.25b. Consistent in current at 50 mV of different concentration is appearance.



(a)



(b)

Figure 5.24 Linear sweep of HRP/PANI coated GC electrode (a) and 50 mV peak current at various aniline concentration at 500 Uml^{-1} HRP in Hydrogen peroxide: Phenol concentration ration (H:P) 0.35 (Rosatto et al., 1999) at scan rate 20 mVs^{-1}

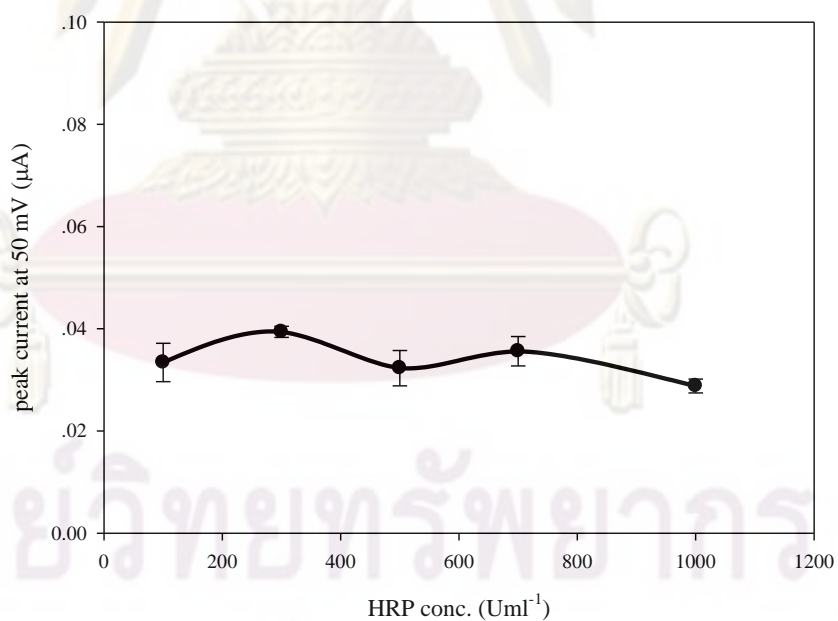
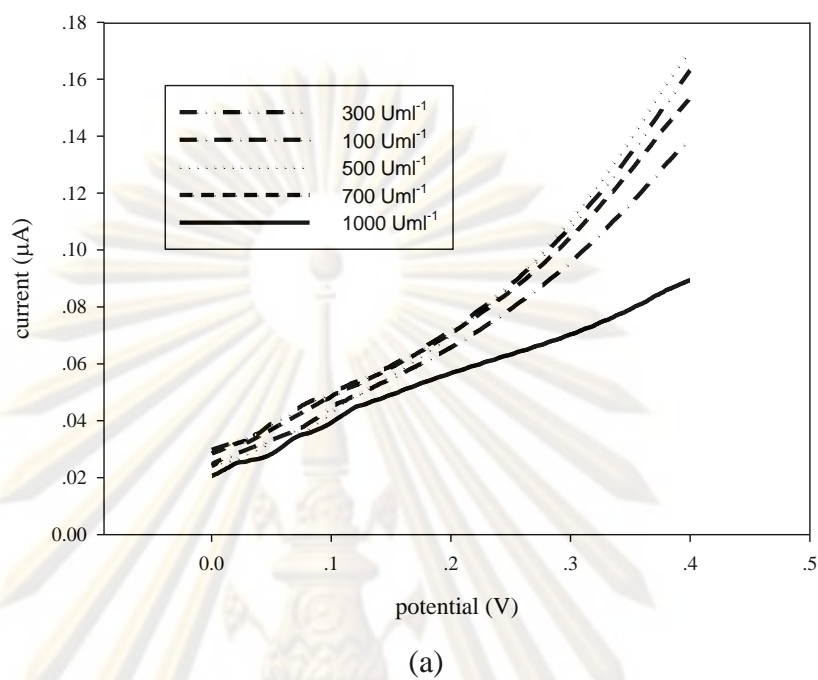


Figure 5.25 Linear sweep of HRP/PANI coated GC electrode (a) and 50 mV peak current at various HRP concentration at 0.3 mM aniline concentration in Hydrogen peroxide: Phenol concentration ration (H:P) 0.35(Rosatto et al., 1999) at scan rate 20 mVs^{-1}

From the Figure 5.25 the increasing in HRP concentration seems insignificantly effect the enzyme activity with phenol concentration which in agreement of Schuhmann et al. (1997). Moreover, the increasing concentration of enzyme in the deposition solution, the nucleophilic side chains at the enzyme interfere with the polymer growth due to the attack at the intermediate radical cations. Hence, at high enzyme concentrations either film formation fails or the deposition time is long, leading to films with dramatically changed morphology. Moreover, since this was investigated at planar electrode which the mass transfer limit may occurred.

However, 300 Uml⁻¹ HRP suggested a good current result since the higher current and small error is appeared. Furthermore, this make certain of the enough amount of enzyme deposited which help avoid the effect that pointed out above.

5.2.2 Microelectrode array

5.2.2.1 The HRP/PANI microelectrode arrays fabrication

For the PPD/HRP/PANI microelectrode arrays ablation, 0.3 mM aniline containing 300U ml⁻¹ HRP in acetate buffer pH 5.5 was deposited onto 17.30 min sonochemically modified electrode surfaces by 20 continuous potential sweeps between -0.2 V and +0.8 V. Figures 5.26 shows the voltammograms obtained from electrochemical deposition of aniline/HRP on modified GC electrodes. It is obviously seen that with the deposition cycle, the peak current observed increases. This is due to the increase of the conductive surface area from accumulation of poly-aniline layers on the electrode surface with each potential sweep following the mechanism in Figure 5.23. While initially the conductivity of coated electrodes is seen to increase, it must be understood that a high number of consecutive potential sweeps will become a limiting factor and the cumulative conductivity through the polymer will start decreasing. This can be explained as the polymer film becomes thicker with each sweep in agreement with results obtained by Tsekenis *et al.*, (2008). However, the peak current seems no increasing at eventual of deposition. The complimentary result was exhibit at non conductive condition for aniline electrodeposition on gold electrode by Tsekenis *et al.*, (2008).

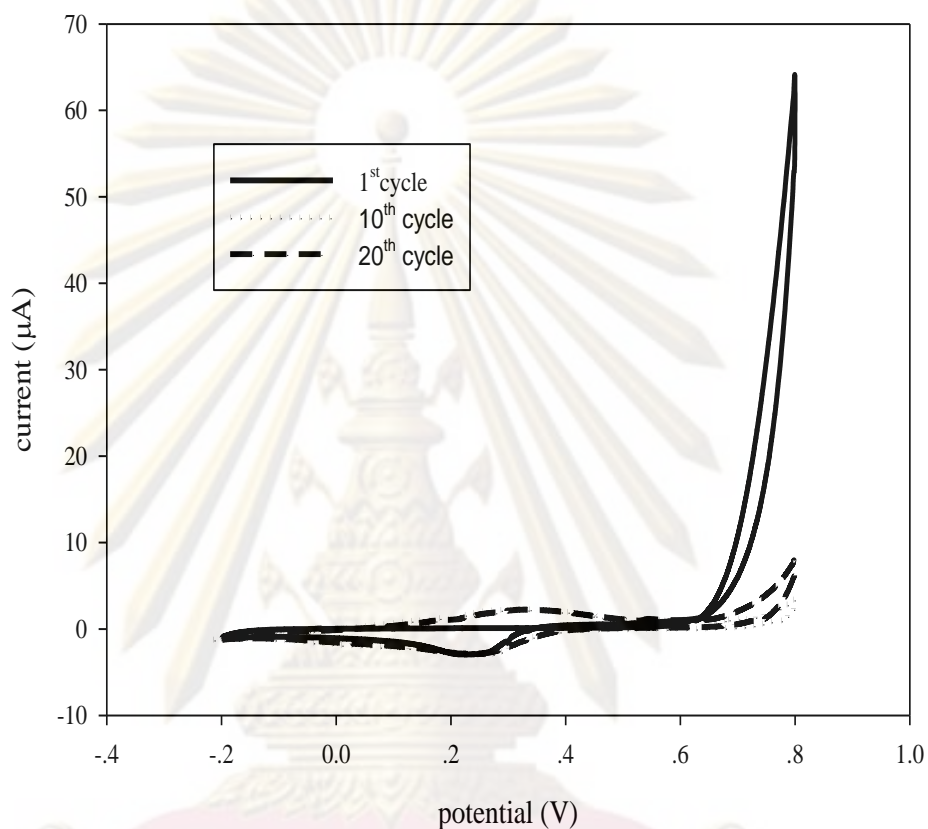
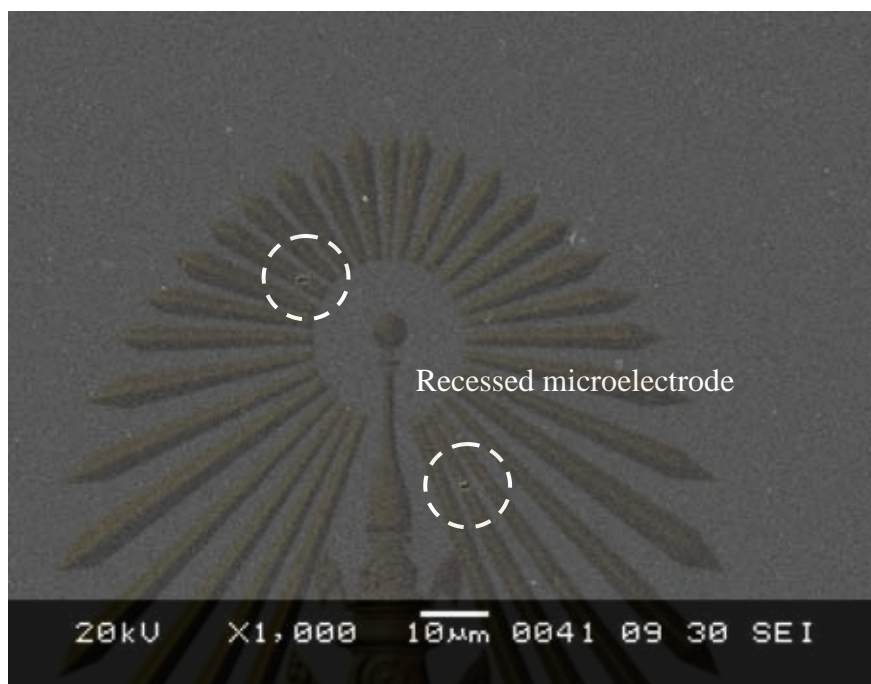
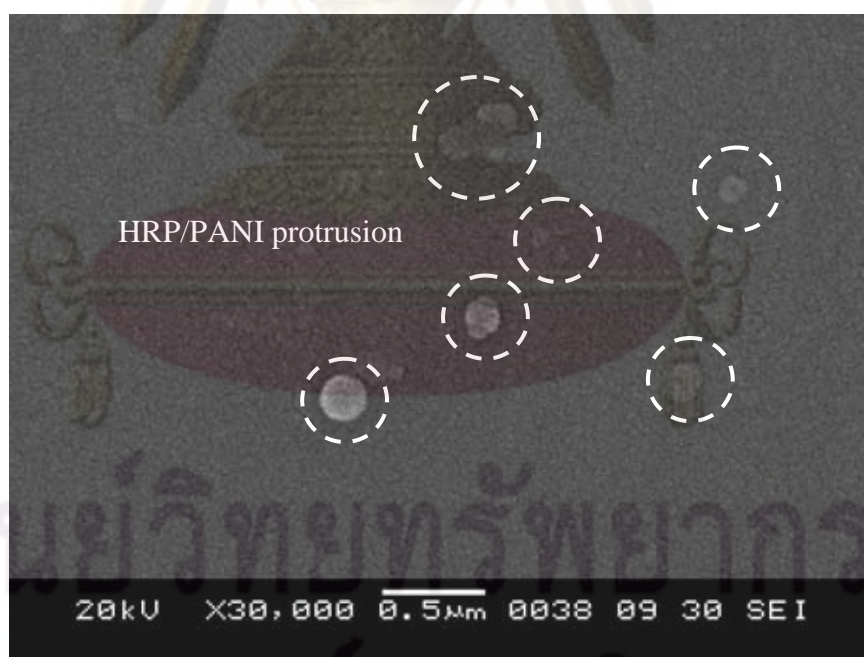


Figure 5.26 Electrochemical deposition (-0.2 V to 0.8 V) of 0.3 mM aniline/ 300 Uml^{-1} HRP electrodeposition on a PPD modified GC electrode in acetate buffer pH 5.5 at scan rate 20 mVs^{-1}

Confirming the HRP/PANI electrodeposited on sonochemically modified GC electrode using the SEM image (Figure 5.27). The HRP /PANI were formed the protrusion at the microelectrode cavities. These protrusions were found in very small sizes ($\sim 0.5 \mu\text{m}$) which suggest the longer in polymerization time may require completing the recessed microelectrode arrays (Figure 5.27a).



(a)

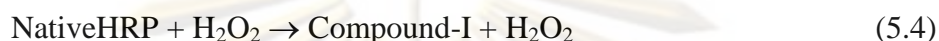


(b)

Figure 5.27 Scanning electron micrographs of PPD/HRP/PANI microelectrode arrays.

5.2.2.2 HRP for phenol detection mechanism

Linear sweeps using a hydrogen peroxide:phenol in acetate buffer (pH 5.5) was used to investigate the electroconductivity of the PPD/HRP/PANI microelectrode arrays. The phenol reaction mechanisms are as follows (Ruzgus et al., 1995):



The HRP is firstly oxidised by H_2O_2 forming compound-I (equation (5.4)) which can then be reduced by phenol resulting in Compound-II and phenol radical (equation (5.5)). Native HRP is then achieved after the reduction of Compound-II with another molecule of phenol (equation (5.6)). Thus, phenol acts as an electron mediator which could be electrochemically reduced back to its initial state at the electrode surface. The reduction current, therefore, is expected to be proportional to the concentration of phenol in the solution if direct electron transfer is insignificant.

5.2.2.3 The Effect of hydrogen peroxide concentration

Basically, H_2O_2 concentration is very important to get a good sensitivity of biosensors for phenol detection (Rosatto et al., 1999). Thus, the proper value of H_2O_2 should be perceived for HRP/PANI microelectrode arrays for phenol detection. Figure 5.28 displays the current response at 50 mV of various H_2O_2 concentrations at 1 μM phenol by using the 300 Uml^{-1} HRP/ 0.3 mM aniline for microelectrode arrays production. The high current response was achieved from at 0.5 μM H_2O_2 . Agreeably with the HRP mechanism, which require two mole of phenol for one mole of H_2O_2 .

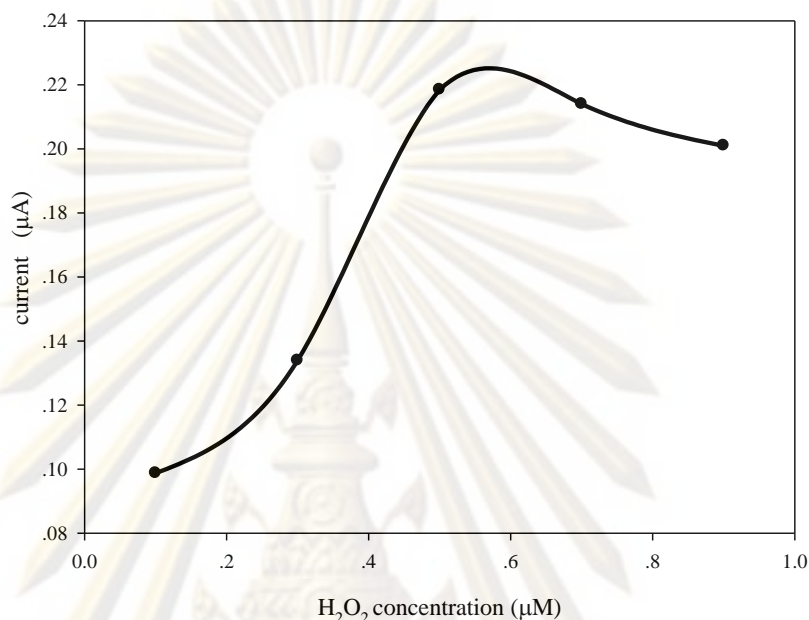


Figure 5.28 Current response at 50 mV of PPD/HRP/PANI microelectrode arrays for various Hydrogen peroxide concentration at 1 μM phenol concentration scan rate 20 mVs^{-1}

5.2.2.4 The PPD/HRP/PANI microelectrode arrays for phenol detection

This research applied phenol for being the model chemical to investigate the microelectrode arrays which modified in the work. Figure 5.29b is the calibration curve for the phenol is made at the H:P ratio 0.7 at 50 mV on the semi-log scale of potential sweep from the linear sweep voltammogram (Figure 5.29a). At 50 mV, the response to acetate at this potential is very small this might improve the reliability of the phenol determination. Furthermore, the most important factor for the determination of phenol is that a consistent potential inclusively used. It should be noted that the current increases as the phenol concentration increase, with maximum current value is obtained at $1 \times 10^{-6} \text{ M}$ phenol. The insignificant differentiation is

displayed in higher phenol concentration than 1×10^{-6} M may be due to the saturated enzyme with substrate at high phenol concentration. Since the phenol concentration range which applied in this research does not show the linear relation with the current response, the kinetic property (Michaelis-Menten constant) may be impracticable determined.

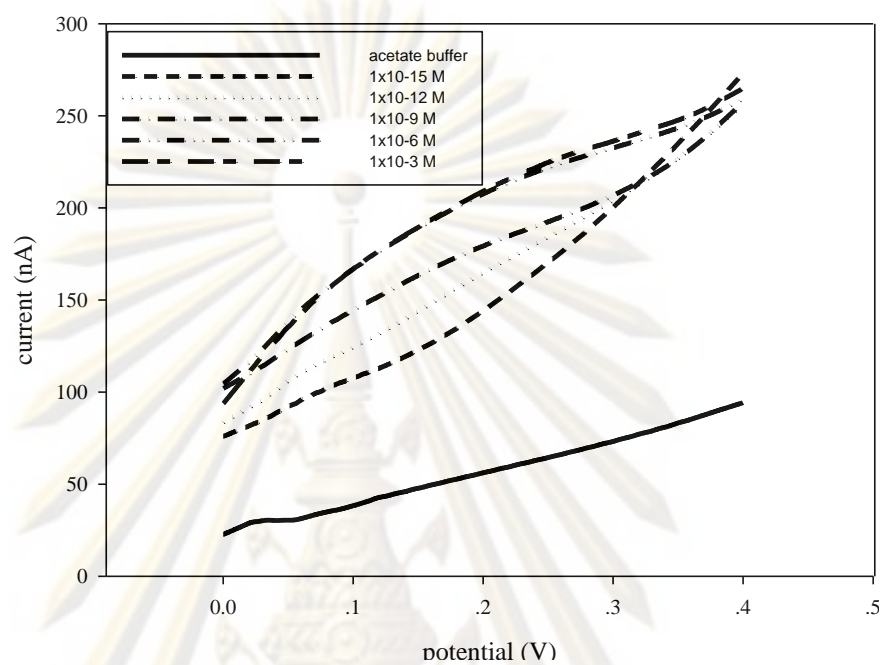
The former sonochemical fabrication for microelectrode arrays were determined the pesticide down to concentration of 1×10^{-17} M by acetylcholinesterase (Pritchard et al., 2004 and Law et al., 2005). From this comprise none of the report for HRP microelectrode array presented the excellent results for phenol detection were obtained with concentration range between 1×10^{-15} and 1×10^{-6} M.

5.3 The PPD/Au/HRP/PANI microelectrode arrays

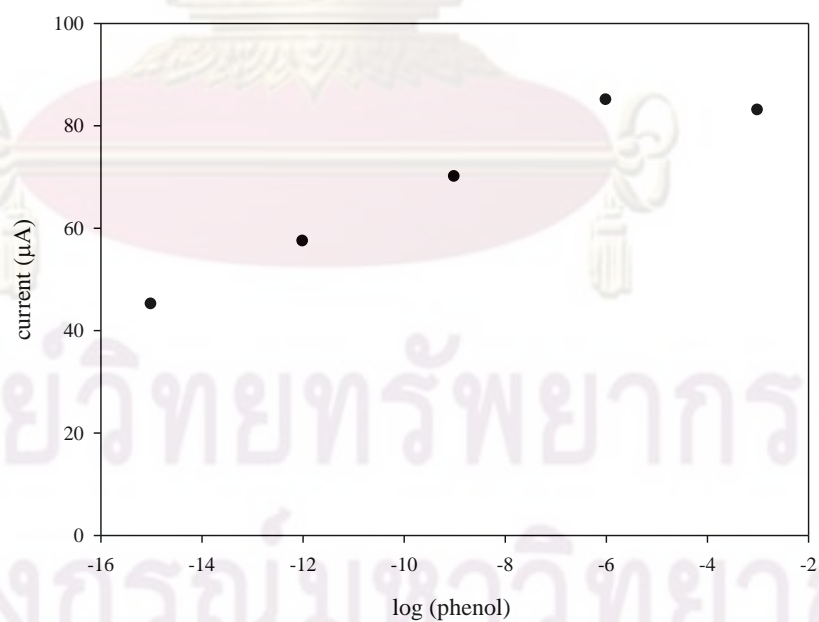
The study of metal particle/conducting polymer composites is interesting for several reasons. First, particles have size and shape dependent properties. Second, the high surface to volume ratio of particles in the composite should result in a large number of binding sites available for chemical sensing or catalysis. Third, the combination of conducting polymers with metallic particles yields materials with new properties (e.g. optical, conducting or catalytic) (Smith et al., 2005).

Much of the research on biosensors involving gold particles has been devoted to enzyme electrodes. There are the unique properties of gold particles, such as good conductivity, useful electrocatalytic ability and biocompatibility, several researchers have been devoted to fabricate electrochemical sensors and biosensors (Granot et al., 2005, Pingarron, et al., 2008).

This study reports on electrochemical synthetic methods and characterization of a new Au/HRP/PANI composite on modified electrode. After sonochemical ablation on PPD coated GC electrode, the 0.5 mM $\text{HAuCl}_4 \cdot 3\text{H}_2\text{O}$ was electrodeposited on the PPD modified electrode before PANI/HRP deposited. The schematic diagram for PPD/Au/HRP/PANI microelectrode arrays is presented in Figure 5.30. Au particle may form the array protrusion in the cavity of the modified electrode.



(a)



(b)

Figure 5.29 Linear sweep of PPD/HRP/PANI microelectrode arrays (a) and 50 mV peak current for various phenol concentration at 0.7 H:P ratio, scan rate 20 mVs^{-1} .

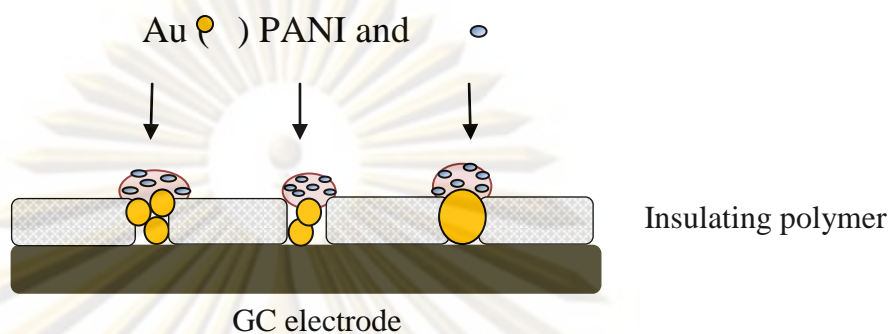
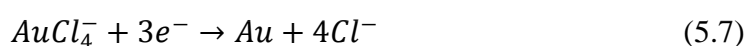


Figure 5.30 The schematic of sonochemical ablation formation of PPD/Au/HRP/PANI microelectrode arrays

5.3.1 Gold particle electrodeposition

In recent years, research efforts on a kind of gold particles deposited for the biosensors have flourished because of their good biological compatibility, excellent conducting capability and high surface-to-volume ratio. The ability of providing a stable immobilization of biomolecules retaining their bioactivity is a major advantage for the preparation of biosensors. There are several reports presented the Au particle composited with poly-aniline by forming the Au particle follow by immersed an electrode into Au particle and polymer solution (Sarma et al., 2002, Yu et al., 1020) Moreover, the Au particles were deposited on PANI thin film by immersion (Sheffer et al., 2009). The deposition of particle separately the polymer matrix achieved the principal advantage resides in the synthetic control possible over both the particles and the matrix (Rosatto et al., 2002). An electrodeposition method is applied for Au particle deposition in this report. Applying voltage induced the Au deposited on the surface by following overall mechanism.



According to this mechanism two charge transfer steps coupled are involved with a preceding chemical reaction



In this research, Au particles were electrodeposited on to the modified microelectrode arrays at -200 mV potential for 30 sec to prevent in particle sizes and quantity. The cyclic voltammetry of Au particle arrays was displayed in Figure 5.31 by using 5 mM ferri/ferro cyanide since no changing in the signal response for the hexaammineruthenium (III) chloride and ferrocenecarboxylic acid (data not show). The sigmoidal was clearly observed even show forward plateau, as described before that this does not directly relate to the array exhibits none microelectrode behaviour. Moreover, in the 5 samples of Au microelectrode arrays which were investigated in the cyclic voltammetry have been show the relative standard deviation 8.17% which slightly higher than the microelectrode arrays achieved from the sonochemically ablation (Figure 5.32).

Furthermore, the microscopic behaviour of Au particles on the microarrays modified electrode is displayed in Figure 5.33. The spherical model of Au particles were furnished in the sonochemical pore arrays, the distribution of the particle is 0.5 – 1 μm . The SEM images show the particles can accumulate more than one in the micro arrays cavities depended on the size of the cavity.

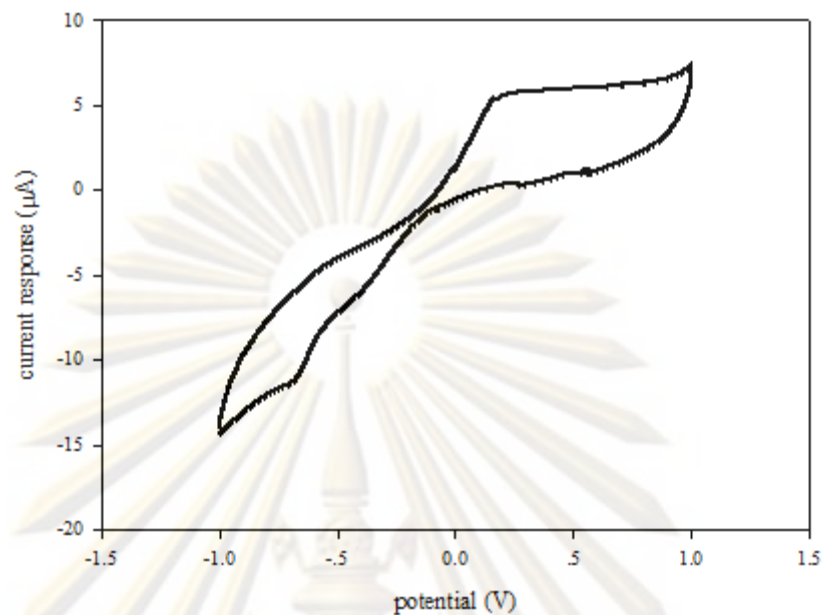


Figure 5.31 Cyclic voltammetry of 5 mM ferri/ferro cyanide of Au particle microelectrode arrays at the electrodeposition time 30 sec, -20 mV.

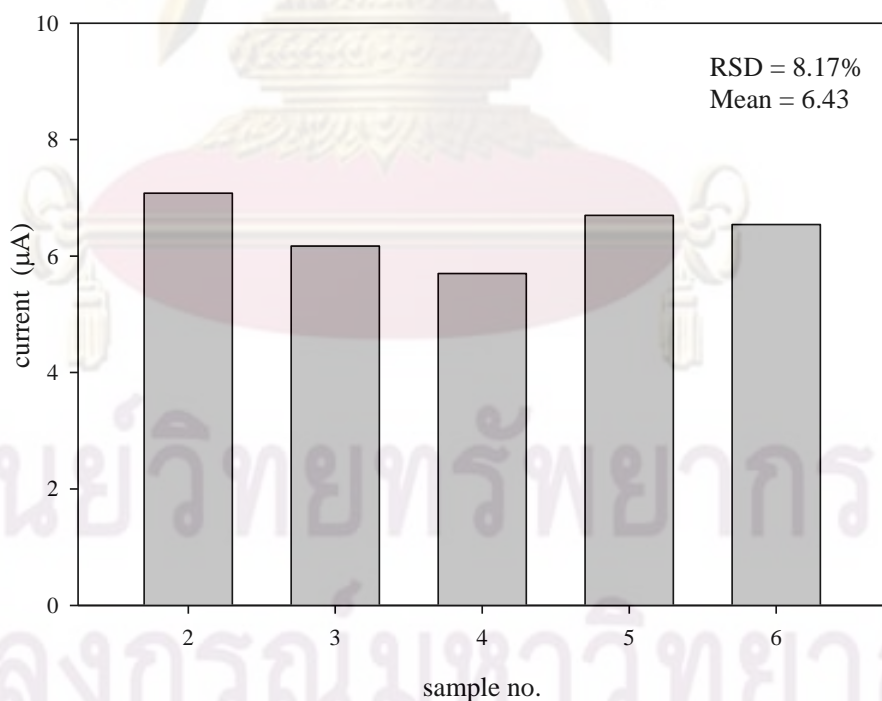
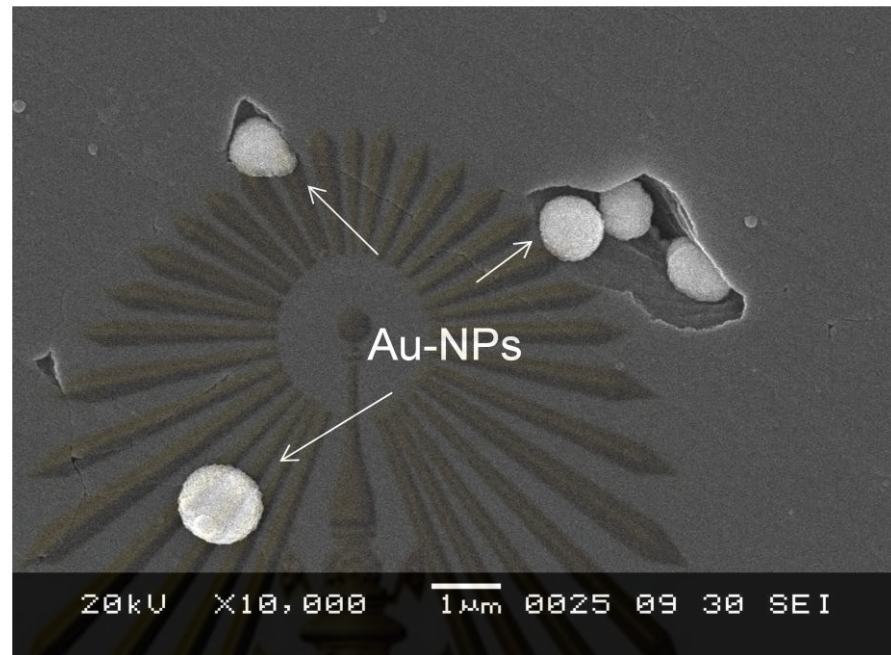
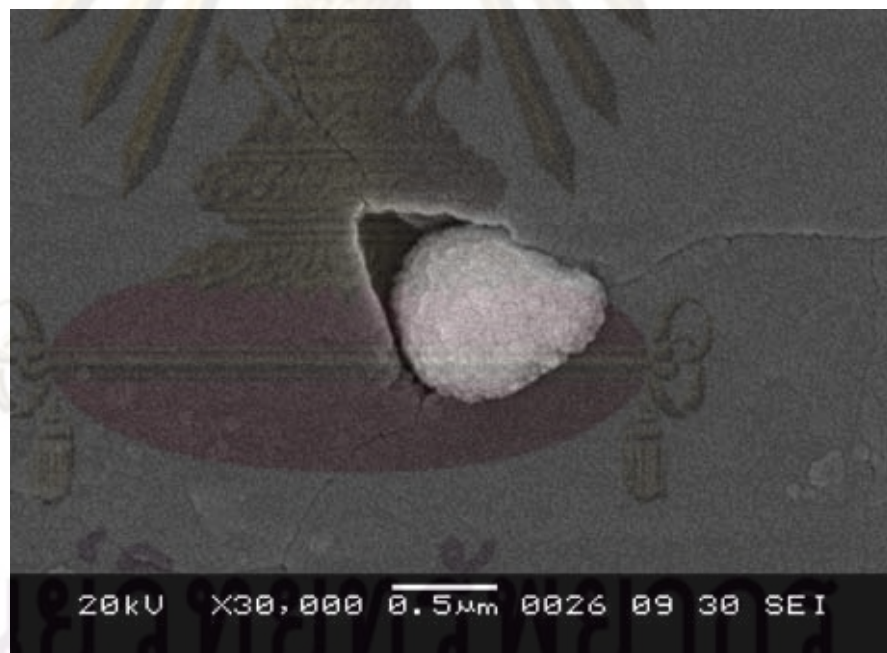


Figure 5.32 Comparison of the current response in 5 mM ferri/ferro cyanide of Au particle microelectrode arrays at the electrodeposition time 30 sec, -20 mV.



(a)



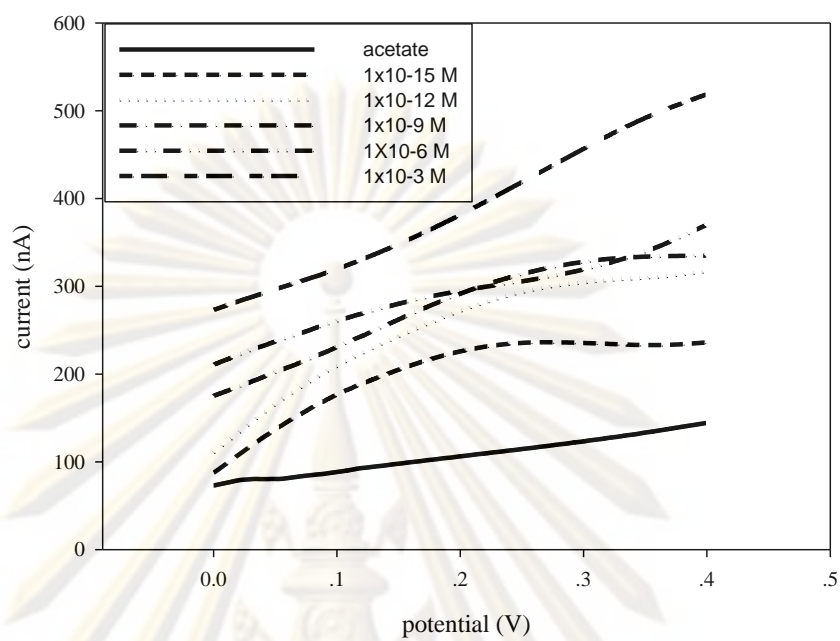
(b)

Figure 5.33 Scanning electron micrographs of Au particles on micro arrays cavities

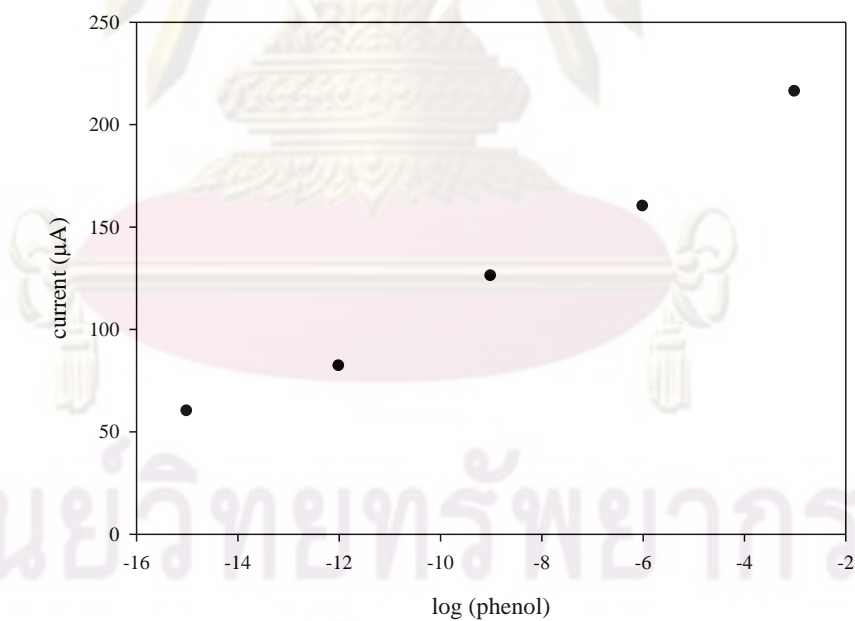
5.3.2 The PPD/Au/HRP/PANI microelectrode arrays for phenol detection

The investigations were carried out to determine the phenol in solution. In order to compare the responses of electrodes fabricated within this work (with and without gold particle modified electrode), the sonochemically fabricated microelectrode array sensors prepared under the similar conditions. For their response to a range of phenol concentrations from 1×10^{-15} M to 1×10^{-3} M were determined by linear sweep (Figure 5.34a). Representative calibration graph is shown in Figure 5.34b.

Good response characteristics are obtained with changes in the concentration of phenol solution and the sensors are seen to exhibit linearity over the investigation concentrations. The current responses do not decline significantly at higher concentrations of phenol as in the PPD/PANI/HRP microelectrode arrays, indicating that both the quantity of reagent deposited and the thickness of the modifying layer do not limit the response of the sensor to phenol. Moreover, Au particles may improve the mass transfer between electrode surface and redox centre in protein since higher surface area were obtained. Granot (2005) reported the chronoamperometric experiments reveal that the charge transport in the poly-aniline /Au-NPs system is ca. 25-fold enhanced as compared to the analogous polyaniline/polystyrene system which confirmed the current improving in this research.



(a)

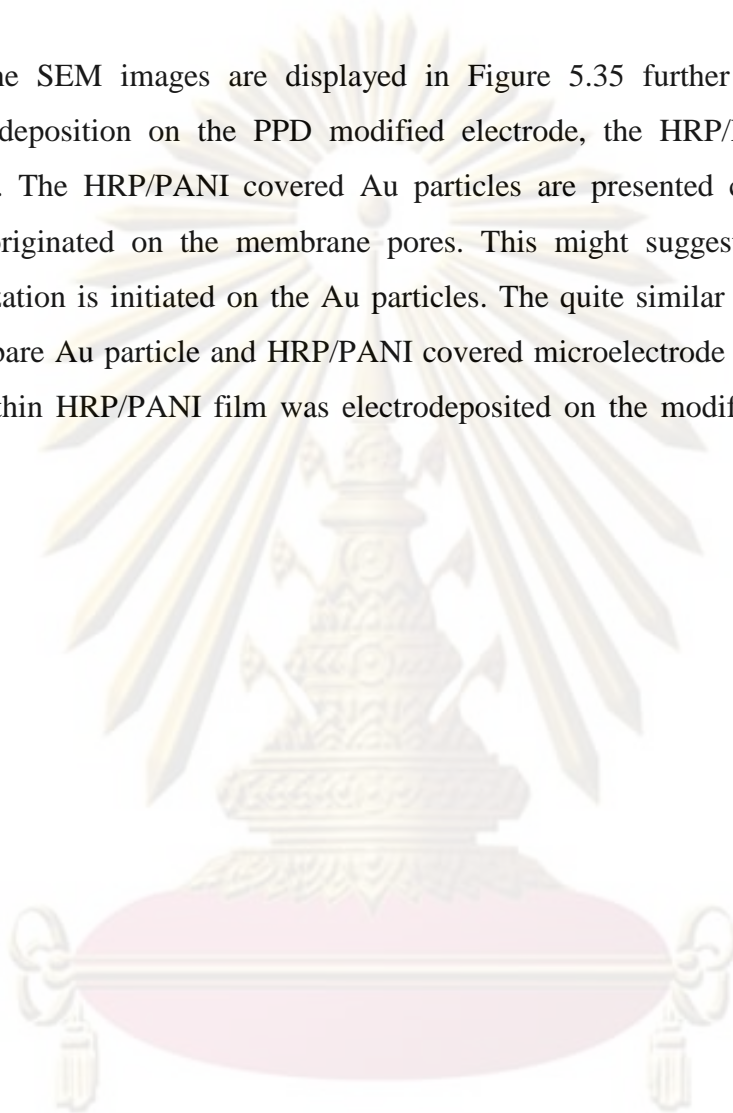


(b)

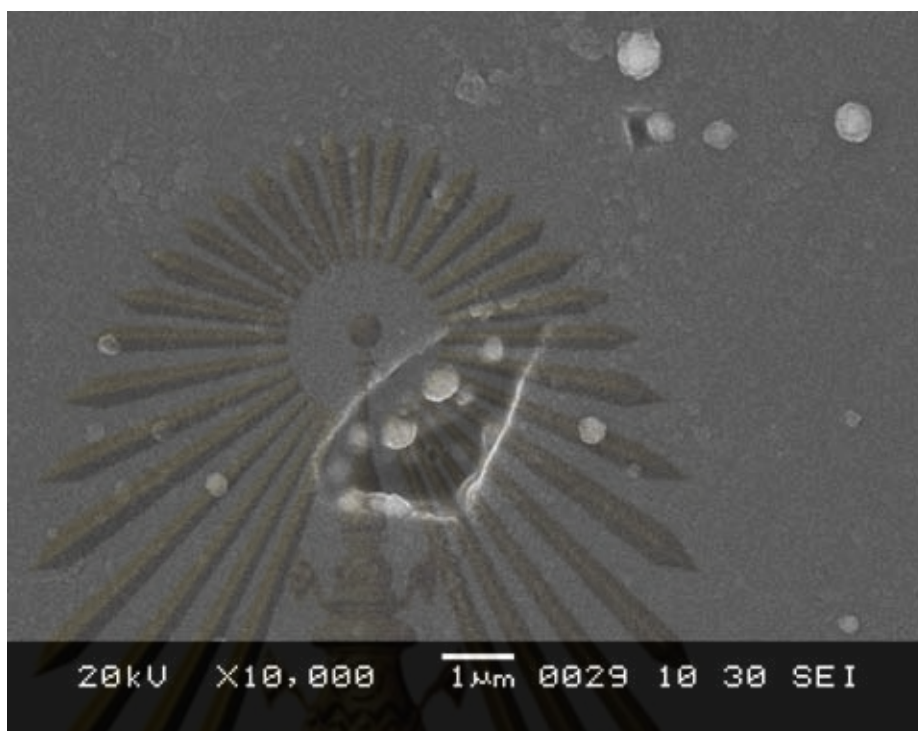
Figure 5.34 Linear sweep of PPD/Au/HRP/PANI microelectrode arrays (a) and 50 mV peak current for various phenol concentration at 0.7 H:P ratio, scan rate 20 mVs^{-1} .

5.3.3 Microscopic characterization of PPD/Au/HRP/PANI microelectrode arrays

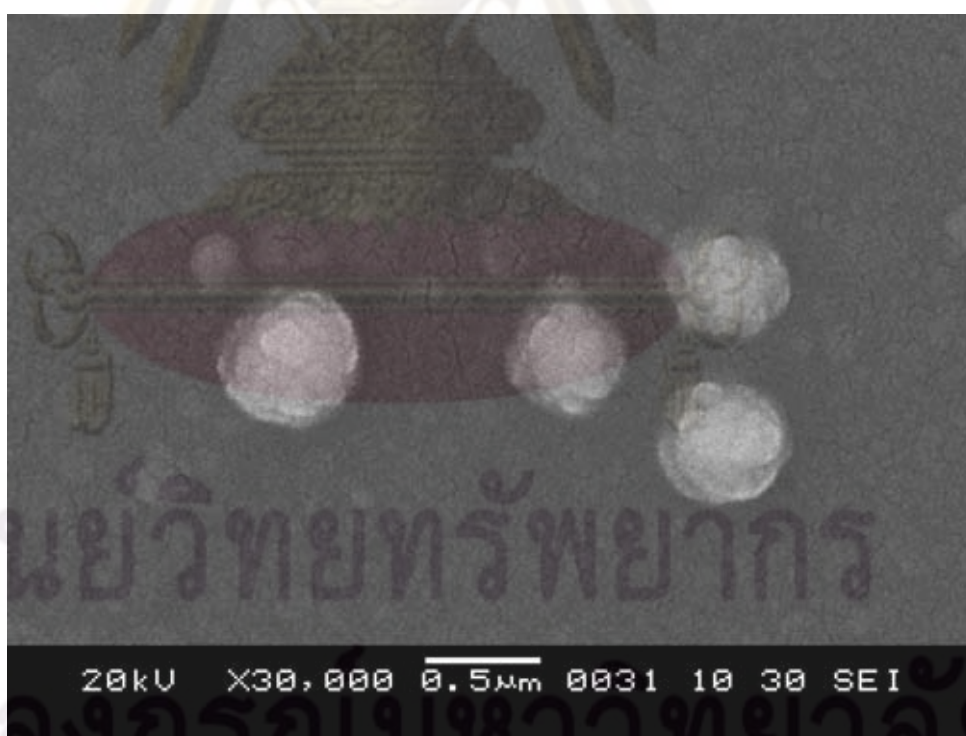
The SEM images are displayed in Figure 5.35 further approved the Au particles deposition on the PPD modified electrode, the HRP/PANI thin film is presented. The HRP/PANI covered Au particles are presented consists of the Au particle originated on the membrane pores. This might suggest that aniline/HRP polymerization is initiated on the Au particles. The quite similar in the particle size between bare Au particle and HRP/PANI covered microelectrode arrays is suggested the very thin HRP/PANI film was electrodeposited on the modified microelectrode arrays.



ศูนย์วิทยทรัพยากร
จุฬาลงกรณ์มหาวิทยาลัย



(a)



(b)

Figure 5.35 Scanning electron micrographs of and PPD/HRP/PANI microelectrode arrays.

5.4 The comparison between PPD/HRP/PANI and PPD/Au/HRP/PANI microelectrode arrays

Throughout this research, an achievement of fabricated microelectrode arrays using sonochemical ablation techniques has been described. The parallel development of a PPD/HRP/PANI microelectrode arrays, coupled with PPD/Au/HRP/PANI microelectrode arrays, is of prime importance to maintain the advantages the microelectrode arrays. This part is presented the comparative area which is often overlooked when considering the commercialisation of such devices. This is including the comparison in an electrochemical analysis, reusability, and reproducibility. These are significantly parameters are sought to support the advantages of this fabrication method and the microelectrode arrays device.

5.4.1 An electrochemical analysis comparison

Linear sweep voltammograms were applied for both PPD/HRP/PANI and PPD/Au/HRP/PANI microelectrode arrays had shown in previous sections. The measurements of phenol in aqueous solutions were tested for their response to a range of phenol concentrations 1×10^{-15} – 1×10^{-3} M. The 50 mV peak current for both types of microelectrode arrays is presented in Figure 5.36. Obviously, the PPD/Au/HRP/PANI microelectrode arrays responses appeared higher measurements for the amount of phenol presented in the sample than the PPD/HRP/PANI microelectrode arrays, approximately 74.38% in average. The explanation for the enhanced precision observed by the Au modified microelectrode arrays over the normal microelectrode arrays, since that the Au particles can improved the electron transfer rate between electrode and immobilized enzyme as act as the catalyst to increase the electrochemical reaction (Li et al., 2010). Thus the current response of the PPD/Au/HRP/PANI microelectrode arrays was effectively increased. Furthermore, the Au particles are help improving the electrochemical response. Since an increasing in surface area of the microelectrode by depositing the particles, the surface concentration of an electroactive species may increase which meaning to increasing

the peak current explanation by using Faraday's law from an equation 5.1 (Yin et al., 2009).

$$I_p = \frac{n^2 F^2 A \Gamma v}{4RT} \quad (5.8)$$

Where, I_p is the peak current, A is an electrode surface area, v is the scan rate, n is the number of electron, R is the universal gas constant, T is the Kelvin temperature, and F is the Faraday constant.

Among the widely reported for the Au particles modified electrode, Yin (2009) reported the effect of Au particles on GC electrode to hydrogen peroxide detection by the similar enzyme as this research. The report presented that the Au particles can dramatically enhance electrochemical response of HRP, resulting an increasing redox currents. Furthermore, the gold particle was used for modified glucose biosensors compare with the non Au particle deposited, reported by Ozdemir (2010). The enhancing in the signal current was observed at the Au particles modified biosensors.

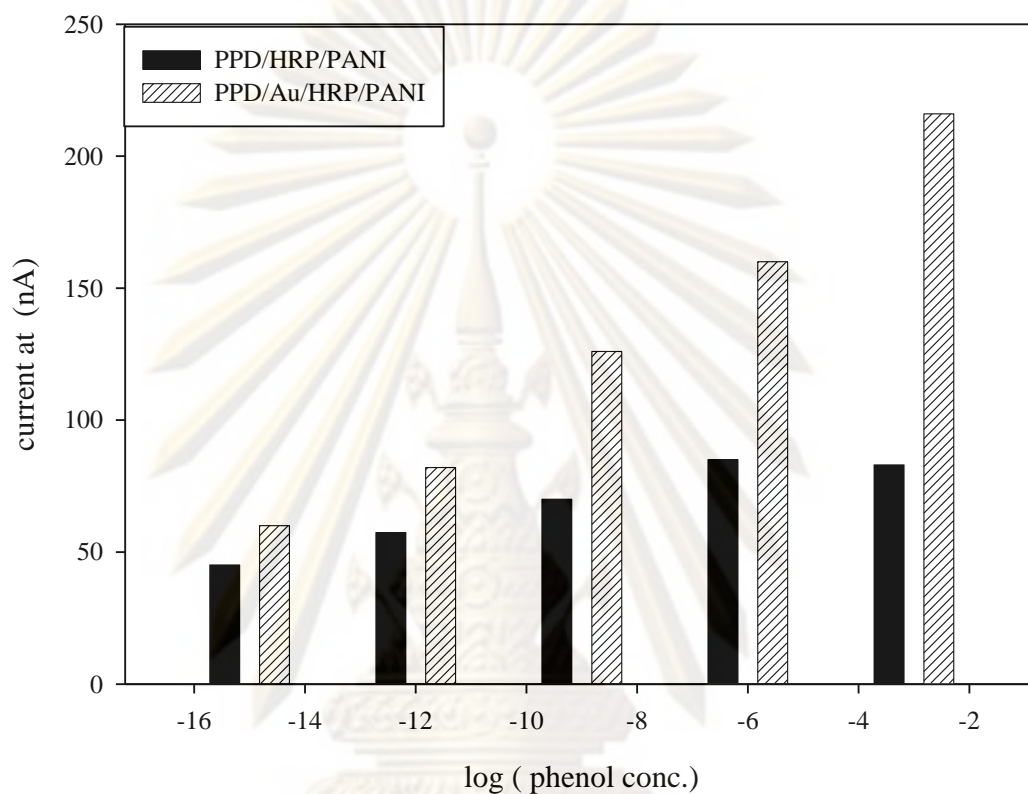


Figure 5.36 The comparison between PPD/HRP/PANI and PPD/Au/HRP/PANI microelectrode arrays peak current at applied voltage 50 mV

ศูนย์วิทยทรัพยากร
จุฬาลงกรณ์มหาวิทยาลัย

5.4.2 Microelectrode arrays reusability

Both the microelectrode arrays with PPD/HRP/PANI and PPD/Au/HRP/PANI are tested for reusability. The reusability of the microelectrode arrays are tested by conducting 10 linear sweep measurements and observing the decline in current response with the repeated uses. These tests are conducted under the same conditions as the previous linear sweep measurements by fixing the phenol concentration at 1×10^{-6} M. Between each trial, the electrode is rinsed with distilled water. After 10 measurements, the current at 1×10^{-6} M phenol are 58.94% and 43.92% of the original current for PPD/HRP/PANI and PPD/Au/HRP/PANI microelectrode arrays, respectively (Figure 5.37 and Figure 5.38, respectively). The Au modified microelectrode arrays may occurred with higher turned over rate of enzyme, the 10th uses current displayed lower current compared with none Au particles. For HRP biosensor from previous report, Panwittayakool (2008) found none current response of HRP biosensor was determined after the first using electrode. The enzyme leaking has been explained the previous result. Contrastingly in this research, the current responses were slightly determined.

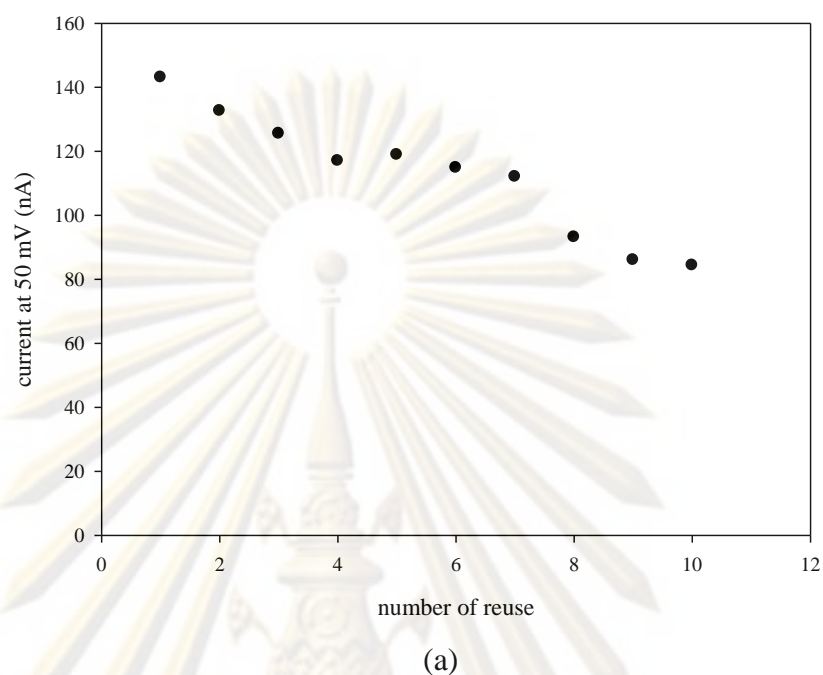


Figure 5.37 Reusability of PPD/HRP/PANI microelectrode arrays(b),the phenol samples (1×10^{-6} M) were analyzed repeatedly using single electrode.

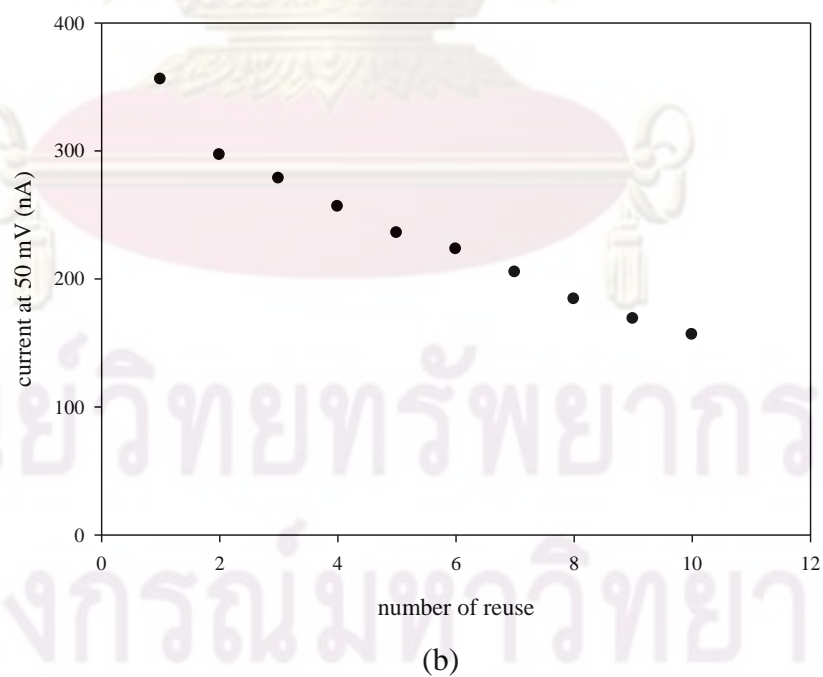


Figure 5.38 Reusability of PPD/Au/HRP/PANI microelectrode arrays(b),the phenol samples (1×10^{-6} M) were analyzed repeatedly using single electrode.

5.5 Conclusion

The development of horseradish peroxidase (HRP) microelectrode arrays for biosensor has been described. The PPD/HRP/PANI and PPD/Au/HRP/PANI microelectrode arrays were fabricated by sonochemically technique.

The poly(o-phenylenediamine) (PPD) were initially deposited at a glassy carbon electrode by potentially cycling the electrode assembly until it became fully insulated by the polymer (50 potential cycles). Cyclic voltammograms relating to the electrodeposition of the film revealed the electropolymerisation as being a self-regulating and thus highly reproducible process, since diminishing peak currents were observed as the electrode became progressively insulated by the film. The thickness of the film deposited upon the gold electrode was estimated via AFM to be approximately 29.53 nm.

Microelectrode array assemblies were produced on the laboratory scale via the ultrasonic ablation of PPD film modified electrode. The ultrasonic ablation time was varied for the microelectrode arrays formation using the cyclic voltammetry. At 17.30 min of sonication time presented the reversible sigmoidal shape, which expresses the microelectrode behaviour. At this time expounded the micron size (5 μm) and sub-micron size (< 1 μm) of microelectrode arrays approximately with the population density 6×10^4 and 17×10^4 pore cm^{-2} , respectively. The reproducibility by using this method for microelectrode arrays fabrication was approximately found at 5.51%RSD.

To achieve an enzyme microelectrode, HRP/PANI and HRP/Au/PANI were later electrodeposited on microelectrode surfaces. Spherical Au particles of around 1 μm were obtained by electrodeposition of Au ions onto microelectrode surfaces. Incorporation of Au in HRP/PANI matrix was postulated to enhance interfacial areas for HRP adsorption as well as functioned as electron conducting pathways between the redox HRP and electrode surface. The significant improvement of microelectrode performances was achieved. Microelectrode arrays incorporated with Au resulted in approximately 74.38 % higher response current in comparison to those without particles. Satisfactory linear ranges were also determined from 1×10^{-15} to 1×10^{-6} , and 1×10^{-15} to 1×10^{-3} M phenol concentration (on a semi-log scale) for PPD/HRP/PANI and PPD/HRP/Au/PANI microelectrode arrays, respectively. In the term of

reusability, after 10 measurements, the current responses were 58.94% and 43.92% of the original current for those PPD/HRP/PANI and PPD/Au/HRP/PANI microelectrode arrays, respectively. Sonochemically fabricated enzyme/Au particles microelectrode arrays showed high potentials for biosensor applications.

5.6 Suggestion for future work

This research has been development of enzyme HRP microelectrode arrays for biosensor by using the sonochemical ablation which gave an approximately 5 % RSD. To achieve this reproducibility the fixing position of electrode was found significantly important, since a little change in position may effect. Moreover, the using homogeneous ultrasonic tank may clarify this effect.

Furthermore, the enzyme enhancement mechanism for the low detection limit and nonlinear relationship of microelectrode arrays

For further microelectrode arrays study, improving of the microelectrode performance would be beneficial in either enzyme biosensor or other sensor field. This research may be the prototype to another microelectrode arrays study.

REFERENCES

- Andreescu, S., Njagi, J., Ispas, C., Victor, E., Manoj Kumar, R., Ozlem, Y. Nanostructured materials for enzyme immobilization and biosensors The New Frontiers of Organic and Composite Nanotechnology. Amsterdam: Elsevier, 2008.
- Adrian W. Bott. Characterization of Chemical Reactions Coupled to Electron Transfer Reactions Using Cyclic Voltammetry Current Separations. Ph.D Thesis Institute of bioscience and technology Cranfield University, 1999.
- Anjos, T. G., Hahn, C. E. W. The development of a membrane-covered microelectrode array gas sensor for oxygen and carbon dioxide measurement. Sensors and Actuators B: Chemical 135(2008):224-229.
- Barton, A. C. Sonochemically fabricated microelectrode arrays for biosensors offering widespread applicability: Part I. Biosensors and Bioelectronics 20 (2004):328-337.
- Barton, A. C. Labelless AC impedimetric antibody-based sensors with pg ml^{-1} sensitivities for point-of-care biomedical applications. Biosensors and Bioelectronics 24(2009):1090–1095.
- Eggs Brian. Biosensor and Introduction, John Wiley and Son Ltd, England, 2000.
- Bouvrette, P., Male, K. B., Luong, J. H. T., & Gibbs, B. F. Amperometric biosensor for diamine using diamine oxidase purified from porcine kidney. Enzyme and Microbial Technology 20(1997):32-38.
- Burmeister, J. J., Gerhardt, G. A. Ceramic-based multisite microelectrode arrays for in vivo electrochemical recordings of glutamate and other neurochemicals. TrAC Trends in Analytical Chemistry 22(2003):498-502.
- Castanön, M. J. L., Ordieres, A. J. M. and Blanco, P. T. 'Amperometric detection of ethanol with poly(o-phenylenediamine)-modified enzyme electrodes. Biosensors and Bioelectronics 12(1997):511-520.
- Chen, Z., Xi, F., Yang, S., Wu, Q., Lin, X. Development of a bienzyme system based on sugar-lectin biospecific interactions for amperometric determination of phenols and aromatic amines. Sensors and Actuators B: Chemical 130(2008):900-907.

- Cosnier, S., Popescu, I. C. Poly(amphiphilic pyrrole) -tyrosinase-peroxidase electrode for amplified flow injection-amperometric detection of phenol. Analytica Chimica Acta 319(1996):145-151.
- Deng., H. and Berkel. G. J. Van. Electrochemical Polymerization of Aniline Investigated Using On-Line Electrochemistry/ Electrospray Mass Spectrometry. Anal. Chem. 71(1999): 4284-4293.
- Ding, T., Wang, H., Xu, S. Zhu, I J. Sonochemical synthesis and characterizations of monodispersed PbSe nanocrystals in polymer solvent. J Cryst Growth 235(2002):517-522.
- Emr, S. A. Yacynych, A. M. Use of polymer-films in amperometric biosensors. Electroanalysis 7(1995):913-923.
- Fei. H, Bin, L., Pingang, H., Jun, H., Yuzhi, F. Electrochemical fabrication of nanoporous polypyrrole film on HOPG using nanobubbles as templates Electrochemistry Communications 11(2009):639–642.
- Foyet, A., Hauser, A., Schefer, W. Template electrochemical deposition and characterization of zinc-nickel alloy nanomaterial. Journal of Electroanalytical Chemistry 604(2007):137-143.
- Gornall, D. G. Study towards the exploitation of sonochemically formed microelectrode arrays for the development of electrochemical sensors. PhD. Thesis Institute of bioscience and technology Cranfield University, 2004.
- Granot, E., Katz, E., Basnar, B., Willner, I. Enhanced Bioelectrocatalysis Using Au-Nanoparticle/Polyaniline Hybrid Systems in Thin Films and Microstructured Rods Assembled on Electrodes. Chem. Mater 17(2005):4600-4609.
- Hedenmo, M., Narvez, A., Domonguez, E., Katakis, I. Improved mediated tyrosinase amperometric enzyme electrodes. Journal of Electroanalytical Chemistry 425(1997): 1-11.
- Hepher, M. J., Duckett, D. and Loening, A. High-speed video microscopy and computer enhanced imagery in the pursuit of bubble dynamics. Ultrasonics Sonochemistry 7(2000):229-233.
- Hernaández-Santos D, G. I.-G. a. M., Garcia AC. Review: metal-nanoparticles based electroanalysis. Electroanalysis 14(2002):11-12.

- Huang, X.J., Yarimaga. O., Kim, J.H., Choi, Y.K. Substrate surface roughness-dependent 3-D complex nanoarchitectures of gold particles from directed electrodeposition. J. Mater. Chem 19(2009): 478–483.
- Hwa-Jung, K., Ming-Hua, P., Seong-Ho, C., Chang-Ho, S., Young-Taeg, L. Development of Amperometric Hydrogen Peroxide Sensor Based on Horseradish Peroxidase-Immobilized Poly(Thiophene-co-EpoxyThiophene): Molecular Diversity Preservation International, 2008.
- Imisides, M. D., John, R., Riley, P. I Wallace, G. G. The use of electropolymerization to produce new sensing surfaces: A review emphasizing electrodeposition of heteroaromatic compounds. Electroanalysis 3(1991):879-889.
- Jun Chen, B. W.-J., Carol Lynam, Orawan Ngamna., Simon Moulton, W. Z., and Gordon G. Wallace. A Simple Means to Immobilize Enzyme into Conducting Polymers via Entrapment. Electrochemical and Solid-State Letters 9(2006), 3-10.
- Kafi, A.K.M., Chen, A. A novel amperometric biosensor for the detection of nitrophenol. Talanta 79(2009):97-102.
- Karel Stulik, C. A., Karel Holub, Vladimir Marecek, Kutner, a. W. Microelectrodes. Definitions, characterization and applications. Pure Appl Chem72(2000):10-11.
- Kim, H.-J., Piao, M.-H., Choi, S.-H., Shin, C.-H., Lee, Y.-T. Development of Amperometric Hydrogen Peroxide Sensor Based on Horseradish Peroxidase-Immobilized Poly(Thiophene-co-EpoxyThiophene). Sensors 8(2008):4110-4118.
- Kim, H. J. C., S. H.; Lee, K. P.; Gopalan, A. I.; Oh, S. H.; Woo, J. C. Fabrication of Functional Poly(thiophene) Electrode for Biosensors. Ultramicroscopy (2007): 12-28.
- Klima, J., Bernard, C. Degrand, C. Sonoelectrochemistry: effects of ultrasound on voltammetric measurements at a solid electrode. J Electroanal Chem 367(1994):297-300.

- Konry, T., Hadad, B., Shemer-Avni, Y., Cosnier, S., Marks, R. S. ITO pattern fabrication of glass platforms for electropolymerization of light sensitive polymer for its conjugation to bioreceptors on a micro-array. Talanta 75(2008):564-571.
- Korkut, S., Keskinler, B., Erhan, E. An amperometric biosensor based on multiwalled carbon nanotube-poly(pyrrole)-horseradish peroxidase nano biocomposite film for determination of phenol derivatives. Talanta 76(2008):1147-1152.
- Kuttruff H. Ultrasonics: Fundamentals and Applications. Elsevier Science Publications, USA, 1991.
- Law, K. A., J. Higson, S. P. Sonochemically fabricated acetylcholinesterase micro-electrode arrays within a flow injection analyser for the determination of organophosphate pesticides. Biosensors and Bioelectronics 20(2005):1914-1924.
- Lee, J.-H., Jang, A., Bhadri, P. R., Myers, R. R., Timmons, W., Beyette, J. F. R., Bishop, P. L., Papautsky, I. Fabrication of microelectrode arrays for in situ sensing of oxidation reduction potentials. Sensors and Actuators B: Chemical 115(2006):220-226.
- Leighton, T. G. The principles of cavitation. In Ultrasound in Food Processing, 151-182. London: Thomson Science, 1998.
- LeRoy A. Diagnosis and treatment of nephrolithiasis: current perspectives. AM.J.Roentgenology 163(1994):1309-1313.
- Li, W., Yuan, R., Chai, Y., Zhou, L., Chen, S., Li, N. Immobilization of horseradish peroxidase on chitosan/silica sol-gel hybrid membranes for the preparation of hydrogen peroxide biosensor. Journal of Biochemical and Biophysical Methods 70(2008):830-837.
- Li, X. G., Huang, M. R., Duan, W. & Yang, Y. L. Novel multifunctional polymers from aromatic diarnines by oxidative polymerizations. Chem Rev 102(2002): 2925-3030.
- Lin, C.-C., Juo, T.-J., Chen, Y.-J., Chiou, C.-H., Wang, H.-W., Liu, Y.-L. Enhanced cyclic voltammetry using 1-D gold nanorods synthesized via AAO template electrochemical deposition. Desalination 233(2008):113-119.

- Lin, J., Qu, W., Zhang, S. Disposable biosensor based on enzyme immobilized on Au-chitosan-modified indium tin oxide electrode with flow injection amperometric analysis. Analytical Biochemistry 360(2007):288-293.
- Li, Y., Schluesener, H.J., Xua, S. Gold nanoparticle-based biosensors. Gold Bulletin 43 (2010):24-41.
- Losito, I., De Giglio, E., Cioffi, N. Malitesta, C. Spectroscopic investigation on polymer films obtained by oxidation of o-phenylenediamine on platinum electrodes at different pHs. J Mater Chem 11(2001):1812-1817.
- Losito, I., Palmisano, F. Zambonin, P. G. o-phenylenediamine electropolymerisation by cyclic voltammetry combined with electrospray ionisation ion trap mass spectroscopy. Anal Chem 75(2003):4988-4995.
- Mason, T. J. Sonochemistry. Oxford: Oxford University Press, 1999.
- Mason, T. J. Beflan, J. Ultrasonics in Industrial Processes: The Problems of Scale-up. Current Trends in Sonochemistry, Edited by G. Price, Royal Society of Chemistry, 1992.
- Mathebe, N. G. R., Morrin, A., Iwuoha, E. I. Electrochemistry and scanning electron microscopy of polyaniline/peroxidase-based biosensor. Talanta 64(2004):115-120.
- Mello, L. D., Sotomayor, M. D. P. T., Kubota, L. T. HRP-based amperometric biosensor for the polyphenols determination in vegetables extract. Sensors and Actuators B: Chemical 96(2003):636-645.
- Marsh, J., Scantlebury J, .D. and Lyon, S.B. Poly(2-allyl)phenyleneoxide electropolymer film grown on steel. Journal of Applied Polymer Science 79 (2001):1563-1571.
- Martinusz K., Czirók E. and Inzelt G. Studies of the formation and redox transformation of poly(o-phenylenediamine) films using a quartz crystal microbalance. Journal of Electroanalytical chemistry 379(1994):437-444.
- Miller D.L., Bao S., Giles R.A., Thrall B.D. Ultrasonic Enhancement of Gene Transfection in Murine Melanoma Tumors. Ultrasound Med. Biol. 25(1999):1425-1430.

- Mills, D.W. Towards a commercial microelectrode array based sensor for improved chlorine detection. EngD Thesis Institute of bioscience and technology Cranfield University, 2005.
- Morf, W. E., de Rooij, N. F. Performance of amperometric sensors based on multiple microelectrode arrays. Sensors and Actuators B: Chemical 44 (1997):538-541.
- Morrin, A., Guzman, A., Killard, A. J., Pingarron, J. M., Smyth, M. R. Characterisation of horseradish peroxidase immobilisation on an electrochemical biosensor by colorimetric and amperometric techniques. Biosensors and Bioelectronics 18(2003):715-720.
- Munteanu, F.-D., Lindgren, A., Emneus, J., Gorton, L., Ruzgas, T., Csoregi, E., Ciucu, A., van Huystee, R. B., Gazaryan, I. G., Lagrimini, L. M. Bioelectrochemical Monitoring of Phenols and Aromatic Amines in Flow Injection Using Novel Plant Peroxidases. Analytical Chemistry 70(1998): 2596-2600.
- Myler, S., Collyer, S. D., Davis, F., Gornall, D. D., Higson, S. P. J. Sonochemically fabricated microelectrode arrays for biosensors: Part III. AC impedimetric study of aerobic and anaerobic response of alcohol oxidase within polyaniline. Biosensors and Bioelectronics 21(2005):666-671.
- Myler, S., Davis, F., Collyer, S. D., Higson, S. P. J. Sonochemically fabricated microelectrode arrays for biosensors--part II: Modification with a polysiloxane coating. Biosensors and Bioelectronics 20(2004): 408-412.
- Njagi, J., and Andreescu, S., Stable enzyme biosensors based on chemically synthesized Au-polypyrrole nanocomposites, Biosensors and Bioelectronics 23(2007):168-175.
- Ordeig, O., Banks, C. E., Davies, T. J., Campo, J. d., Muoz, F. X., Compton, R. G. The linear sweep voltammetry of random arrays of microdisc electrodes: Fitting of experimental data. Journal of Electroanalytical Chemistry 592(2006):126-130.
- Orozco, J., Fernández-Sánchez, C., and Jiménez-Jorquera, C. Gold nanoparticle-modified ultramicroelectrode arrays : A suitable transducer platform for the development of biosensors. Procedia Chemistry 1(2009): 666-669.

- Ozdemir, C., Yen, F., Odac, D., Timur, S. Electrochemical glucose biosensing by pyranose oxidase immobilized in gold nanoparticle-polyaniline/AgCl/gelatin nanocomposite matrix. Food Chemistry 119(2010):380–385.
- Pingarrón, J.M., Yáñez-Sedeño, P., González-Cortés, A. Gold nanoparticle-based electrochemical biosensors. Electrochimica Acta 53(2008):5848-5866.
- Pritchard, J., Law, K., Vakurov, A., Millner, P., Higson, S. P. J. Sonochemically fabricated enzyme microelectrode arrays for the environmental monitoring of pesticides. Biosensors and Bioelectronics 20(2004):765-772.
- Ramirez-Fernandez F.J. , S., W.J. , Peixoto, N. Integrated sensors and microsystems. Revista Mexicana De Ftsica 52(2006): 4.
- Rivas, G. A., Rubianes, M. D., Rodrogez, M. C., Ferreyra, N. F., Luque, G. L., Pedano, M. L., Miscoria, S. A., & Parrado, C. n. Carbon nanotubes for electrochemical biosensing. Talanta74(2007):291-307.
- Rosatto, S. S., Kubota, L. T., de Oliveira Neto, G. Biosensor for phenol based on the direct electron transfer blocking of peroxidase immobilising on silica-titanium. Analytica Chimica Acta 390(1999):65-72.
- Rosatto, S. S., Sotomayor, P. T., Kubota, L. T., Gushikem, Y. SiO₂/Nb₂O₅ sol-gel as a support for HRP immobilization in biosensor preparation for phenol detection. Electrochimica Acta 47 (2002):4451-4458.
- Ruzgas, T., Gorton, L., Emnous, J., Marko-Varga, G. Kinetic models of horseradish peroxidase action on a graphite electrode. Journal of Electroanalytical Chemistry 391(1995):41-49.
- Samuel P. Kounaves, W. D., and Pamela R. Hallock. Iridium-Based Ultramicroelectrode Array Fabricated by Microlithography. Anal. Chem 66(1994):6.
- Sarma, T. K., Devasish C., Anumita, P., Arun C. Synthesis of Au nanoparticle–conductive polyaniline composite using H₂O₂ as oxidising as well as reducing agent. Chem. Commun. (2002):1048–1049.
- Sasaki, K. Pharmacokinetic study of a gallium-porphyrin photo- and sono-sensitizer, ATX-70, in tumor-bearing mice. Jpn J Cancer Res 92(2001):989-995.

- Sayyah, S. M., El-Deeb, M. M., Kamal, S. M., Azooz, R. E. Electropolymerization of O-Phenylenediamine on Pt-Electrode from Aqueous Acidic Solution: Kinetic, Mechanism, Electrochemical Studies and Characterization of the Polymer Obtained Journal of Applied Polymer Science 112(2009):3695–3706.
- Schuhmann, W., Kranz, C., Wohlschliiger, H., Strohmeier, J. Pulse technique for the electrochemical deposition of polymer films on electrode surfaces. Biosensors & Bioelectronics 12(1997):1157-1167.
- Seo, K.D. Horseradish Peroxidase (HRP) Immobilized Poly(aniline-co-m-aminophenol) Film Electrodes fabrication and Evaluation as Hydrogen Peroxide Sensor. Sensors 7(2007):719-729.
- Simm, A. O., Ward-Jones, S., Banks, C. E., Compton, R. G. Novel Methods for the Production of Silver Microelectrode-Arrays: Their Characterisation by Atomic Force Microscopy and Application to the Electro-reduction of Halothane. Analytical Sciences 21(2005):667-671.
- Shlamovitz G.Z., Iakobishvili Z., Matz I., Golovchiner G., Lev E. and Siegel R.J. In vitro ultrasound augmented clot dissolution—what is the optimal timing of ultrasound application. Cardiovasc Drugs Ther 16(2002):521–526
- Stett, A., Biological application of microelectrode arrays in drug discovery and basic research. Analytical and Bioanalytical Chemistry 377(2003):486-495.
- Shaohua, Z., Yuanjie, T., Huihui, Y., Minbo L. Direct electrochemistry of glucose oxidase on screen-printed electrodes through one-step enzyme immobilization process with silica sol–gel/polyvinyl alcohol hybrid film. Sensors and Actuators B: Chemical 133(2008): 555–560.
- Sheffer, M., Daniel, M. Control of locally deposited gold nanoparticle on polyaniline films. Electrochimica Acta 54(2009): 2951–2956.
- Shuqun C., Xinda Z., Zhaoyou T., Yao Y., Susu B., Dechu Q. Effects of high-intensity focused ultrasound and anti-angiogenic agents on the ablation of experimental liver cancers. Chinese Journal of Digestive Diseases 1(2000):35-38.
- Suslick, K S. Sonochemistry. Science 247(1990):1439-1445.

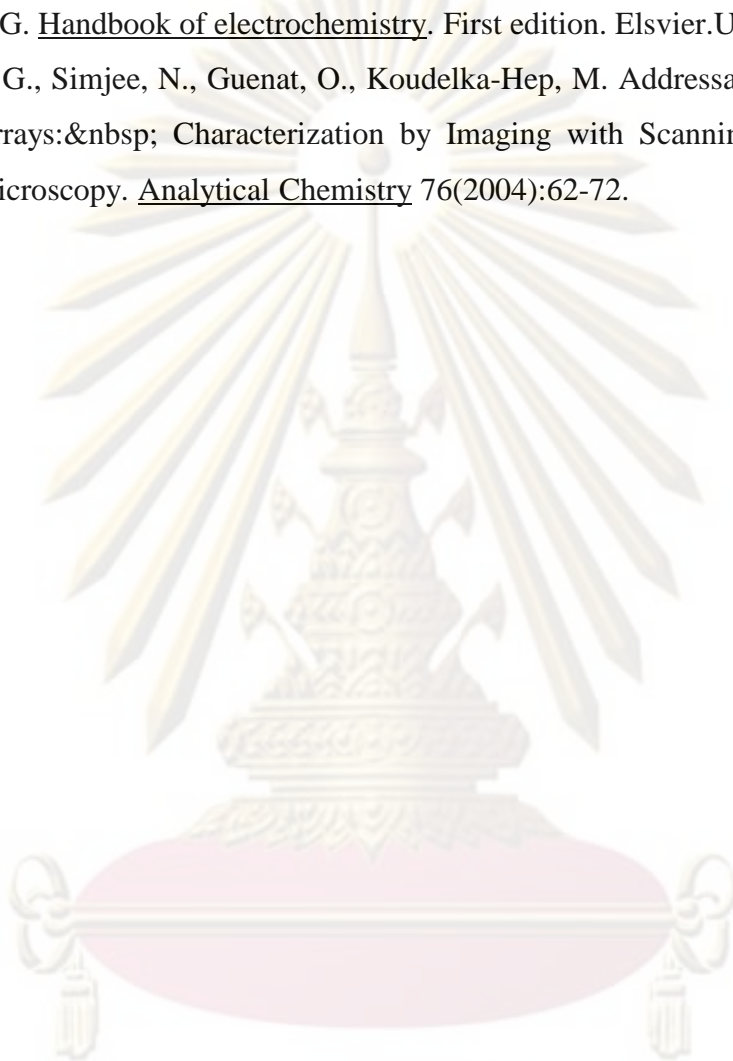
- Thanachasai, S., Rokutanazono, S., Yoshida, S., Watanabe, T. Novel Hydrogen Peroxide Sensors Based on Peroxidase-Carrying Poly{pyrrole-co-[4-(3-pyrrolyl) butanesulfonate]} Copolymer Films. Analytical Sciences 18(2002):773-777.
- Theron, P., Pichat, P., Petrier, C., Guillard, C. Water treatment by T102 photocatalysis and/or ultrasound. degradations of phenyltrifluoromethyl ketone, a trifluoroacetic-acid-forming pollutant, and octan-1-ol, a very hydrophobic pollutant. Water Sci Technol 44(2001):263-270.
- Tsekenis, G., et al. Label-less Immunosensor Assay for Myelin Basic Protein Based upon an AC Impedance Protocol. Anal. Chem. 80 (2008): 2058–2062.
- Tuziuti, T., Yasui, K. and Iida, Y. Spatial study on a multibubble system for sonochemistry by laser-light scattering. Ultrasonics Sonochemistry 12(2005):73-77.
- Walton, D. J. Phull, S. S. Sonoelectrochemistry. In Advances In Sonochemistry, 205-285. London: JAI Press. 1996.
- Wang Joseph. Analytical electrochemistry. Third edition. New Jersey: John Wiley & Sons, 2007.
- Wang, H.-S., Pan, Q.-X., & Wang, G.-X. A Biosensor Based on Immobilization of Horseradish Peroxidase in Chitosan Matrix Cross-linked with Glyoxal for Amperometric Determination of Hydrogen Peroxide. Sensors 5(2005):266-276.
- Welch, C. M., Banks, C. E., Simm, A. O., Compton, R. G. Silver nanoparticle assemblies supported on glassy-carbon electrodes for the electro-analytical detection of hydrogen peroxide. Analytical and Bioanalytical Chemistry 382(2005):12-21.
- Wu, S., Zhao, H., Ju, H., Shi, C., Zhao, J. Electrodeposition of silver-DNA hybrid nanoparticles for electrochemical sensing of hydrogen peroxide and glucose. Electrochemistry Communications 8(2006):1197-1203.
- Xia, H., Zhang, C. & Wang, Q. Study on ultrasonic-induced encapsulating emulsion polymerization in the presence of nanoparticles. J Appl Polym Sci 80(2001): 1130-1139.

- Xiao, L., Streeter, I., Wildgoose, G. G., Compton, R. G. Fabricating random arrays of boron doped diamond nano-disc electrodes: Towards achieving maximum Faradaic current with minimum capacitive charging. Sensors and Actuators B: Chemical 133(2008): 118-127.
- Xu, J.-Z., Zhang, Y., Li, G.-X., Zhu, J.-J. An electrochemical biosensor constructed by nanosized silver particles doped sol-gel film. Materials Science and Engineering: C 24(2004):833-836.
- Xu, Q., Mao, C., Liu, N.-N., Zhu, J.-J., Shen, J. Immobilization of horseradish peroxidase on O-carboxymethylated chitosan/sol-gel matrix. Reactive and Functional Polymers 66(2006):863-870.
- Xu, S., Peng, B., Han, X. A third-generation H₂O₂ biosensor based on horseradish peroxidase-labeled Au nanoparticles self-assembled to hollow porous polymeric nanospheres. Biosensors and Bioelectronics 22(2007):1807-1810.
- Yasui, K., Tuziuti, T. and Iida, Y. Dependence of the characteristics of bubbles on types of sonochemical reactors. Ultrasonics Sonochemistry 12(2005):43-51.
- Yi, X., Huang-Xian, J., Hong-Yuan, C. Direct Electrochemistry of Horseradish Peroxidase Immobilized on a Colloid/Cysteamine-Modified Gold Electrode. Analytical Biochemistry 278(2000):22-28.
- Yin, H, Ai, S., Shi, S., and Zhu, L. A novel hydrogen peroxide biosensor based on horseradish peroxidase immobilized on gold nanoparticles-silk fibroin modified glassy carbon electrode and direct electrochemistry of horseradish peroxidase. Sensors and Actuators B 137 (2009):747-753.
- Yim, B, Nagata.Y., Maeda., Y. Sonolytic degradation of phthalic acid esters in aqueous solutions. Acceleration of hydrolysis by sonochemical ablation. J Phys Chem 106(2002):104-107.
- Yu, Q. Z. Polyaniline/Au&Fe₃O₄@Au sub-microcables fabricated by electrospinning and electroless deposition. Materials Science and Engineering B ,2010.
- Zhang Z., Lei C., Sun W., Liu ,H., Deng J. Electrochemical immobilization of horseradish peroxidase on an electro-activated glassy carbon electrode. Journal of Electroanalytical Chemistry 419(1996): 85-91.

Zhu, L., Yang, R., Zhai, J., Tian, C. Biezomatic glucose biosensor based on co-immobilization of peroxidase and glucose oxidase on a carbon nanotubes electrode. Biosensors and Bioelectronics 23(2007):528-535.

Zoski, C. G. Handbook of electrochemistry. First edition. Elsevier.UK, 2003.

Zoski, C. G., Simjee, N., Guenat, O., Koudelka-Hep, M. Addressable Microelectrode Arrays; Characterization by Imaging with Scanning Electrochemical Microscopy. Analytical Chemistry 76(2004):62-72.



ศูนย์วิทยทรัพยากร
จุฬาลงกรณ์มหาวิทยาลัย



APPENDIX

ศูนย์วิทยทรัพยากร
จุฬาลงกรณ์มหาวิทยาลัย

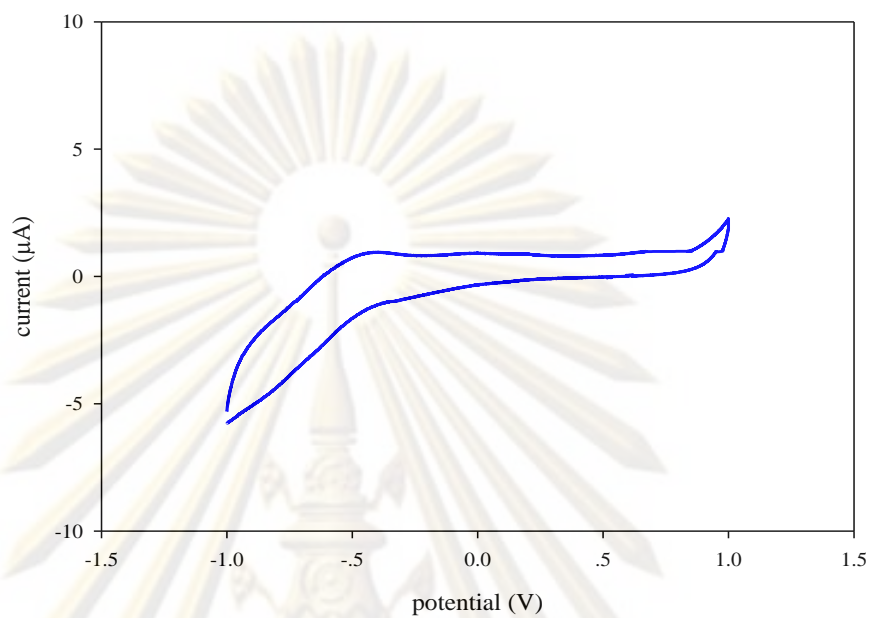


APPENDIX A PRE EXPERIMENTATION

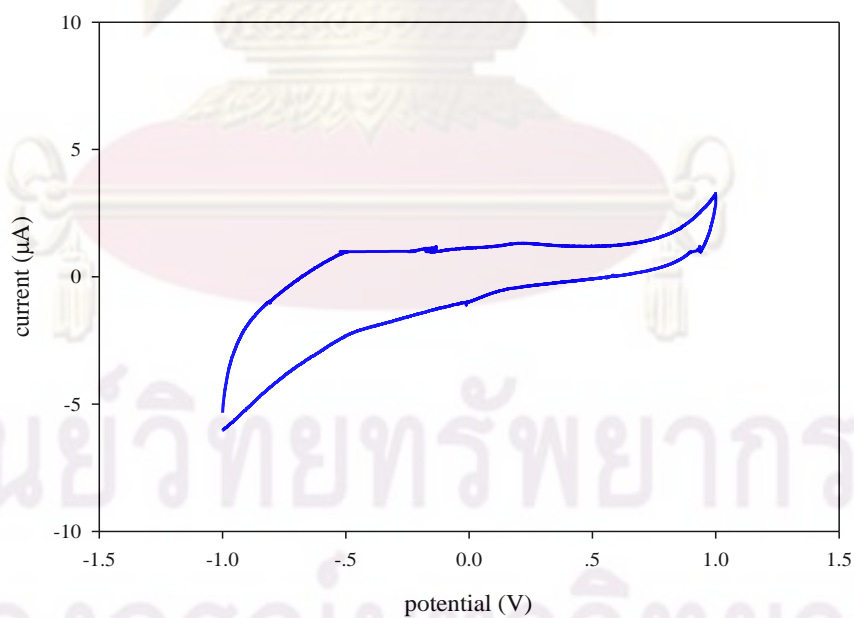
A.1 *o*PD electrodeposition on GC electrode

The 1,2 phenylenediamine dihydrochloride (*o*PD) was electropolymerised on GC electrode by potential sweep between 0 and 1000 mV versus Ag/AgCl (Reference electrode) and Pt (Counter electrode) at various scan rate (10, 20, 30, 40, and 50 mVs⁻¹). Then, the PPD coated electrode was dried for 2 hours and rinsed with demonized water for remove unpolymerized molecules. The cyclic voltammogram was applied by the PPD coated electrode was immerse in 5 mM ferri/ferro cyanide which was prepared in phosphate buffer (pH 7.4) and measuring the current between -1000 and 1000 mV versus Ag/AgCl and Pt electrode with scan rate 20 mVs⁻¹.

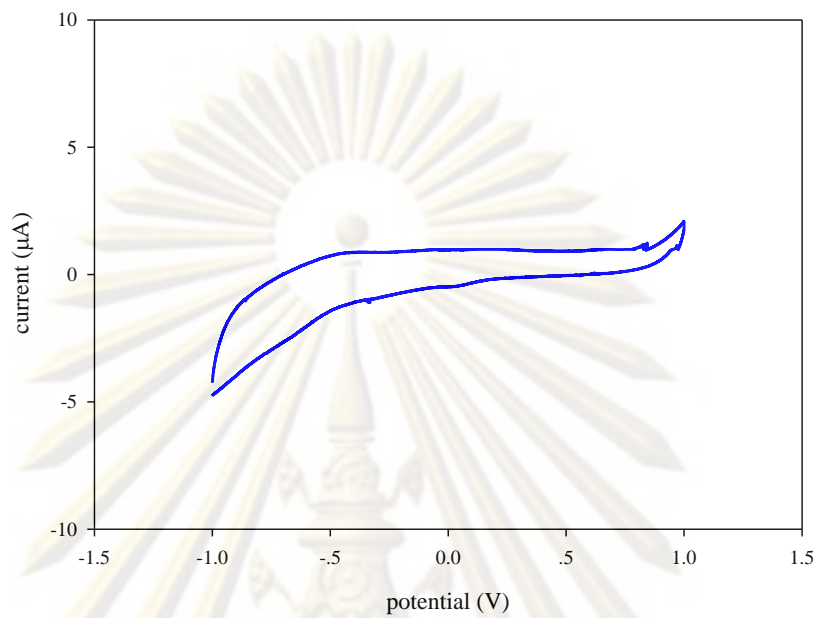
The effect of various scan rates was determined for electropolymerization of PPD on GC electrode in the first place. Cyclic voltammogram is shown in Figure A.1. The voltammogram from various scan rates is quite similar in the most conditions. Meanwhile, the voltammogram at scan rate 50 mVs⁻¹ was different from others. This might be because of at this mode had a faster scan rate than others the polymerization process was not suitable to form the polymer thin film. Additionally, the Fe³⁺ peak current at about 0.35 V in different scan rate is shown in the Figure A.2. At scan rate 10 and 20 mVs⁻¹ are shown the low peak current, while another scan rates are presented higher peak current. Since the elecetropolymerization at scan rate 10 mVs⁻¹ is taken very long time, the scan rate 20 mVs⁻¹ is applied for the polymerization in all case.



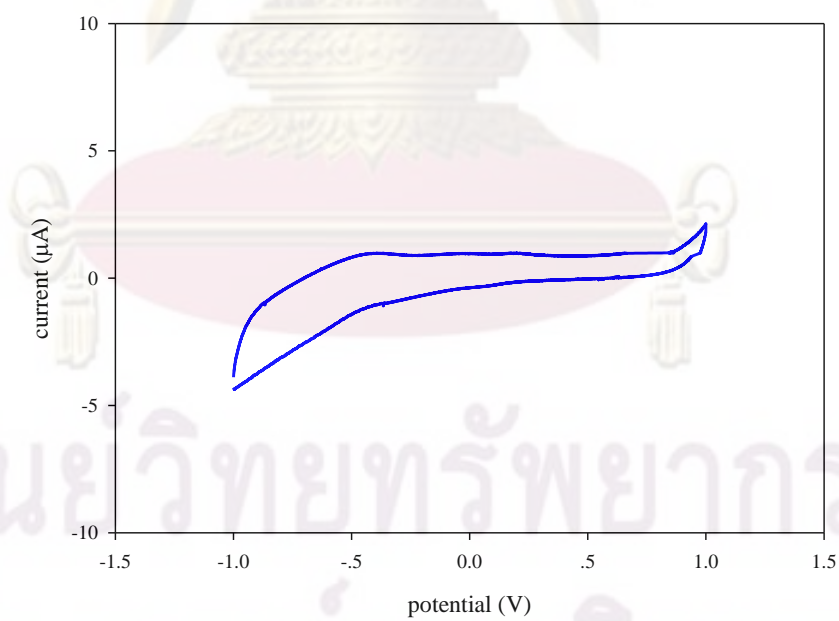
(a)



(b)



(c)



(d)

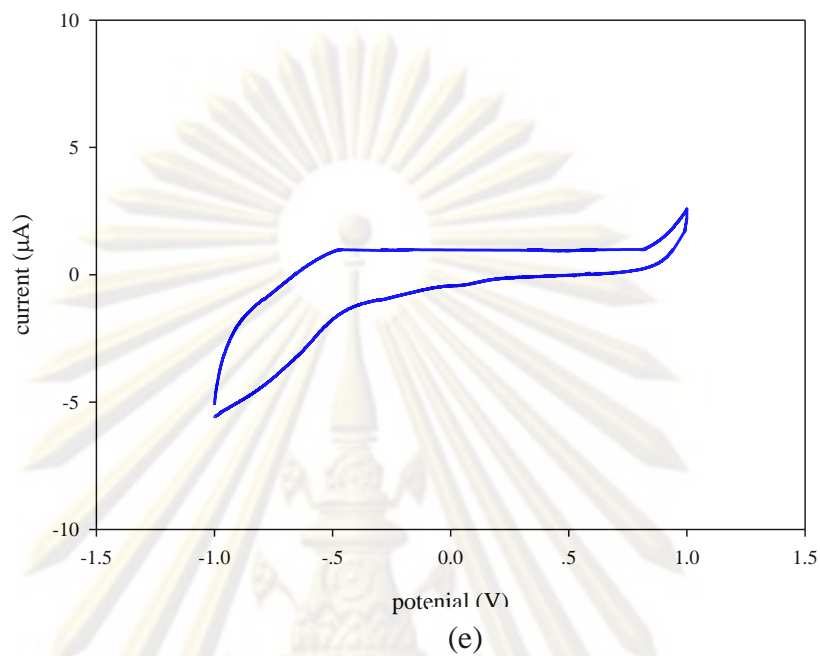


Figure A.1 Cyclic voltammogram of PPD coated GC electrode for 50 cycles at scan rate 10 (a), 20 (b), 30 (c), 40 (d), and 50 mVs^{-1} (e) in 5 mM ferri/ferrocyanide.

ศูนย์วิทยทรัพยากร
จุฬาลงกรณ์มหาวิทยาลัย

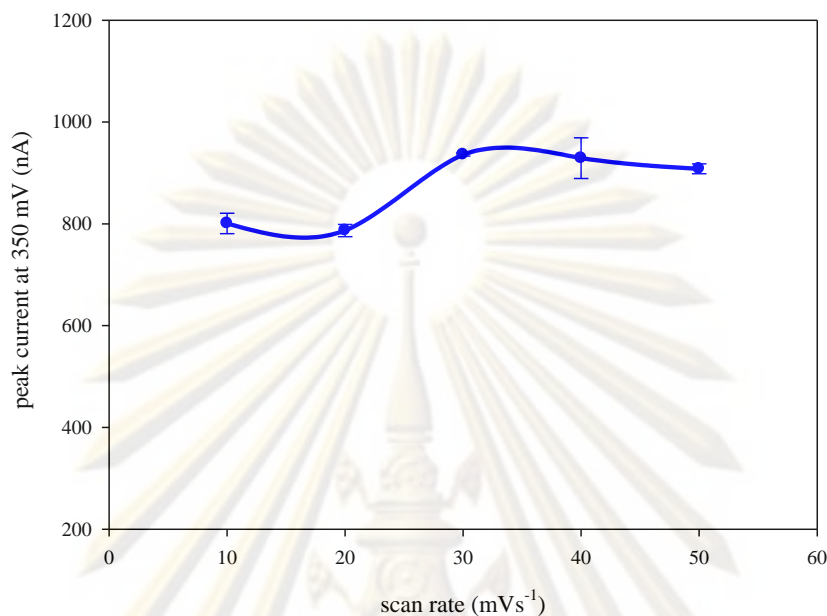
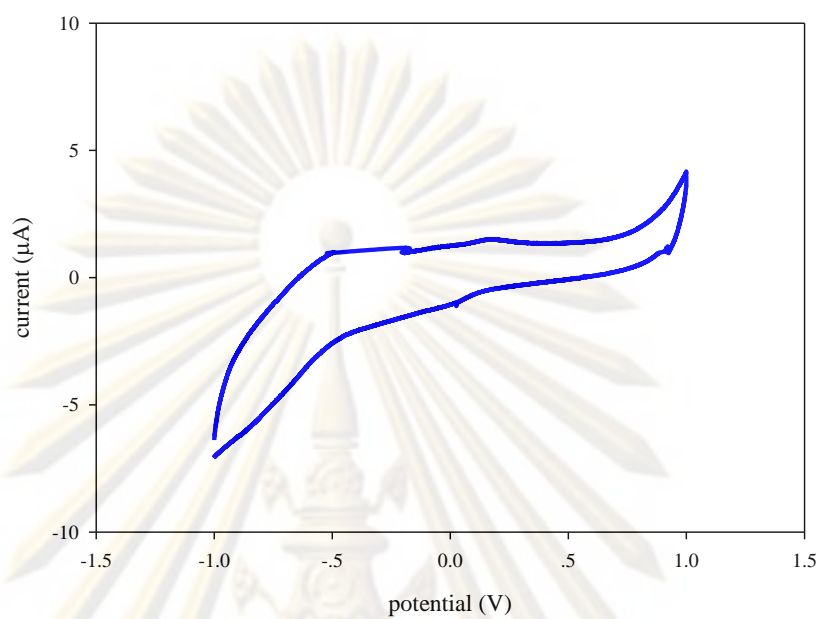
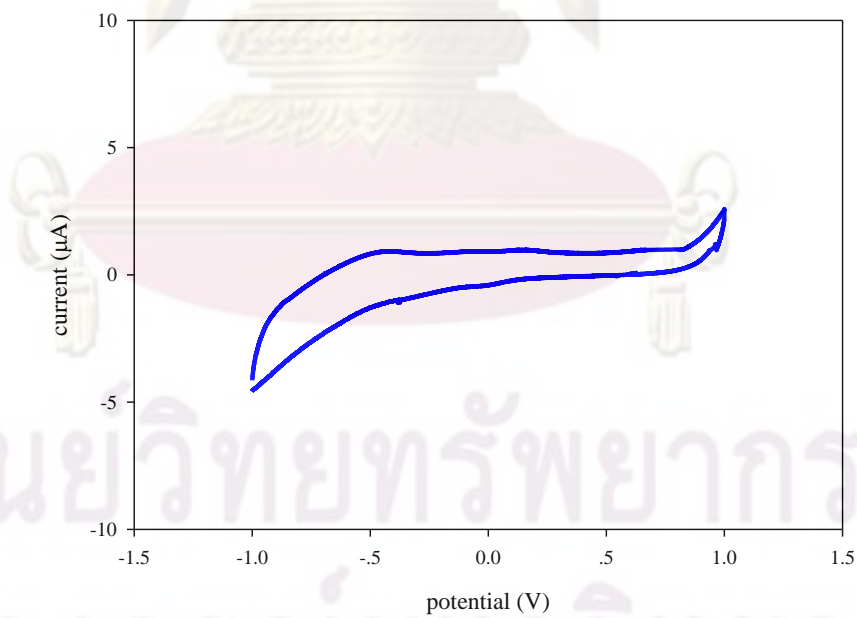


Figure A.2 The relation between the peak current at 0.35 V of the forward scan in 5 mM ferri/ferro cyanide at various scan rates.

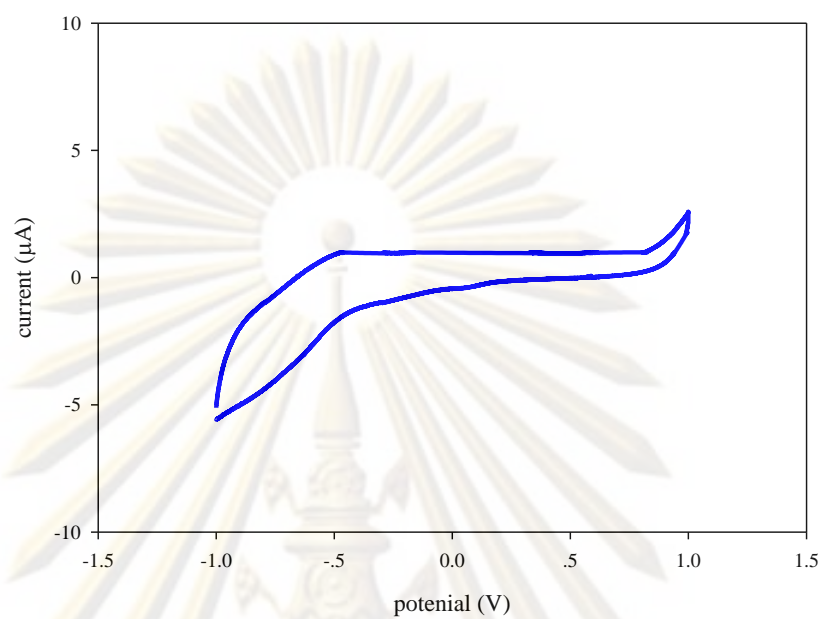
In electropolymerization process of thin film, the number of electrodeposition cycle is important for film formation. The 10, 30, 50, and 70 cycle were studied for PPD coated at scan rate 50 mVs^{-1} on GC electrode. Figure A.3 is shown the cyclic voltammogram of these processes in 5 mM ferri/ferro cyanide. Even though the voltammogram are quite similar, but the peaks current are different (Figure A.4). The lower polymerization cycle (10 cycles) presented the higher peak current. This possibly because of the polymerization was not perfect at low polymerization cycle. Nevertheless at higher polymerization cycle (70 cycles) achieved slightly higher peak current than 50 cycles, at the 50 polymerization cycle seem to be the suitable cycle for PPD polymerization. Because at higher polymerization cycle the polymerization time is much longer but obtained the same peak current



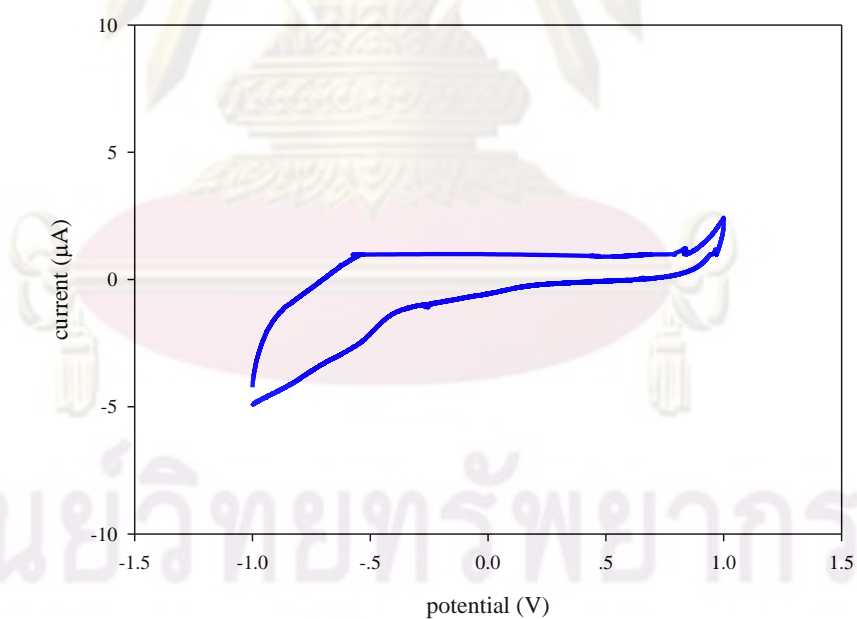
(a)



(b)



(c)



(d)

Figure A.3 Cyclic voltammogram of PPD coated GC electrode for 10 cycles (a), 30 cycles (b), 50 cycles(c), and 70 cycle (d) at scan rate 20 mVs⁻¹ in 5 mM ferri/ferro cyanide.

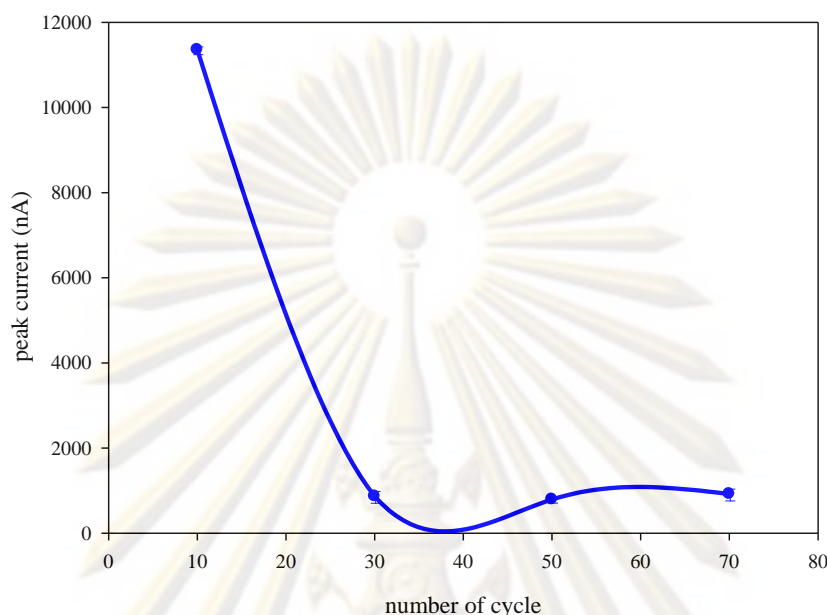


Figure A.4 The relation between peak current at 0.35 V of forward scan and the number of cycle in 5 mM ferri/ferro cyanide at scan rate 20 mVs⁻¹.

The *o*PD concentration was the next parameter for the polymerization process. Six *o*PD concentrations are investigated in this process. The cyclic voltammograms are not shown in this report. Moreover, the relation between peak current at 0.35 V and the disparate concentration is shown in Figure A.5. Although the smallest peak current was obtained at 0.5 mM monomer, at 5 mM of monomer is the appropriate concentration for polymerization. This due to the stationary peak current is acquired between 1 and 10 mM of monomer concentration. Furthermore, the higher peaks current are presented at higher concentrations which are possibly because of the electrochemistry measurement error. However, the high concentration polymerization was not the asset condition in this process.

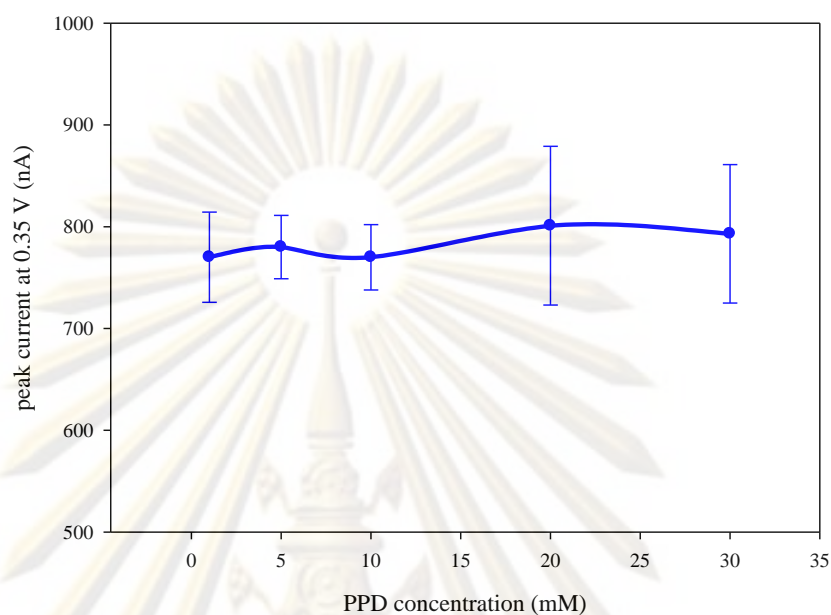


Figure A.5 The relation between peak current at 0.35 V of forward scan and the monomer concentration in 5 mM ferri/ferro cyanide at scan rate 20 mVs^{-1} .

Summary

The applicable condition for 1,2 phenylenediamine dihydrochloride (*o*PD) polymerization is at 5 mM of monomer for 20 cycles at scan rate 20 mVs^{-1} . For cyclic voltammogram determination, the 5 mM ferri/ferro cyanide was applied at scan rate 20 mVs^{-1} .

ศูนย์วิทยทรัพยากร
จุฬาลงกรณ์มหาวิทยาลัย

VITA

Lerdluck Kaewvimol, was born in Anghong, Thailand, graduated in 1997, from Anghong Patthamarot Wittayakhom School. She entered Silpakorn University in June as a Biotechnology major in the faculty of Industrial Technology. Lerdluck continued her Master's degree in Chemical Engineering at Chulalongkorn University. After she graduated in May 2004, Lerdluck be the research assistance at Thailand Institute of Scientific and Technological Research. Lerdluck decided to continue her Ph.D. in Chemical Engineering, Chulalongkorn University with a MUA research scholar in 2007. During her 4 years with studying and researching, Lerdluck took the program to continue her research at school of Health, Cranfield University, United Kingdom for six months. After that, she came back to finish her Ph.D. at Chulalongkorn University in 2010.



ศูนย์วิทยทรัพยากร
จุฬาลงกรณ์มหาวิทยาลัย